学位論文

Theoretical modeling and phylogenetic analysis of cyanobacterial promoters regarding the rise of atmospheric oxygen in the Paleoproterozoic

（原生代初期における大気酸素濃度上昇に関する
理論研究とシアノバクテリアの
プロモーター分子系統解析）

平成 27 年 12 月 博士（理学）申請

東京大学大学院理学系研究科
地球惑星科学専攻

原田 真理子

Abstract

The early Paleoproterozoic is a remarkable period in the Earth's history, marked by the rise of atmospheric oxygen, global glaciations (a snowball Earth event), and the evolution of life (emergence of eukaryotes). Geochemical studies suggest that the rise of oxygen was a transition from oxygen poor to oxygen rich steady states of the atmosphere, accompanied with an overshoot of oxygen levels. However, the trigger for the transition has been unclear, leaving its linkage to the snowball glaciation and consequences to the biological evolution poorly understood.

In the first half of this thesis (Part I: Transition to an oxygen-rich atmosphere triggered by the Paleoproterozoic snowball Earth event), the trigger for the rise of oxygen is discussed by numerical calculations using biogeochemical cycle models. In this study, I focus on the climate jump at the end of the snowball glaciation as a trigger for the rise of oxygen. Numerical results suggest that the super-greenhouse conditions after the deglaciation cause intense nutrient riverine input to the oceans via chemical weathering. In the nutrient-rich oceans, bloom of cyanobacteria causes increases in burial of organic carbon into the sediments and releases massive oxygen into the atmosphere. The large perturbations into the global redox balance result in a rapid transition from oxygen-poor ($< 10^{-5}$ PAL, PAL: Present Atmospheric Levels) to oxygen-rich ($> 10^{-2}$ PAL) conditions within $\sim 10^{4}$ years after the deglaciation. The transition is followed by an overshoot of oxygen to 0.1−1 PAL lasting for 10^{6}−10^{8} years. The magnitude and time scale of the overshoot vary depending on the initial and boundary conditions. However, only under the conditions assuming typical "hard snowball Earth" scenario, an extensive and long-term overshoot (~1 PAL lasting for $\sim 10^{8}$ years) occurs. Such an extensive overshoot causes the oxidation of deep oceans and the long-term accumulation of oceanic sulphate ions, which are in good agreement with the geochemical records. Therefore, I suggest that the oxygen transition in the Paleoproterozoic was accompanied with an extensive overshoot

reaches ~ 1 PAL and that the snowball glaciation would be a strong candidate as the trigger for the rise of oxygen.

In the second half of the thesis (Part II: Rise of oxygen and evolution of DNA sequences of the promoters in cyanobacteria), the phylogenetic analysis of cyanobacteria is performed in order to estimate the consequences of the rise of oxygen to the biological evolution. Contrary to previous studies that have mainly discussed the evolution of morphologies and habitat of cyanobacteria, this study focuses on the evolution of the gene expression levels of oxygen catalysing enzymes, which can be directly correlated to the changes in environmental oxygen levels. The ancestral sequences of DNA that regulates gene expression levels (i.e., promoter sequences) of RubiCO (ribulose 1,5-bisphosphate carboxylase/oxygenase) and Fe-SOD (Fe-superoxide dismutase) are obtained from phylogenetic analysis. In order to estimate the gene expression levels, the obtained sequences are compared to the promoters of genes that should be highly expressed (rRNA and ribosomal proteins). The results show that the similarity between ancestral sequences of Fe-SOD promoters and the promoters of highly expressed genes was low at the time of the emergence of cyanobacteria. The similarity increases at the branching nodes diverged at 2.5−2.0 Ga, which roughly coincides with the rise of atmospheric oxygen reported from geochemical records. This implies that the gene expression levels of Fe-SOD increased in response to the rise in atmospheric oxygen. In contrast, the results suggest that the gene expression levels of RubsiCO have been generally high throughout the history, implying no relationship with the changes in the oxygen levels, although the similar result as Fe-SOD is also obtained from one of models used in this study,. Such discrepancies imply that, regarding the carbon fixation, the adaptation to the oxygen-rich conditions might have been compensated by the evolution of other biochemical characteristics rather than increasing gene expression (e.g., increases in the activity of the enzyme). Although improvement may be required in future works, I suggest that methodologies of ancestral promoter analysis developed in this study will become novel tools that provide the evidence connecting biological evolution and the environmental changes in the Earth's history.

In this dissertation, relationships among three major events in the Paleoproterozoic (i.e., the rise of atmospheric oxygen, snowball glaciation, and the evolution of life) are studied by numerical calculation and phylogenetic analysis. I propose that the cyanobacterial bloom just after the snowball deglaciation triggered the rise of oxygen and that the rise of oxygen caused the adaptive evolution of cyanobacteria. This would be the first study to provide a comprehensive and quantitative scenario for the co-evolution of environment and life in the Paleoproterozoic, suggesting the occurrence of interaction between the climate, chemical composition of atmosphere-ocean system, and biosphere.

Acknowledgments

First, I would like to express my sincere appreciation to Prof. Eiichi Tajika and Prof. Akihiko Yamagishi for their erudite supervision. It is their continuous leading and encouragement that have leaded my study to the successful completion.

I would like to express my deep and sincere thanks to Dr. Yasuhito Sekine, for his kind guidance and encouragement during my Ph. D. I would like to thank Dr. Shin-ichi Yokobori and Mr. Ryutaro Furukawa for their guidance and helpful discussions in promoter analysis. I am grateful to Dr. Kazumi Ozaki for his support in developing numerical models and for always giving me critical comments.

I wish to thank Prof. K. Endo, Prof. T. Murakami, Prof. R. Tada, Prof. H. Nagahara, Prof. S. Sugita, Dr. Y. Abe, Dr. M. Ikoma, Dr. M. Tamakoshi, Dr. S. Akanuma, and Dr. S. Takahashi for their critical review and comments for this thesis. The member of the research group at the University of Tokyo, Mr. Y. Watanabe, Mr. S. Kadoya, Mr. Y. Chang, Ms. K. Oide, Mr. Y. Nakagawa, and Mr. Kobayashi T. are greatly acknowledged. I am grateful to the member of the research group at the Tokyo University of Pharmacy and Life Sciences, especially Dr. Y. Kawaguchi, Mr. S. Yagi, Ms. A. Kaji, Mr. K. Takahashi, Ms. A. Nagano, Ms. M. Bessho, Mr. T. Sasamoto, Mr. H. Ogasawara, Mr. T. Nakayama, Ms. Y. Murano, Ms. A. Yamashita, and Mr. T. Kumagawa. I would like to thank Dr. A. Takigawa, Dr. R. Sakai, Mr. T. Kodama and Dr. S. Tachibana for their encouragements. I am grateful for the kind support by S. Fujiwara and Y. Hirata. I also thank financial support by JSPS Research Fellowship for young scientists. And finally, my sincerest thanks to my family.

December 17, 2015

Mariko Harada

Contents

General Introduction

The rise of oxygen in the Paleoproterozoic

Molecular oxygen (O_2) consists ~21% of the Earth's atmosphere today. However, lines of evidence indicate that the atmosphere was originally poor in O_2. Photochemical models constrain the O_2 level before the origin of life to < 10^{-12} PAL (PAL: Present Atmospheric Level) (Kasting et al., 1979). Sulphur isotope data from sedimentary rocks before 2.45 Ga show mass independent fractionations (MIF-S), suggesting the absence of UV shieling by an ozone layer due to low atmospheric O_2 concentrations (Farquhar, 2000; Farquhar et al., 2007). Photochemical models suggest that the O_2 levels required for the ozone layer formation are 10^{-5}–10^{-2} PAL (Pavlov and Kasting, 2002), indicating 10^{-5} PAL as the upper limit for the atmospheric O_2 before 2.45 Ga. Recent studies show that there are several factors which affect MIF-S signal other than O_2 concentrations (e.g., atmospheric methane concentration, sulfur input flux, and the presence of hydrocarbon) (Zahnle et al., 2006; Claire et al., 2014). Thus, it should be noted that the quantitative O_2 levels required for MIF-S signal would be still uncertain. However, reducing atmospheric conditions before ~2.4 Ga is plausible, supported by paleosol data (Rye and Holland, 1998) and the occurrence of detrital reduced minerals (i.e., uraninite and pyrite) in the Archean sedimentary rocks (Papineau et al., 2007; Young, 2002). A transition

from a reducing (< 10^{-5} PAL) to an oxidising atmosphere (> 10^{-3}-10^{-2} PAL) is marked by the disappearance of the MIF-S and of detrital uraninite and pyrites, the global occurrence of red bed, and paleosol records after 2.45-2.2 Ga (Bekker et al., 2004; Murakami et al., 2011; Planavsky et al., 2014; Rye and Holland, 1998). Although there are still uncertainties in the quantitative levels of O_2 and the exact timing of the rise of O_2, lines of evidence show a clear transition from O_2-poor to O_2-rich atmospheres in the early Paleoproterozoic. The oxidation event is called the "Great Oxidation Event" (the GOE) (Fig 1.1; e.g., Canfield, 2005; Holland, 2002; Karhu and Holland, 1996).

The major and irreversible shift in Earth's redox state during the GOE can be understood as a jump form low to high steady states of atmospheric O_2 concentrations (Claire et al., 2006; Goldblatt et al., 2006). The transition to an oxidising atmosphere might have been triggered by the imbalance of the global redox budget (i.e., decreases in O_2 consumption and/or increases in O_2 generation). Some previous works propose that the decrease in influx of reduced materials to the atmosphere-ocean system caused the decrease in O_2 consumption, and, in turn, triggered the transition. Gaillard et al. (2011) and Kump and Barley (2007) focus on the changes in the redox state of volcanic gases due to the changes in degassing pressure. They suggest that switch from submarine to subaerial volcanisms caused the redox state of emanating volcanic gases more oxidizing, and consequently, results in decrease in the total influx of reducing materials. Numerical studies hypothesise that the hydrogen escape to space gradually caused oxidation of the continents, resulting in decrease in influx of reduced gases emitted from metamorphic processes (e.g., Catling and Claire, 2005; Claire et al., 2006). Numerical calculation by Goldblatt et al. (2006) suggest that the decrease in influx of reduced materials from the Earth's interior, conceptually assumed as reduced iron (Fe^{2+}) in this model, caused the decrease in O_2 consumption. Besides, other pervious studies show that an increase in O_2 generation can be induced by the increase of the burial rate of organic carbon generated by oxygenic photosynthesis. Numerical model shows that the small increase in the net primary productivity and burial of organic carbon can also cause the jump between low and high steady state levels of atmospheric O_2 (Goldblatt et al., 2006). Several different hypotheses regarding the

Paleoproterozoic rise of O_2 have been proposed so far, however, the causal mechanisms which may have triggered and caused the GOE is still unclear.

Recent geochemical studies indicate that the rise of oxygen might have accompanied an extensive, long-term overshoot (Fig. 0.1; e.g., Lyons et al., 2014). The global deposition of sulphate evaporites at 2.22−2.08 Ga (Bekker and Holland, 2012; Schröder et al., 2008) suggests the sufficiently high riverine input of sulphate ions to the ocean during this period, hence, oxidative weathering of continental sulphides under strongly oxidising atmosphere. Geochemical evidence of deep ocean oxygenation at ~2.1 Ga has been reported in Francevillian Supergroup, the Republic of Gabon (Canfield et al., 2013), implying the high atmospheric O_2 levels. Sulphur isotope data at 2.2−2.1 Ga (Planavsky et al., 2012) and the episodic uranium enrichment in the sedimentary rocks (Partin et al., 2013) also support the occurrence of the overshoot. The transition to an oxygen-rich atmosphere including the dynamic overshoot can be called as “the Great Oxygen Transition (the GOT)” (Lyons et al., 2014). Contrary to the conventional, unidirectional model of the rise of O_2, the GOT requires large-scale perturbation of biogeochemical cycle as a trigger. However, previous studies only focus on explaining unidirectional increase in the atmospheric O_2, and there has been no models account for this novel view of the rise of O_2.

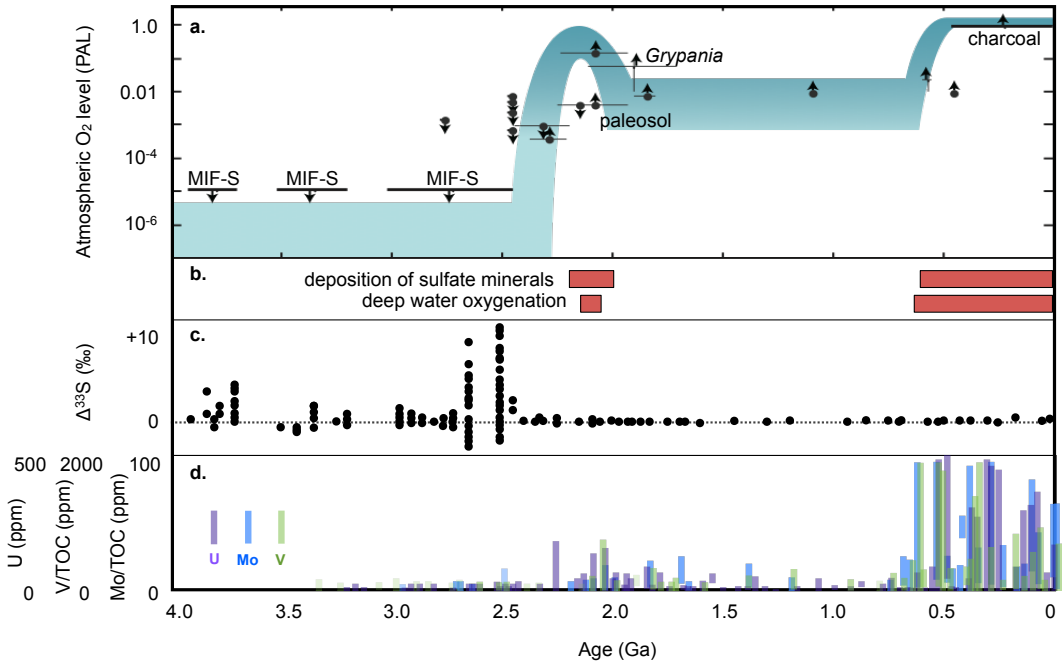

Fig.0.1 Evolution of atmospheric oxygen levels. a, Oxygen levels constrained by proxies (Goldblatt et al., 2006 and references therein). Shaded blue area show possible evolutionary track of atmospheric oxygen levels (Lyons et al., 2014). **b,** Evidence of deposition of sulphate minerals and deep water oxygenation (Canfield et al., 2013; Schröder et al., 2008; Turner and Bekker, 2015). **c,** Signals of mass independent fractionation of sulphur isotopes (Farquhar et al., 2007). **d,** Records of the enrichment of redox sensitive trace metals in sedimentary rocks (Partin et al., 2013; Sahoo et al., 2012; Scott et al., 2008).

The Paleoproterozoic glaciations

The early Paleoproterozoic is also known as a period of repeated glaciations (i.e., the early Paleoproterozoic glaciations). Glacial deposits at this age have been globally reported from North America, South Africa, Western Australia and Fennoscandia (e.g., Ojakangas, 1988; Marmo et al., 1988; Young, 1991; Kohonen and Marmo, 1992; Kirschvink et al., 2000; Ojakangas et al., 2001a, 2001b; Bekker et al., 2001, 2004; Young, 2004). The depositional age is spanning from ~2.45 to 2.22 Ga (Rasmussen et al., 2013). Although stratigraphic correlations between the glacial deposits are still controversial, it is suggested that there have been at least three, probably four, glaciations during this period (e.g., Kopp et al., 2005). The linkage between glaciations and the rise of O_2 has been indicated by several geochemical studies. In the Huronian Supergroup, Ontario, Canada, enrichment of redox sensitive elements (e.g., Os, Re, Mo, Mn) immediately above the glacial deposits suggests that the atmospheric O_2 levels increased at the time of deglaciation (Goto et al., 2013; Sekine et al., 2011a, 2011b). The Makganyene Diamictite Formation deposited at ~2.22 Ga in the Transvaal Supergroup, Griqualand West region, South Africa, is considered to have been glacial deposits formed in low latitude (~11°), indicating that the glaciation was the snowball Earth event (Evans et al., 1997). The glacial diamictites are directly overlain by manganese and iron formations, which implies that the atmospheric O_2 rose immediately after the snowball Earth event (Kirschvink et al., 2000; Kopp et al., 2005). The evidence of the deposition of sulphate minerals is found above the manganese and iron formation (Schröder et al., 2008), suggesting that the rise of O_2 after the snowball Earth was a long-lasting event.

Causal linkage between the early Paleoproterozoic glaciations and the rise of O_2 has been poorly understood. Previous studies suggest that the rise of O_2 caused the glaciations (Kasting et al., 2001; Kirschvink, 2002; Kopp et al., 2005; Claire et al., 2006; Goldblatt et al., 2006). In the Arhcean, methane (CH_4) would have been a major greenhouse gas which maintained warm climate. These studies suggest that the oxidation of the atmosphere caused the collapse of CH_4 in the atmosphere. This might resulted in the rapid decrease in the greenhouse effect, leading to the glaciation (Kasting et al., 2001; Kirschvink, 2002; Kopp et al., 2005; Claire et al., 2006;

Goldblatt et al., 2006). However, the models do not account for the rise of O_2 after the glaciations. The oxidation was possibly caused by blooming of photosynthetic cyanobacteria after the snowball Earth event (Kirschvink et al., 2000; Kopp et al., 2005). However, it is highly uncertain how the snowball Earth event affected the biosphere and atmospheric O_2 levels.

Adaptive evolution of life to the rise of oxygen

Biological evolutions coincided with the rise of O_2 in the Paleoproterozoic. The oldest fossil of eukaryotes (*Grypania spiralis*) has been found in the 2.1-1.9 Ga Negaunee Iron Formation, Michigan, USA (Han and Runnegar, 1992). Molecular clock analysis show that the last common ancestor of extent eukaryotes appeared in 1.866-1.679 Ga (Parfrey et al., 2011), which is roughly consistent with the fossil records. It is suggested that, in general, high O_2 levels are advantageous for the evolution of complicated life. Aerobic respiration yields ~30 ATP molecules per oxidised glucose molecule during cellular respiration, which is ~15 times more efficient than anaerobic respiration (Rich, 2003). Biosynthesis of membrane lipids (sterols and unsaturated fatty acids) of eukaryotes requires molecular oxygen, (Runnegar, 1991). Simultaneous occurrence of the rise of O_2 and biological innovation in the Paleoproterozoic strongly implies causal linkage between them, however, there has been no direct evidence to support the hypothetical relationships.

The evolution of cyanobacteria would also have been deeply related to the rise of O_2. Given that cyanobacteria are photosynthetic bacteria live in the euphotic zone of the oceans, they would have been greatly affected by the changes in the atmospheric O_2 levels. Further, because there are only cyanobacteria that were able to produce molecular oxygen before the emergence of eukaryotic algae, their emergence and evolution should have contributed to the rise of O_2 (i.e., the GOE). Indeed, phylogenetic and molecular clock analyses of cyanobacteria have been revealed that the major diversification of extant cyanobacteria occurred in the Paleoproterozoic (e.g., Blank and Sánchez-Baracaldo, 2010; Sánchez-Baracaldo et al., 2014, 2005; Schirrmeister et al., 2015, 2013; Shih et al., 2013; Tomitani et al., 2006). However, because the previous studies only focus on the evolution of

morphology or habitats, direct correlation between the environmental O_2 levels and the evolution of cyanobacteria has been poorly understood. Some previous works suggest that evolution of some morphological traits and/or habitat change of cyanobacteria may account for the rise of O_2 (e.g., Blank and Sánchez-Baracaldo, 2010; Schirrmeister et al., 2013, 2015). However, the evolution of such characteristics of cyanobacteria might not directly correlate to the environmental O_2 levels. Further analysis using an indicator that directly reflects the environmental O_2 levels will be required to assess these hypothetical causal linkages between the rise of O_2 and the evolution of cyanobacteria.

The evolution of enzymes which use O_2 or chemical components related to O_2 as substrate might reflect the rise of environmental O_2. Studying the evolution of such enzymes will be the first step for the better understanding of relationships between the rise of O_2 and the adaptive evolution of life. For instance, the efficiency of metabolism such as detoxification of reactive oxygen species, carbon fixation in the photosynthesis, and aerobic respiration can be affected by the changes in environmental O_2 levels. These reactions are enzymicaly catalyzed by superoxide dismutase, catalase (SOD), ribulose 1,5-bisphosphate carboxylase/oxygenase (rubisco), and cytochrome *c* oxidase, respectively. The amount of synthesis (gene expression levels) the enzymes must have been evolved in response to the rise of O_2. Although several previous works have analysed the origin and evolution of the enzymes, there have been no study to discuss the evolution of such a biochemical feature.

The evolution of gene expression can be evaluated by the phylogenetic analysis of DNA sequences which controls the gene expression levels. The DNA sequences are called promoter sequences. Introducing the knowledge of molecular biology into phylogenetic analysis and developing a novel methodology to analyse promoter sequences of O_2-related enzymes enables us to understand the direct adaptive evolution of life to the rise of O_2. As mentioned above, cyanobacteria are bacterial organisms live in the place where directly affect by the rise of atmospheric O_2. Thus they might be good targets to introduce such a new methodology. If it is proved that the rise of O_2 is recorded in the DNA sequences of cyanobacteria the

same principles and methodologies can be applied in other organisms, including eukaryotes.

Objectives of this thesis

The early Paleoproterozoic is marked by a major phase changes in the atmosphere-ocean chemistry, climate, and biosphere. (i.e., the rise of atmospheric O_2 several glaciations including a snowball Earth event, and the evolution of eukaryotes and cyanobacteria). The rise of O_2 has been accompanied with an overshoot of oxygen levels; however, the trigger and causal mechanisms of the rise of O_2 have been unclear, leaving its linkage to the snowball Earth event poorly understood. Moreover, due to lack of evidence, consequence of the rise of O_2 to the biological evolution has been largely uncertain.

In this thesis, I aim to evaluate the causal mechanisms of the rise of O_2 in the Paleoproterozoic and to discuss its linkage to the other three events. In Part I, by developing a biogeochemical cycle model, the causal mechanisms of the rise of O_2 and the overshoot are evaluated, focusing on the Paleoproterozoic snowball Earth event as a trigger. Using biogeochemical cycle models, I quantify the rise of O_2 just after the snowball deglaciation, and compare the results with geological records. In Part II, the consequences of the rise of O_2 to the biological evolution are discussed by a novel methodology. From phylogenetic analysis of cyanobacterial promoter sequences, the gene expression levels of O_2 catalysing enzymes are estimated. The results are compared with the evolutionary track of atmospheric O_2 over Earth's history. Finally, in Conclusion, I summarise the findings obtained in the studies for this thesis.

Part I: Transition to an oxygen-rich atmosphere triggered by the Paleoproterozoic snowball Earth event

1.1. Previous theoretical studies for the Great Oxidation Event

As reviewed in General Introduction, several hypothetical triggers for the rise of O_2 (the GOE) have been proposed so far. In order to assess the validity of the hypothesis, it would be fundamental to develop a quantitative model which can estimate atmospheric O_2 levels through a balance of oxygen fluxes into and out of the atmosphere, and to estimate the time scales and magnitudes of resulting change in O_2 levels. Through comparing the numerical results with observations of the geological records, the trigger for the rise of O_2 can be constrained. However, as a mechanism to stabilize atmospheric oxygen levels has not been known well, there have been only two studies that have quantitatively calculated the time evolution of the atmospheric O_2 levels during the GOE (Claire et al., 2006; Goldblatt et al., 2006). One is the work by Goldblatt and co-workers. They develop a biogeochemical cycle model coupled with a model of atmospheric photochemistry and constrain atmospheric oxygen levels through many of atmospheric photochemical reactions. In this model, the atmospheric O_2 levels are stabilized by the negative feed back loop

with regards to O_2 which are derived from the O_2 dependant photochemical CH_4 oxidation and biological O_2 production. The study proposes that the rise of O_2 can be interpreted as a jump between two steady states of atmospheric O_2 and that the jump can be triggered by a small increase in oxidant input from the biosphere and/or a decrease in reductant input from Earth's interior. The other work is by Claire et al. (2006), which also includes biogeochemical cycles and atmospheric photochemistry in the model. In this model, the atmospheric O_2 levels are controlled by strong O_2 dependence of the rates of photochemical reactions and oxidative weathering of continental organic carbon. They suggest that the rise of O_2 was triggered by the gradual oxidation of continents due to the continuous escape of hydrogen to space (Claire et al., 2006). In both of the models, when the atmospheric O_2 level reaches > 10^{-5} PAL, the levels of O_2 increases rapidly and irreversibly by a positive feedback loop with regards to O_2, that is, increases in O_2 levels induce decreases in the oxidizing efficiency of CH_4 in the atmosphere, a process which further increases the O_2 levels. Owing to this mechanism and the ideas for stabilizing the O_2 levels, these two models successfully account for an event-like, unidirectional jump in O_2 levels from low (<10^{-5} PAL) to high (> 0.01 PAL) levels. Their works, however, do not explain the rise of O_2 levels with an intense overshoot suggested by recent geochemical works (Bekker and Holland, 2012; Schröder et al., 2008). This is because the two studies hypothesize the small perturbation or gradual oxidation of surface environments as a trigger for the rise of O_2. A dynamic transition accompanied with the overshoot appears to require strong forcing toward oxidation as a trigger.

1.2. The Paleoproterozoic snowball Earth event as a trigger for the rise of oxygen

In this study, I propose the Paleoproterozoic snowball Earth event ended at 2.2 Ga (Evans et al., 1997; Kirschvink et al., 2000) as a trigger for the transition from a O_2-poor to an O_2-rich atmosphere with an overshoot of O_2 levels. The simultaneous occurrence of the snowball Earth event and the rise of O_2 strongly suggest that there

have been a causal linkage between these two events (Kirschvink et al., 2000). In the Transvaal Supergroup, Griqualand West region, South Africa, a massive deposition of manganese-iron oxides is found directly above a low-latitude glacial diamictites, which implies the rise of O_2 might have caused by the glaciation (Kirschvink et al., 2000; Kopp et al., 2005). The evidence of the deposition of sulphate minerals is found above the manganese and iron formation (Schröder et al., 2008), suggesting that the snowball-induced O_2 rise was a massive and long-lasting event.

Previous studies suggest that a long-term shutdown of atmosphere–ocean interactions during the snowball glaciation results in the accumulation of volcanic carbon dioxide (CO_2) in the atmosphere. Theoretical models show that the buildup of CO_2 to a level of ~0.7 atm at ~2.2 Ga eventually causes a climate jump to an ice-free greenhouse state (Caldeira and Kasting, 1992; Tajika, 2003). Such a greenhouse climate during deglaciation should have induced a strong perturbation of the biogeochemical cycle. It is however highly uncertain how this perturbation caused by the climate jump affected the atmospheric O_2 levels. I therefore investigate the perturbation to the biogeochemical cycle due to the climate jump which ended the Paleoproterozoic snowball Earth event at 2.2 Ga.

1.3. Biogeochemical cycle model

In this study, I evaluate responses in the atmosphere–ocean system to a climate jump at the termination of the snowball glaciation, by using a biogeochemical cycle model. Surface temperature, which is calculated from the amount of atmospheric CO_2, affects a net primary production and biogeochemical processes in the oceans by changing the input fluxes of nutrients and cations to the oceans through chemical weathering of the continents. Atmospheric levels of O_2 and methane (CH_4) are calculated from the mass balance between the input and output of both oxidants and reductants based on a redox balance model (Goldblatt et al., 2006), which has a bistability of O_2 levels for a given net primary production. Details of the model are described below.

1.3.1. Model description and experimental design

The model consists of three boxes: atmosphere, surface ocean, and deep ocean (Fig. 1.1), where the abundances of gaseous molecules, such as CO_2, O_2, and CH_4 and/or dissolved species including dissolved inorganic carbon (DIC), alkalinity, phosphate (PO_4), O_2, and calcium ion (Ca^{2+}) are calculated. These boxes exchange key elements through atmosphere–ocean interactions, biogeochemical reactions and ocean circulations. Removal of elements from the atmosphere–ocean system occurs through carbonate precipitation and organic carbon burial to seafloor sediments as well as H_2 escape from the atmosphere to space, whereas supplies of elements take place via chemical weathering of the continents, reductant input and volcanic degassing from mantle (Fig. 1.1). Surface temperatures are calculated from atmospheric CO_2 concentration, based on parameterization of the numerical results from a radiative–convective climate modelling of Kasting and Ackerman (1986).

In the surface ocean, organic carbon is produced by cyanobacteria through oxygenic photosynthesis, and is, in turn, exported to the deep ocean. In the deep ocean, most of exported organic carbon is assumed to be decomposed through aerobic respiration and methanogenesis. In the atmosphere, CH_4 produced by methanogenesis is oxidized finally to form CO_2, and O_2 is consumed. Thus, the net production rate of O_2 in the atmosphere-ocean system corresponds to the rate of organic carbon burial in the ocean. The rate of organic carbon burial is assumed to be proportional to the rate of export production. The rate of export production is expressed as a function of phospate concentrations in the surface ocean (Yamanaka and Tajika, 1996). Phosphate riverine input is proportional to the rate of chemical weathering of silicate and carbonate minerals on the continents. Accordingly, the biological production rate of O_2 is strongly affected by surface temperature. It has been widely accepted that there are linkages in the Earth's system between global warming, an enhancement of nutrient supply via continental weathering, and an increase in oceanic biological productivity (e.g., oceanic anoxic events in the Phanerozoic) (e.g., Jenkyns, 2010). In this model, the chemical weathering rate is described as functions of both partial pressure of CO_2 and surface temperature, multiplied by the factor representing weathering efficiency (Berner, 1991; Tajika,

2003). The biological production of CH_4 occurs through decomposition of organic matter by methanogenesis.

As the initial conditions, 0.7 atm of atmospheric CO_2 is assumed because this level is required to end the snowball glaciation in the Paleoproterozoic (Tajika, 2003). Then, time evolution of each component in the atmosphere-ocean system after the snowball deglaciation is explored. In sensitivity tests, various values of initial conditions, such as the atmospheric CO_2 and oceanic phosphate concentration, the weathering efficiency and phosphorous cycles in the oceans are used (Fig. 1.4 and Figs. 1.5–1.8) (see Section 1.5.3 for more details on the sensitivity tests).

In order to evaluate temporal variations in abundances of the gaseous and dissolved species, mass balance equations are solved for given fluxes through particular biogeochemical processes under particular conditions after the end of the snowball Earth event. The model equations and parameters are described in the following sections.

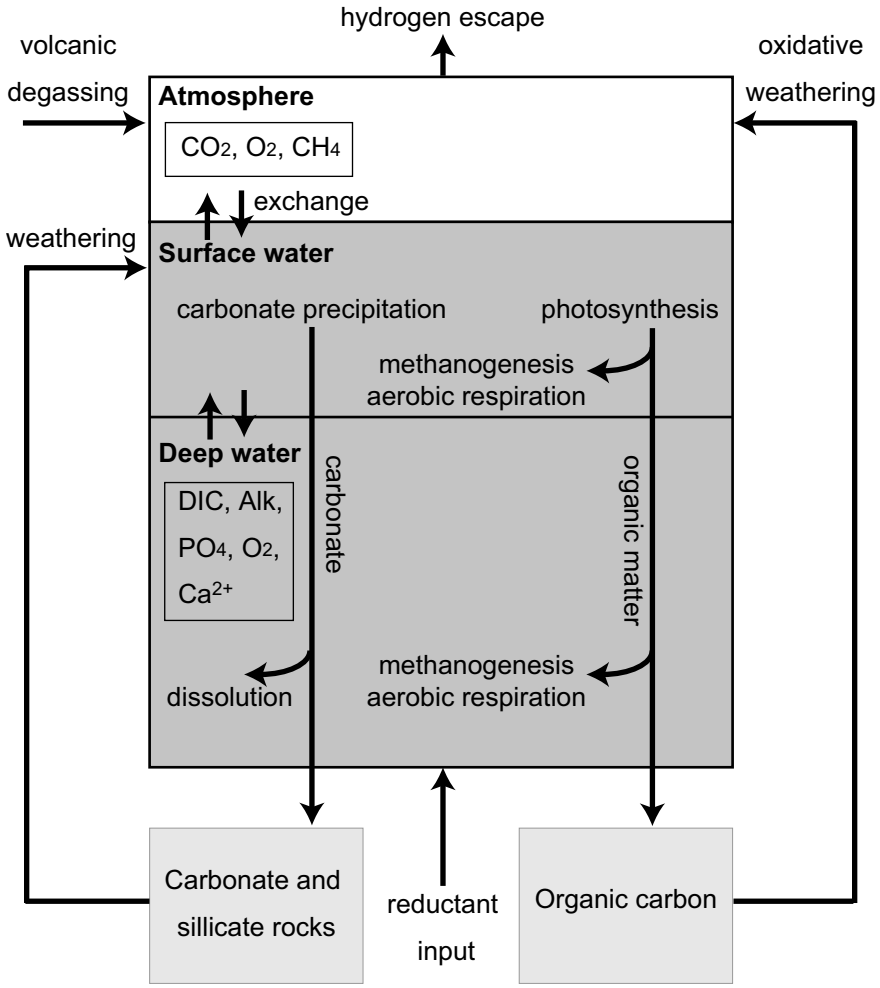

Fig. 1.1 Diagram of the biogeochemical cycle model. Atmosphere-ocean system are represented by three boxes, i.e., atmosphere, surface ocean, and deep ocean. Arrows express exchange of key elements between boxes, as well as external inputs to and outputs from the atmosphere-ocean system.

1.3.2. Governing equations

As mentioned in the previous section, the biogeochemical cycle model consists of three boxes representing the atmosphere, surface ocean, and deep ocean. The model simulates biogeochemical processes in the Paleoproterozoic atmosphere and ocean by solving the mass balance of several components in each box. In this section, mass balance equations and fluxes of both the gaseous and dissolved species in the model are described. I first describe the mass balance equations that determine the variations in abundances of gaseous and dissolved species in the atmosphere-ocean system (Section 1.3.3). Then, I explain each flux of these species in interactions between the boxes as shown in Fig. 1.1 (Section 1.3.5-1.3.13). The equations and parameters are summarized in Tables 1.1–1.4.

1.3.3. Mass balance equations

In the mass balance calculations of CO_2, O_2, and CH_4, the atmosphere and surface ocean reservoirs are treated as one box. At each time step, the mass of the components in the atmosphere-surface ocean box are separated into the two boxes (i.e., the atmosphere box and the surface ocean box), assuming that gas exchange between the atmosphere and surface ocean is in equilibrium.

Inorganic Carbon: Mass balances of inorganic carbon reservoir in the atmosphere-surface ocean box ($\mathbf{C}_{AS}$) and deep ocean box ($\mathbf{C}_{D}$) are expressed as follows.

$$\frac{d\mathbf{C}_{AS}}{dt} = F_{vc} + F_{wo\_C} + F_{esc\_H} + F_{oxi\_M} + F_{wc} - F_{pc} - F_{po\_C} + F_{cir\_C},$$

$$\frac{d\mathbf{C}_{D}}{dt} = F_{dc} + F_{dgD\_C} - F_{cir\_C}.$$

Inorganic carbon in the atmosphere-surface ocean box is provided through degassing from Earth's interior (F_{vc}), oxidative weathering of terrestrial organic matter (F_{wo_C}),

and carbonate weathering on the continents (F_{wc}). In addition, hydrogen escape at the top of atmosphere to space (F_{esc_H}) and photochemical methane oxidation (F_{oxi_M}) are considered as inputs of CO_2 in the atmosphere through net chemical reactions as shown below (Goldblatt et al., 2006). Hydrogen escape is considered to be diffusion limited, thereby, it depends on methane concentration in the atmosphere (Goldblatt et al., 2006):

$$\text{Hydrogen escape:} \quad CH_4 + O_2 + h\nu \rightarrow 4H(\text{space}) + CO_2,$$

$$\text{Photochemical methane oxidation in the atmosphere:} \quad CH_4 + 2O_2 \rightarrow 2H_2O + CO_2.$$

For the sink of C_{AS}, we consider carbonate precipitation (F_{pc}) and export production (F_{po_C}). In the deep ocean, the inorganic carbon reservoir ($\mathbf{C}_D$) increases by carbonate dissolution (F_{dc}) and degradation of marine organic matter (F_{dgD_C}). The surface and deep oceans exchange DIC by the ocean circulation (F_{cir_C}).

Oxygen and methane: Mass balance calculations of oxygen reservoirs (oxygen in the atmosphere-surface ocean: $\mathbf{O}_{AS}$, and oxygen in the deep ocean: $\mathbf{O}_D$) and methane reservoir (methane in the atmosphere-surface ocean: $\mathbf{M}_{AS}$) are basically followed on the basis of the previous model of global redox balance (Goldblatt et al., 2006), which uses parameterization of the numerical results of detailed photochemical models. The model is modified by adding a deep ocean box in the aim of calculating export production and degradation of particulate organic matter in the deep ocean. For simplicity, methane budget in the deep ocean is not calculated in this model, assuming that methane produced in the deep ocean is directly provided into the atmosphere. Mass balance equations of $\mathbf{O}_{AS}$, $\mathbf{O}_D$, and $\mathbf{M}_{AS}$ are expressed as follows.

$$\frac{d\mathbf{O}_{AS}}{dt} = F_{po\_O} - F_{wo\_O} - F_{oxi\_O} - F_{esc\_H} + F_{cir\_O},$$

$$\frac{d\mathbf{O}_D}{dt} = -F_{cir\_O} - F_{dgD\_O},$$

$$\frac{d\mathbf{M}_{\mathrm{AS}}}{dt} = F_{dgS\_M} + F_{dgD\_M} + F_{wo\_M} - F_{oxi\_M} - F_{esc\_H}.$$

Oxygen in the atmosphere-surface ocean box ($\mathbf{O}_{\mathrm{AS}}$) is produced by export production (F_{po_O}). For sink of $\mathbf{O}_{\mathrm{AS}}$, I consider oxidative weathering of terrestrial organic carbon (F_{wo_O}), photochemical methane oxidation (F_{oxi_O}), and hydrogen escape at the top of atmosphere to space (F_{esc_H}). In the deep ocean box, oxygen ($\mathbf{O}_{\mathrm{D}}$) is provided through an exchange between the surface and deep oceans (F_{cir_O}) and is consumed by decomposition of particulate organic matter (F_{dgD_O}). The sources of methane in the atmosphere-surface ocean box ($\mathbf{M}_{\mathrm{AS}}$) are methanogenesis in the anaerobic decomposition of organic matter in the surface and deep oceans (F_{dgS_M} and F_{dgD_M}, respectively), as well as methanogenic degradation of terrestrial organic matter (F_{wo_M}). Methane in the atmosphere and surface ocean is consumed by photochemical methane oxidation (F_{oxi_M}) and hydrogen escape at the top of atmosphere to space (F_{esc_H}).

Calcium and phosphate: Calcium ions in the surface ocean ($\mathbf{Ca}_{\mathrm{S}}$) are delivered through weathering of carbonate and silicate rocks on the continents (F_{wc} and F_{ws}, respectively). Calcium ions are removed from the surface ocean through carbonate precipitation (F_{pc}) ($Ca^{2+} + CO_3^{2-} \rightarrow CaCO_3$). Dissolution of carbonate particles in the deep ocean (F_{dc}) is also considered in this model, which is in turn a source of calcium ions in the deep ocean ($\mathbf{Ca}_{\mathrm{D}}$). An exchange between the surface and deep oceans is expressed by the ocean circulation (F_{Cir_Ca}).

$$\frac{d\mathbf{Ca}_{\mathrm{S}}}{dt} = F_{wc} + F_{ws} - F_{pc} + F_{cir\_Ca},$$

$$\frac{d\mathbf{Ca}_{\mathrm{D}}}{dt} = F_{dc} - F_{cir\_Ca}.$$

Phosphate, a vital nutrient for marine biota, is supplied to the oceans through continental weathering (F_{rp}). Budget of phosphate in the surface ocean ($\mathbf{P}_{\mathrm{S}}$) is supply due to F_{rp} and net supply of phosphate to the surface ocean due to upwelling (F_{cir_P}),

and is removed by the export production from the surface ocean (F_{po_P}). Phosphate in the deep ocean ($\mathbf{P}_D$) is provided through the decomposition of organic matter (F_{dgD_P}).

$$\frac{d\mathbf{P}_S}{dt} = F_{rp} - F_{po\_P} + F_{cir\_P} ,$$

$$\frac{d\mathbf{P}_D}{dt} = F_{dgD\_P} - F_{cir\_P} .$$

Regarding alkalinity in the surface and deep oceans ($\mathbf{Alk}_S$ and $\mathbf{Alk}_D$, respectively), only Ca^{2+} budget is calculated in this model. The variations in alkalinity in the surface and deep oceans are thus twice the variations of calcium ions in these boxes.

$$\frac{d\mathbf{Alk}_S}{dt} = 2 \times \left(F_{wc} + F_{ws} - F_{pc} + F_{cir\_Ca} \right) ,$$

$$\frac{d\mathbf{Alk}_D}{dt} = 2 \times \left(F_{dc} - F_{cir\_Ca} \right) .$$

1.3.4. Aqueous carbon system

This model assumes that the inorganic carbonate system in the atmosphere and ocean are in equilibrium. Temperature dependencies of solubility constant and dissolution constants of the reactions are calculated based on the equations given by (Weiss, 1974) and (Dickson and Millero, 1987).

1.3.5. Temperature calculation

Global surface temperature (T_k) in K as a function of partial pressure of atmospheric CO_2 (pCO_2) in atm is estimated from parameterized formula based on the results of a one-dimensional radiative-convective equilibrium model (Kasting and Ackerman, 1986) as follows:

$$T_k\left(pCO_2\right) = b_1 \cdot pCO_2^{b_2} + T_{eff} \quad ,$$

$$\frac{1}{4} \cdot S_t \cdot \left(1 - A\right) = \sigma T_{eff}^4 \quad ,$$

where S_t, T_{eff}, A, and σ are the solar constant, effective global temperature, planetary albedo, and the Stephen-Boltzmann constant, respectively. According to the compiled results of a radiative-conductive model (Kasting and Ackerman, 1986), the constants b_1 and b_2 are 111.56 and 0.163, respectively, for S_t/S_0 = 1.0 (T_{eff} = 255 K) and 61.98 and 0.294, respectively, for S_t/S_0 = 0.7 (T_{eff} = 235 K), where S_0 is the present value of solar constant. The global surface temperature at ~2.2 Ga [S_t/S_0 = 0.83 (Gough, 1981)] is estimated by linear interpolation between the temperatures for S_t/S_0 = 1.0, and 0.7.

1.3.6. Weathering of carbonate and silicate minerals on the continents

Chemical weathering of silicate and carbonate minerals are expressed as follows:

$$CaSiO_3 + 2CO_2 + H_2O \rightarrow Ca^{2+} + 2HCO_3^- + SiO_2$$

$$CaCO_3 + CO_2 + H_2O \rightarrow Ca^{2+}\ 2HCO_3^-$$

The rates of global chemical weathering of silicate and carbonate minerals (F_{ws} and F_{wc}, respectively) on the continents are described as a function of $p\mathrm{CO_2}$ and global surface temperature, T_k, as follows:

$$F_{ws} = f_a \cdot f_e \cdot f_b(p\mathrm{CO_2}, T_k) \cdot F_{ws}^{*} = f_w \cdot f_b(p\mathrm{CO_2}, T_k) \cdot F_{ws}^{*},$$

$$F_{wc} = f_a \cdot f_e \cdot f_b(p\mathrm{CO_2}, T_k) \cdot F_{wc}^{*} = f_w \cdot f_b(p\mathrm{CO_2}, T_k) \cdot F_{wc}^{*},$$

where F_{ws}^{*} and F_{wc}^{*} are the present-day values of chemical weathering rates of silicate and carbonate, respectively ($F_{ws}^{*} = 6.65 \times 10^{12}$ mol/yr and $F_{wc}^{*} = 13.35 \times 10^{12}$ mol/yr) (Berner, 1991). The factor f_w ($= f_a \cdot f_e$) represents the relative weathering efficiency, where f_a and f_e are the relative continental area and soil biological activity normalized by the present-day values. In Paleoproterozoic, f_w would have been much lower than that of the present-day ($f_w < 1$), because continental areas would have been smaller than that of today ($f_a < 1$), and because there were no vascular land plants ($f_e < 1$). I assume $f_a = 0.4$–0.8 based on the previous estimates of the evolution of continental crust (Hawkesworth and Kemp, 2006; Hawkesworth et al., 2010), and $f_e = 0.1$–0.25, based on observations comparing the weathering fluxes between vegetated and unvegetated regions (Moulton et al., 2000). The factor f_b represents the dependency of chemical weathering rate on both $p\mathrm{CO_2}$ and surface temperature. Based on the previous weathering experiments and modelling (Tajika, 2003; Walker et al., 1981), f_b is simply expressed as follows:

$$f_b(p\mathrm{CO_2}, T_k) = \left(\frac{p\mathrm{CO_2}}{p\mathrm{CO_2^{*}}}\right)^{n} \cdot \frac{\exp\left(-\dfrac{E}{RT_k}\right)}{\exp\left(-\dfrac{E}{RT_k^{*}}\right)},$$

where n, E, and R represent the exponent of pCO_2 dependency, activation energy, and gas constant, respectively. We assume the values of E and n as same as those used in the previous studies (Tajika, 2003; Walker et al., 1981), i.e., E = 15 kcal/mol and n = 0.3. The terms pCO_2^* and T_k^* are the reference values of atmospheric CO_2 concentration and global surface temperature, respectively, which are obtained using the present-day solar constant (S_t/S_0 = 1) and weathering efficiency (f_w = 1).

The weathering rates F_{ws} and F_{wc} might also be influenced by continental runoff or uplift. However, the effect of runoff is not considered in this model because a previous study suggests that the post-snowball, greenhouse climate does not enhance the efficiency of runoff significantly (Le Hir et al., 2009). The degree of continental uplift is uncertain in the Paleoproterozoic, thus I assume that the degree of continental uplift in the Paleoproterozoic is similar to that of today for simplicity.

Weathering may be limited by the transport of glacial tills (Mills et al., 2011), rather than kinetics. Thus, I evaluate the effect of transport limitation on the results based on the method by Mills et al. (2011), considering the maximum and minimum assumptions for the amount of glacial tills (R_{max} = 10^{20} and 10^{18} mol, respectively) (Mills et al., 2011). As will be shown in the section 1.5.3, the results show that the transport limitation of continental weathering would not change conclusion of this study significantly.

1.3.7. Riverine input of phosphorus

Phosphorus riverine input (F_{rp}) is assumed to be proportional to the silicate and carbonate weathering rates (F_{ws} and F_{wc}, respectively) as follows:

$$F_{rp} = \frac{F_{ws} + F_{wc}}{F_{ws}^* + F_{wc}^*} F_{rp}^* .$$

The term F_{rp}^{*} represents the riverine input rate of phosphorus as a form of phosphate at present, which is estimated from a burial flux of phosphorus into the sediments in the steady state of the model.

1.3.8. Biological productivity and burial of organic carbon

Export production (F_{po}) is expressed as a function of phosphate concentration in the surface ocean ($[PO_4]_s$ in mol/L) as follows:

$$F_{po} = R_{cp} \cdot [PO_4]_S \cdot \frac{[PO_4]_S}{[PO_4]_S + \gamma_p} ,$$

where R_{cp} is a carbon to phosphorus ratio of organic matter, and γ_p is the half saturation constant. The net primary production (F_{pp}) and burial rate of organic carbon (F_{bo}) are evaluated from export production, assuming that they are proportional to the export production as follows:

$$F_{pp} = \frac{1}{f} \cdot F_{po} ,$$

$$F_{bo} = \alpha \cdot F_{po} = \beta \cdot F_{pp} ,$$

$$\beta = \alpha \cdot f ,$$

where a parameter f is the fraction of organic matter exported from the surface ocean to the deep ocean to the net primary production, and α represents burial efficiency of organic matter into sediments.

The net primary production (F_{pp}) is taken to be a sum of oxygenic and anoxygenic photosynthesis (F_{oph} and F_{red}, respectively) as follows:

$$F_{pp} = F_{oph} + F_{red} .$$

According to the previous redox balance model (Goldblatt et al., 2006), I consider that productivity due to anoxygenic photosynthesis may have been dominated by iron-oxidizing phototrophic bacteria which is controlled by a supply of ferrous iron, as it works as an electron donor for anoxygenic photosynthesis ($Fe^{2+} + CO_2 + 11H_2O + h\nu \rightarrow 4Fe(OH)_3 + CH_2O + 8H^+$). The flux of ferrous iron in the ocean is given by the net input flux of reductant from the mantle.

Based on the estimates of the net primary productivity and organic carbon burial rates today (Goldblatt et al., 2006), we can evaluate $\beta \sim 0.003$. Observations of the modern oceans (Eppley and Peterson, 1979) suggest that global f value is ~0.2. Thus, α would be on the order of ~0.01 in the present-day oceans. However, these values in the Proterozoic oceans are highly uncertain. In this study, I assume a fixed value of β, for simplicity, and perform a sensitivity study by varying values of f and α (see Section 1.5.3). For R_{cp}, I simply assume it to be the same as that of the Redfield ratio at present. The half saturation constant γ_p is determined so as to reproduce the observations of biological productivity and phosphate concentration in the present-day oceans (Paytan and McLaughlin, 2007).

1.3.9. Decomposition of organic carbon

Proportions of organic matter decomposed in the surface and deep oceans are expressed as follows:

Surface ocean: $(1 - f)\, F_{pp}$,

Deep ocean: $(1 - \alpha)\, F_{po}$.

Decomposition is assumed to occur owing to aerobic respiration and/or methanogenesis, depending on oxygen concentration in the oceans (Goldblatt et al., 2006). Fractions of organic matter decomposed by aerobic respiration ($CH_2O + O_2 \rightarrow H_2O + CO_2$) in the surface and deep oceans are expressed as follows:

Surface ocean: $\gamma_{(O_2)S} \cdot (1 - f) F_{pp}$,

Deep ocean: $\gamma_{(O_2)D} \cdot (1 - \alpha) F_{po}$.

The terms $\gamma_{(O2)S}$ and $\gamma_{(O2)D}$ are the fractions for the surface and deep oceans, respectively, which are expressed as a function of dissolved oxygen concentration in the surface ocean and deep ocean as follows:

$$\gamma_{(O_2)S} = \frac{\mathbf{O}_{AS}}{\mathbf{O}_{AS} + d_\gamma} = \frac{[O_2]_S}{[O_2]_S + d_\gamma^{'}} ,$$

$$\gamma_{(O_2)D} = \frac{[O_2]_D}{[O_2]_D + d_\gamma^{'}} ,$$

where d_γ = 1.36 × 10^{19} mol and $d_\gamma^{'}$ = 3.81 × 10^{-4} mol/L. These constants are determined so that the model may reproduce the relationship between the oxygen level and fraction of organic matter decomposed by aerobic respiration, or methanogenesis (Goldblatt et al., 2006).

1.3.10. Productions and consumptions of methane, oxygen, and inorganic carbon

Methane production rates in the surface and deep oceans by organic matter decomposition ($2CH_2O \rightarrow CH_4 + CO_2$) are expressed as follows:

$$\text{Surface ocean: } \frac{1}{2}\left(1-\gamma_{(O_2)S}\right)\cdot\left(1-f\right)F_{pp},$$

$$\text{Deep ocean: } \frac{1}{2}\left(1-\gamma_{(O_2)D}\right)\cdot\left(1-\alpha\right)F_{po}.$$

Methane consumption rates in the surface and deep oceans due to oxidization by methanotrophs ($CH_4 + 2O_2 \rightarrow 2H_2O + CO_2$), which corresponds to CO_2 generation rates, are also calculated as a function of oxygen availability as follows:

$$\text{Surface ocean: } \frac{1}{2}\delta_{(O_2)S}\left(1-\gamma_{(O_2)S}\right)\cdot\left(1-f\right)F_{pp},$$

$$\text{Deep ocean: } \frac{1}{2}\delta_{(O_2)D}\left(1-\gamma_{(O_2)D}\right)\cdot\left(1-\alpha\right)F_{po}.$$

The terms $\delta_{(O2)S}$ and $\delta_{(O2)D}$ are expressed as functions of dissolved oxygen concentrations in thesurface ocean and deep ocean as follows:

$$\delta_{(O_2)S} = \frac{\mathbf{O}_{AS}}{\mathbf{O}_{AS}+d_\delta} = \frac{[\mathrm{O}_2]_S}{[\mathrm{O}_2]_S+d_\delta'},$$

$$\delta_{(O_2)D} = \frac{[O_2]_D}{[O_2]_D + d_\delta^{'}},$$

where d_δ = 2.73 × 10^{17} mol and $d_\delta^{'}$ = 7.64 × 10^{-6} mol/L. These constants are determined so that the model may reproduce the relationship between the oxygen levels and fraction of CH_4 consumed by methanotrophs (Goldblatt et al., 2006).

The net production rates of CH_4 through organic matter decomposition in the surface and deep oceans are expressed as follows (Goldblatt et al., 2006):

$$F_{dgS\_M} = \frac{1}{2}\Phi_{(O_2)S}(1-f)F_{npp},$$

$$F_{dgD\_M} = \frac{1}{2}\Phi_{(O_2)D}(1-\alpha)F_{po},$$

where $\Phi_{(O2)S}$ and $\Phi_{(O2)D}$ are functions of oxygen (Goldblatt et al., 2006):

$$\Phi_{(O_2)S} = \left(1-\gamma_{(O_2)S}\right)\cdot\left(1-\delta_{(O_2)S}\right).$$

$$\Phi_{(O_2)D} = \left(1-\gamma_{(O_2)D}\right)\cdot\left(1-\delta_{(O_2)D}\right).$$

The net production rate (F_{po_O}) of O_2, which corresponds to the export production from the surface oceans, and net consumption rate (F_{dgD_O}) of O_2 through organic matter decomposition in the deep ocean are expressed as follows:

$$F_{po\_O} = F_{pp} - \left(1 - \Phi_{(O_2)S}\right)(1-f)F_{pp} \,,$$

$$F_{dgD\_O} = \left(1 - \Phi_{(O_2)D}\right)(1-\alpha)F_{po} \,.$$

The net removal rate of inorganic carbon from the surface ocean due to the export production (F_{po_C}) and net production rate of CO_2 due to organic matter decomposition in the deep ocean (F_{dgD_C}) are expressed as follows:

$$F_{po\_C} = F_{pp} + \left\{\gamma_{(O_2)S} + \frac{1}{2}\cdot\left(1+\delta_{(O_2)S}\right)\left(1-\gamma_{(O_2)S}\right)\right\}\left(1-f\right)F_{pp} \,,$$

$$F_{dgD\_C} = \left\{\gamma_{(O_2)D} + \frac{1}{2}\cdot\left(1+\delta_{(O_2)D}\right)\left(1-\gamma_{(O_2)D}\right)\right\}\left(1-\alpha\right)F_{po} \,.$$

1.3.11. Oxidative weathering of the continents

In this model, organic carbon exposed on the continents is decomposed due to oxidative weathering which pruduces CO_2 and CH_4 (Goldblatt et al., 2006). Thus, the net consumption rates of O_2, as well as production rates of CO_2 and CH_4, through oxidative weathering are also expressed as a function of atmospheric O_2 concentration as follows (Goldblatt et al., 2006):

$$F_{wo\_C} = \left\{\gamma_{(O_2)S} + \frac{1}{2}\cdot\left(1+\delta_{(O_2)S}\right)\left(1-\gamma_{(O_2)S}\right)\right\}F_{wo} \,,$$

$$F_{wo\_M} = \frac{1}{2}\Phi_{(O_2)S}F_{wo} \,,$$

$$F_{wo\_O} = \left(1 - \Phi_{(O_2)S}\right)F_{wo} \,.$$

1.3.12. Carbonate precipitation and dissolution

Carbonate precipitation and dissolution rates, expressed as F_{pc} and F_{dc}, respectively, are estimated from the degree of saturation with respect to calcite (Ω_{cal}). In the present oceans, carbonate precipitation by non-biological processes does not occur despite the surface seawater is generally oversaturated with respect to calcite (Millero, 2007). In this study, we set the solubility product K_{sp} as a product of the Ca^{2+} and CO_3^{2-} concentrations ($[Ca^{2+}]^*$ and $[CO_3^{2-}]^*$, respectively) in the surface water of the oceans today, assuming that calcite can be precipitated from the surface water when $[Ca^{2+}][CO_3^{2-}]$ becomes larger than K_{sp}.

$$\Omega_{cal} = \frac{[Ca^{2+}][CO_3^{2-}]}{K_{sp}},$$

$$K_{sp} = [Ca^{2+}]^*[CO_3^{2-}]^*.$$

The calcite precipitation rate (F_{pc}) is calculated in order to satisfy the following equations.

$$\begin{cases} K_{sp} = \left([Ca^{2+}]_s - \Delta t \cdot F_{pc}\right)\left([CO_3^{2-}]_s - \Delta t \cdot F_{pc}\right) & \left(\Omega_{cal} \geq 1\right) \\ F_{pc} = 0 & \left(\Omega_{cal} < 1\right) \end{cases}$$

Calcite precipitates if the degree of saturation exceeds unity ($\Omega_{cal} > 1$), in a manner that the degree of saturation maintains $\Omega_{cal} = 1$ in the oceans in each time step. If $\Omega_{cal} < 1$, calcite precipitation does not occur.

Calcite particles produced in the surface ocean settle down into the deep ocean, and they dissolve there depending on the degree of saturation. The calcite dissolution rate (F_{dc}) is obtained in order to satisfy the equations described below: calcite particles dissolve if the deep ocean is undersaturated with respect to calcite ($\Omega_{cal} < 1$), while, if the deep ocean is supersaturated with respect to calcite ($\Omega_{cal} > 1$), calcite dissolution does not occur ($F_{dc} = 0$).

$$\begin{cases} F_{dc} = 0 & \left(\Omega_{cal} \geq 1\right) \\ K_{sp} = \left([\mathrm{Ca}^{2+}]_d + \Delta t \cdot F_{dc}\right)\left([\mathrm{CO}_3^{2-}]_d + \Delta t \cdot F_{dc}\right) & \left(\Omega_{cal} < 1\right) \end{cases}$$

All of the equations used for mass balance calculation and flux evaluations are summarised in tables below (Tables 1.1-1.4) .

1.3.13. Redox balance calculation

I calculate atmospheric levels of O_2 and CH_4 through the mass balance between the input and output of both oxidants and reductants, based on a redox balance model of Goldblatt et al. (2006). The model includes O_2 and CH_4 production from biosphere, hydrogen escape from the atmosphere to space, oxidative weathering of the continents, reductant inputs from Earth's interior, and photochemical methane oxidation in the atmosphere. The rate of hydrogen escape is limited by diffusion, which is assumed to be proportional to the atmospheric CH_4 concentration. The steady states of O_2 are achieved when the hydrogen escape balances the net reductant input from the Earth's interior. The model results show a bistability (i.e., two steady state solutions) of O_2 levels for given net primary production and net reductant input owing to the non-linear dependency of the methane oxidation rate to the atmospheric oxygen levels derived from the results of photochemical models (Goldblatt et al., 2006). Goldblatt et al. (2006) suggests that the atmosphere-ocean system would have

been in the bistable region in the Paleoproterozoic, based on estimates of the Paleoproterozoic net reductant intput rate and net primary productivity. In this study, I adopt this assumption, and start calculations from the low hysteresis branch of O_2 in the bistable region.

Table 1.1 *Mass balance Equations, and their symbols and descriptions.*

Symbol	Description	Mass balance equation (mol/yr)
$\mathbf{C}_{AS}$	Inorganic carbon in the atmosphere and surface ocean	$\frac{d\mathbf{C}_{AS}}{dt} = F_{vc} + F_{wo\_C} + F_{esc\_H} + F_{oxi\_M} + F_{wc} - F_{pc} - F_{po\_C} + F_{cir\_C}$
$\mathbf{C}_{D}$	Inorganic carbon in the deep ocean	$\frac{d\mathbf{C}_{D}}{dt} = F_{dc} + F_{dgD\_C} - F_{cir\_C}$
$\mathbf{O}_{AS}$	Oxygen (O_2) in the atmosphere and surface ocean	$\frac{d\mathbf{O}_{AS}}{dt} = F_{po\_O} - F_{wo\_O} - F_{oxi\_O} - F_{esc\_H} + F_{cir\_O}$
$\mathbf{O}_{D}$	O_2 in the deep ocean	$\frac{d\mathbf{O}_{D}}{dt} = -F_{cir\_O} - F_{dgD\_O}$
$\mathbf{M}_{AS}$	Methane (CH_4) in the atmosphere and surface ocean	$\frac{d\mathbf{M}_{AS}}{dt} = F_{dgS\_M} + F_{dgD\_M} + F_{wo\_M} - F_{oxi\_M} - F_{esc\_H}$
$\mathbf{Ca}_{S}$	Calcium ions (Ca^{2+}) in the surface ocean	$\frac{d\mathbf{Ca}_{S}}{dt} = F_{wc} + F_{ws} - F_{pc} + F_{cir\_Ca}$
$\mathbf{Ca}_{D}$	Calcium ions in the deep ocean	$\frac{d\mathbf{Ca}_{D}}{dt} = F_{dc} - F_{cir\_Ca}$
$\mathbf{P}_{S}$	Phosphorus ions (PO_4^{3-}) in the surface ocean	$\frac{d\mathbf{P}_{S}}{dt} = F_{rp} - F_{po\_P} + F_{cir\_P}$
$\mathbf{P}_{D}$	Phosphorus ions in the deep ocean	$\frac{d\mathbf{P}_{D}}{dt} = F_{dgD\_P} - F_{cir\_P}$
$\mathbf{Alk}_{S}$	Alkalinity in the surface ocean	$\frac{d\mathbf{Alk}_{S}}{dt} = 2 \times \left(F_{wc} + F_{ws} - F_{pc} + F_{cir\_Ca} \right)$
$\mathbf{Alk}_{D}$	Alkalinity in the deep ocean	$\frac{d\mathbf{Alk}_{D}}{dt} = 2 \times \left(F_{dc} - F_{cir\_Ca} \right)$

Table 1.2. *Symbols that are used to express fluxes between the boxes*.

Symbol	Description
F_{vc}	volcanic degasing flux of CO_2
F_{red}	reductant (Fe^{2+}) input (= anoxygenic photosynthesis rate)
F_{wc}	weathering of carbonate rocks
F_{ws}	weathering of silicate rocks
F_{rp}	phosphorus river input
F_{wo}	amount organic carbon expose on land
F_{wo_M}	CH_4 produced by weathering of terrestrial organic matter
F_{wo_C}	CO_2 produced by weathering of terrestrial organic matter
F_{wo_O}	O_2 consumed by weathering of terrestrial organic matter
F_{pp}	net primary production
F_{po_P}	phosphorus uptake by export production
F_{po}	export production
F_{oph}	oxygenic photosynthesis
F_{dgS_M}	CH_4 production by decomposition of particulate organic matter in the surface water
F_{dgD_M}	CH_4 production by decomposition of particulate organic matter in the deep water
F_{dgS_C}	CO_2 production by decomposition of particulate organic matter in the surface water
F_{po_C}	net removal rate of inorganic carbon from the surface ocean due to the export production
F_{dgD_C}	CO_2 production by decomposition of particulate organic matter in the deep water
F_{dgS_O}	O_2 consumption by decomposition of particulate organic matter in the surface water
F_{po_O}	net production rate of O_2 by export production
F_{dgD_O}	O_2 consumption by decomposition of particulate organic matter in the deep water
F_{dgD_P}	phosphorus recycling in the deep ocean
F_{bo}	burial of organic carbon
F_{pc}	precipitation of carbonate carbon
F_{dc}	dissolution of carbonate carbon
F_{ds_X}	upwelling of dissolved component $\mathbf{X_D}$ **(X = C, O, Ca, P, Alk)**
F_{sd_X}	down welling of dissolved component $\mathbf{X_S}$ **(X = C, O, Ca, P, Alk)**
F_{cir_X}	net supply of net supply of dissolved component **X** to the surface ocean due to upwelling,
F_{oxi_M}	CH_4 consumption by photochemical oxidation of CH_4

Table 1.3 *Equations and parameters used to express fluxes between the boxes*

Symbol	unit	Description	Equation / parameter	Ref.
F_{vc}	mol/yr	volcanic degasing flux of CO_2	6.65×10^{12} (const.)	this study
F_{red}	mol/yr	reductant (Fe^{2+}) input (= anoxygenic photosynthesis rate)	0.3×10^{12} (const.)	(Goldblatt et al., 2006)
F_{wc}	mol/yr	weathering of carbonate rocks	$F_{wc} = f_a \cdot f_e \cdot f_b \cdot F_{wc}^*$	this study
F_{ws}	mol/yr	weathering of silicate rocks	$F_{ws} = f_a \cdot f_e \cdot f_b \cdot F_{ws}^*$	this study
F_{rp}	mol/yr	phosphorus river input	$F_{rp} = \frac{F_{ws} + F_{wc}}{F_{ws}^* + F_{wc}^*} F_{rp}^*$	this study
F_{wo}	mol/yr	amount organic carbon expose on land	10×10^{12} (const.)	this study
F_{wo_M}	mol/yr	CH_4 produced by weathering of terrestrial organic matter	$F_{wo\_M} = \frac{1}{2}\Phi_{(O_2)S} F_{wo}$	(Goldblatt et al., 2006)
F_{wo_C}	mol/yr	CO_2 produced by weathering of terrestrial organic matter	$F_{wo\_C} = \left\{\gamma_{(O_2)S} + \frac{1}{2}\cdot(1+\delta_S)(1-\gamma_S)\right\} F_{wo}$	(Goldblatt et al., 2006)
F_{wo_O}	mol/yr	O_2 consumed by weathering of terrestrial organic matter	$F_{wo\_O} = \left(1-\Phi_{(O_2)S}\right) F_{wo}$	(Goldblatt et al., 2006)
F_{pp}	mol/yr	net primary production	$F_{pp} = \frac{F_{po}}{f}$	this study
F_{po_P}	mol/yr	phosphorus uptake by export production	$F_{po\_P} = \frac{F_{po}}{R_{cp}}$	this study
F_{po}	mol/yr	export production	$F_{po} = R_{cp} \cdot [PO_4]_S \cdot \frac{[PO_4]_S}{[PO_4]_S + \gamma_p}$	(Yamanaka and Tajika, 1996)
F_{oph}	mol/yr	oxygenic photosynthesis	$F_{oph} = F_{pp} - F_{red}$	
F_{dgS_M}	mol/yr	CH_4 production by decomposition of particulate organic matter in the surface water	$F_{dgS\_M} = \frac{1}{2}\Phi_{(O_2)S}(1-f)F_{pp}$	(Goldblatt et al., 2006)
F_{dgD_M}	mol/yr	CH_4 production by decomposition of particulate organic matter in the deep water	$F_{dgD\_M} = \frac{1}{2}\Phi_{(O_2)D}(1-\alpha)F_{po}$	(Goldblatt et al., 2006), this study
F_{dgS_C}	mol/yr	CO_2 production by decomposition of particulate organic matter in the surface water	$F_{dgS\_C} = \left\{\gamma_{(O_2)S} + \frac{1}{2}\cdot(1+\delta_S)(1-\gamma_S)\right\}(1-f)F_{pp}$	(Goldblatt et al., 2006)
F_{po_C}	mol/yr	net removal rate of inorganic carbon from the surface ocean due to the export production	$F_{po\_C} = F_{pp} - \left\{\gamma_{(O_2)S} + \frac{1}{2}\cdot(1+\delta_{(O_2)S})(1-\gamma_{(O_2)S})\right\}(1-f)F_{pp}$	this study

Table 1.3 *(continued)*

Symbol	unit	Description	Equation / parameter	Ref.
F_{dgD_C}	mol/yr	CO_2 production by decomposition of particulate organic matter in the deep water	$F_{dgD\_C} = \left\{\gamma_{(O_2)D} + \frac{1}{2}\cdot(1+\delta_D)(1-\gamma_D)\right\}(1-\alpha)F_{po}$	(Goldblatt et al., 2006), this study
F_{dgS_O}	mol/yr	O_2 consumption by decomposition of particulate organic matter in the surface water	$F_{dgS\_O} = (1-\Phi_{(O_2)S})(1-f)F_{pp}$	(Goldblatt et al., 2006)
F_{po_O}	mol/yr	net production rate of O_2 by export production	$F_{po\_O} = F_{oph} - (1-\Phi_{(O_2)S})(1-f)F_{pp}$	this study
F_{dgD_O}	mol/yr	O_2 consumption by decomposition of particulate organic matter in the deep water	$F_{dgD\_O} = (1-\Phi_{(O_2)D})(1-\alpha)F_{po}$	(Goldblatt et al., 2006), this study
F_{dgD_P}	mol/yr	phosphorus recycling in the deep ocean	$F_{dgD\_P} = \frac{1}{R_{cp}}(1-\alpha)F_{po}$	this study
F_{bo}	mol/yr	burial of organic carbon	$F_{bo} = \alpha\cdot f\cdot F_{pp}$	this study
F_{pc}	mol/yr	precipitation of carbonate carbon	$\begin{cases} K_{sp} = ([Ca^{2+}]_s - \Delta t\cdot F_{pc})([CO_3^{2-}]_s - \Delta t\cdot F_{pc}) & (\Omega_{cal}\geq 1) \\ F_{pc} = 0 & (\Omega_{cal}<1) \end{cases}$	this study
F_{dc}	mol/yr	dissolution of carbonate carbon	$\begin{cases} F_{dc} = 0 & (\Omega_{cal}\geq 1) \\ K_{sp} = ([Ca^{2+}]_D + \Delta t\cdot F_{dc})([CO_3^{2-}]_D + \Delta t\cdot F_{dc}) & (\Omega_{cal}<1) \end{cases}$	this study
F_{ds_X}	mol/yr	upwelling of dissolved component $\mathbf{X_D}$ **X** = **C**, **O**, **Ca**, **P**, **Alk**	$F_{ds\_X} = [X]_D\cdot W,\quad [X]_D = \frac{\mathbf{X}_D}{V_D}$	this study
F_{sd_X}	mol/yr	down welling of dissolved component $\mathbf{X_S}$ **X** = **C**, **O**, **Ca**, **P**, **Alk**	$F_{sd\_X} = [X]_S\cdot W,\quad [X]_S = \frac{\mathbf{X}_S}{V_S}$	this study
F_{cir_X}	mol/yr	net supply of net supply of dissolved component **X** to the surface ocean due to upwelling,	$F_{cir\_X} = F_{ds\_X} - F_{sd\_X}$	this study
F_{oxi_M}	mol/yr	CH_4 consumption by photochemical oxidation of CH_4	$F_{oxi\_M} = \frac{1}{2}\mathbf{M}^{0.7}\cdot\Psi_{(O_2)S}$	this study

Table 1.3 *(continued)*

Symbol	unit	Description	Equation / parameter	Ref.
F_{oxi_O}	mol/yr	O_2 consumption by photochemical oxidation of CH_4	$F_{oxi\_O} = \mathbf{M}^{0.7} \cdot \Psi_{(O_2)S}$	(Goldblatt et al., 2006)
F_{esc_H}	mol/yr	hydrogen escape	$F_{esc\_H} = s\mathbf{M}$	(Goldblatt et al., 2006)
f_b		kinetic control on weathering	$f_b = \left(\frac{p\mathrm{CO}_2}{p\mathrm{CO}_2^*}\right)^n \cdot \frac{\exp\left(-\frac{E}{RT}\right)}{\exp\left(-\frac{E}{RT^*}\right)}$	(Tajika, 2003)
$\gamma_{(O2)S}$		fraction of organic matter decomposed by aerobic respiration in atmosphere and surface water	$\gamma_{(O_2)S} = \frac{\mathbf{O}_{AS}}{\mathbf{O}_{AS} + d_\gamma} = \frac{[\mathrm{O}_2]_S}{[\mathrm{O}_2]_S + d_\gamma'}$	(Goldblatt et al., 2006)
$\gamma_{(O2)D}$		fraction of organic matter decomposed by aerobic respiration in deep water	$\gamma_{(O_2)D} = \frac{[\mathrm{O}_2]_D}{[\mathrm{O}_2]_D + d_\gamma'}$	this study
$\delta_{(O2)S}$		fraction of methane decomposed by methanoreoph in atmosphere and surface water	$\delta_{(O_2)S} = \frac{\mathbf{O}_{AS}}{\mathbf{O}_{AS} + d_\delta} = \frac{[\mathrm{O}_2]_S}{[\mathrm{O}_2]_S + d_\delta'}$	(Goldblatt et al., 2006)
$\delta_{(O2)D}$		fraction of methane decomposed by methanoreoph in atmosphere and deep water	$\delta_{(O_2)D} = \frac{[\mathrm{O}_2]_D}{[\mathrm{O}_2]_D + d_\delta'}$	this study
$\Phi_{(O2)S}$		fraction of organic matter anaerobically decomposed in atmosphere and surface ocean	$\Phi_{(O_2)S} = \left(1 - \gamma_{(O_2)S}\right) \cdot \left(1 - \delta_{(O_2)S}\right)$	(Goldblatt et al., 2006)
$\Phi_{(O2)D}$		fraction of organic matter anaerobically decomposed in atmosphere and deep ocean	$\Phi_{(O_2)D} = \left(1 - \gamma_{(O_2)D}\right) \cdot \left(1 - \delta_{(O_2)D}\right)$	(Goldblatt et al., 2006)
W_{cal}		degree of saturation of calcite	$W_{cal} = [Ca^{2+}][CO_3^{2-}] / K_{sp}$	this study
$\Psi_{(O2)}$		oxidation parameter	$10^{a_1\psi^4 + a_2\psi^3 + a_3\psi^2 + a_4\psi + a_5}, \quad \psi = \log \mathbf{O}_{AS}$	(Goldblatt et al., 2006)
T_k	K	global surface temperatures	$T_k = T_k^{S_t/S_0=1.0} - \left(T_k^{S_t/S_0=1.0} - T_k^{S_t/S_0=0.7}\right) \frac{1.0 - S_t/S_0}{1.0 - 0.7}$	this study
$T_k^{St/S0=1.0}$	K	global surface temperatures (S_t/S_0 = 1.0)	$T_k^{S_t/S_0=1.0}\left(p\mathrm{CO}_2\right) = 111.56 \cdot p\mathrm{CO}_2^{0.163} + 255.0$	(Kasting and Ackerman, 1986), this study
$T_k^{St/S0=0.7}$	K	bal surface temperatures (S_t/S_0 = 1.0)	$T_k^{S_t/S_0=0.7}\left(p\mathrm{CO}_2\right) = 61.98 \cdot p\mathrm{CO}_2^{0.294} + 235.0$	(Kasting and Ackerman, 1986), this study

Table 1.4 *Constants used in the model, and their symbols and descriptions.*

Symbol	unit	Description	Value	Ref.
f_a		relative continental area	0.4-0.8	(Hawkesworth and Kemp, 2006), (Hawkesworth et al., 2010)
f_e		relative soil biological activity	0.1-0.25	(Moulton et al., 2000)
F_{ws}^*	mol/yr	silicate weathering rate in the present	6.65×10^{12}	(Berner, 1991)
F_{wc}^*	mol/yr	carbonate weathering rate in the present	13.35×10^{12}	(Berner, 1991)
F_{rp}^*	mol/yr	present riverine input	0.09×10^{12}	this study
f		fraction of export production	0.0027-0.25	this study
γ_P	mol/L	half saturation constant for the export production	10^{-6}	this study
a		burial efficiency	1-0.01	this study
s	s^{-1}	scale constant for hydrogen escape	§2.03×10^{-5}	(Goldblatt et al., 2006)
pCO_2^*	atm	present pCO_2	3.15×10^{-4}	this study
T^*	K	present global temperature	285	this study
E	kcal mol^{-1}	activation energy	15	(Tajika, 2003)
R	kcal $K^{-1}mol^{-1}$	gas constant	1.99×10^{-3}	this study
n		exponent of pCO_2 dependency of weathering	0.3	(Tajika, 2003), (Berner, 1994), (Walker et al., 1981)
d_r	mol	half saturation constant for aerobic respiration	1.36×10^{19}	(Goldblatt et al., 2006)
d_{meop}	mol	half saturation constant for methanotroph	2.73×10^{17}	(Goldblatt et al., 2006)
d_r'	mol/L	half saturation constant for aerobic respiration	8.29×10^{-5}	this study
d_x'	mol/L	half saturation constant for methanotroph	1.66×10^{-6}	this study
W	L/yr	ocean circulation rate	5.99×10^{17}	(Hotinski et al., 2000)
V_S	L	volume of the surace ocean	0.05×10^{21}	this study
V_D	L	volume of the deep ocean	1.37×10^{21}	this study
K_{sp}	mol^2L^{-2}	solubility product of calcite	$10^{-5.902}$	this study
S_t/S_0		relative solar constant	0.83 (2.2 Ga)	(Gough, 1981)
R_{cp}		C/P ratio in the organic matter	106	this study
a_1		constant for methane oxidation parameter	§0.003006	(Goldblatt et al., 2006)
a_2		constant for methane oxidation parameter	§-0.1655	(Goldblatt et al., 2006)
a_3		constant for methane oxidation parameter	§3.2305	(Goldblatt et al., 2006)
a_4		constant for methane oxidation parameter	§-25.8343	(Goldblatt et al., 2006)
a_5		constant for methane oxidation parameter	§71.5398	(Goldblatt et al., 2006)

§ The values are corrected after the publication of Goldblatt et al. (2006). The corrected values are: to $s = 3.7 \times 10^{-5}$, $a_1 = 0.0030084$, $a_2 = -0.1655405$, $a_3 = 3.2305351$, $a_4 = -25.8343054$, and $a_5 = 71.5397861$. This will not affect conclusions significantly.

1.3.14. Initial and boundary conditions

Initial conditions: Calculations are started from a low branch of stable steady state of atmospheric oxygen (i.e., ~10^{-6} PAL) (Goldblatt et al., 2006). The initial amounts of dissolved O_2 in the oceans are given by assuming equilibrium between the atmosphere and ocean. Concentrations of dissolved species/ions and alkalinity in the post-snowball ocean are highly uncertain. Concerning initial DIC and Ca^{2+} concentrations and alkalinity, I set their values as same as those of the present-day levels for simplicity.

Sensitivity study is performed by varying initial atmospheric CO_2 and initial oceanic PO_4, because these factors might affect the results significantly. As for the initial PO_4 concentration in the nominal case, I consider the value of ~1.5×10^{-6} mol/L, which is the steady-state level for given boundary conditions (see below) and close to the value of the present-day ocean (Paytan and McLaughlin, 2007). I also vary the initial PO_4 concentration up to 100 times the present-day value. I consider 0.7 atm of an initial partial pressure of atmospheric CO_2 as the nominal case, because this level of CO_2 is required to escape from a snowball glaciation for the solar luminosity in the Paleoproterozoic (Tajika, 2003). To investigate the sensitivity of initial CO_2, I perform calculations for initial CO_2 of 0.086 and 0.3 atm in addition to the nominal case.

Boundary conditions: The rates of CO_2 degassing, reductant input, oxidative weathering of organic carbon, and ocean circulation rate are fixed to constant values. On the other hand, I vary the relative weathering efficiency (f_w) and the fraction of export production to the net primary production (f), given large uncertainties in these parameters in the Paleoproterozoic oceans. I consider $f_w = 0.09$ for the nominal case and change f_w from 0.05 to 0.2 given a possible range of f_w in the Paleoproterozoic. The present study also considers $f = 0.027$ for the nominal case, because this value can reproduce the phosphorus concentration in the present-day ocean. The value for f is varied from 0.25 to 0.0027 in a sensitivity study.

1.4. Results

1.4.1. Rise of oxygen in the aftermath of snowball Earth

Figure 1.2 shows the evolution of surface environments after the snowball glaciation. Based on characteristic processes and timescales, I divide a series of environmental changes into two stages (Fig. 1.2).

Stage I (<~10^5 years after the termination of the snowball glaciation) is characterized by the intense chemical weathering of continents, nutrient (PO_4) enrichment in the oceans and a transition between oxygen steady-state levels. During this stage, carbonate precipitation is temporarily inhibited because the oceans are highly undersaturated with respect to carbonate, owing to high levels of atmospheric CO_2 accumulated during the glaciation (Fig. 1.2d). The high levels of atmospheric CO_2 and high surface temperatures are prolonged over ~10^5 years (≥0.3 atm and ≥300 K, respectively) (Fig. 1.2a). Under transient super-greenhouse conditions, chemical weathering of the continents proceeds rapidly (Fig. 1.2b), and extremely high levels of the riverine input fluxes result in oceans to be highly enriched in phosphate (5–10 times that of the present-day level) at 10^4–10^6 years after the glaciation (Fig. 1.2c).

In response to the nutrient enrichments, primary production is enhanced in the oceans (Fig. 1.2d). As a consequence of elevated primary production followed by an elevated rate of organic carbon burial, the atmospheric O_2 level exceeds ~10^{-5} PAL (Fig. 1.2e). This level is proposed as the threshold for triggering a positive feedback loop with regards to O_2, that is, when the atmospheric O_2 level reaches this level, an ozone layer forms to decrease the oxidizing efficiency of CH_4, in the atmosphere, leading to further increase in O_2 levels (Claire et al., 2006; Goldblatt et al., 2006). Once the positive feedback is initiated, atmospheric O_2 rapidly increases, jumping to a higher steady-state branch irreversibly (Fig. 1.3).

Stage II (10^5–10^8 years after glaciation) is marked by the deposition of cap carbonate, climate stabilization, and oxygen overshoot. As a result of a supply of cations from continental weathering over ~10^5 years, the oceans become saturated

with respect to calcium carbonate (Fig. 1.2d). The timing of carbonate precipitation depends on weathering efficiency. However, regardless of such uncertainties, the carbonate precipitation always occurs after the O_2 transition (Fig.1.2). After the carbonate precipitation (10^5–10^6 years), the atmospheric CO_2 levels and surface temperatures reach steady states (Fig. 1.2a and 1.2b). As a consequence of stabilization of climate, phosphate concentrations and organic carbon burial rate in the ocean also reach steady states in ~10^6 years (Fig. 1.2c and 1.2d).

However, even under stable conditions in climate and carbon cycles, atmospheric O_2 does not reach a final equilibrium but overshoots to ~1 PAL over a period of 10^6–10^8 years after the snowball glaciation (Fig. 1.2e). The accumulation of O_2 in the atmosphere is caused by the excess of net organic carbon reservoir change relative to reductant inputs during the first 10^6 years after the glaciation (Figs. 1.2d and 1.2f). This means that the O_2 levels during the period are not equilibrated and increase unidirectionally. Under highly oxygenated conditions during the overshoot, methanogenesis is suppressed, leading to a decline in atmospheric CH_4 levels (Fig. 1.2e). This reduces the rate of hydrogen escape from the atmosphere to space (Fig. 1.2f), which results in a decrease in a net oxidation rate, or an increase in a net reduction rate, in the atmosphere-ocean system. Consequently, the accumulated O_2 is gradually consumed through the oxidation of excess reductants in the atmosphere-ocean system (e.g., reductants provided from Earth's interior) (Fig. 1.2e). The timescale of the overshoot is controlled by a balance between the amount of accumulated O_2 and net reduction rate. The steady-state level of ~0.01 PAL of O_2, which corresponds to a high hysteresis branch of the steady state (Goldblatt et al., 2006), is achieved ~10^8 years after the glaciation (Fig. 1.3) when the rate of hydrogen escape is balanced strictly by the net reduction rate (Fig. 1.2f).

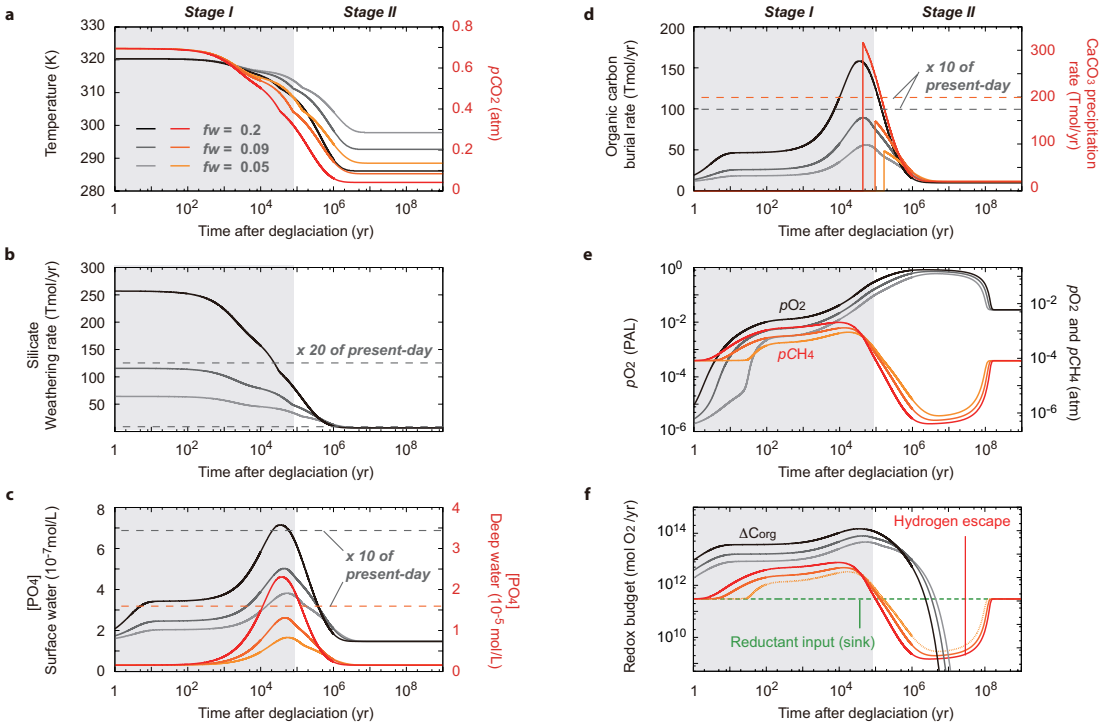

Fig.1.2 Time variations in fluxes and reservoirs after the snowball glaciation. a, Surface temperatures (black) and partial pressures of CO_2 (pCO_2; red). **b,** Weathering rates of silicate rock (black). **c,** Phosphate concentrations in the surface ocean (black) and deep ocean (red). **d,** Rates of carbonate precipitation ($CaCO_3$; red) and organic carbon burial (black). **e,** Partial pressures of atmospheric O_2 (pO_2; black) and CH_4 (pCH_4; red). **f,** Net organic carbon reservoir change, ΔC_{org} (burial rate minus weathering rate of organic carbon; black), the rate of hydrogen escape to space (red), and the input rate of reductants from the mantle (green). I assume f_w = 0.09 as the nominal case.

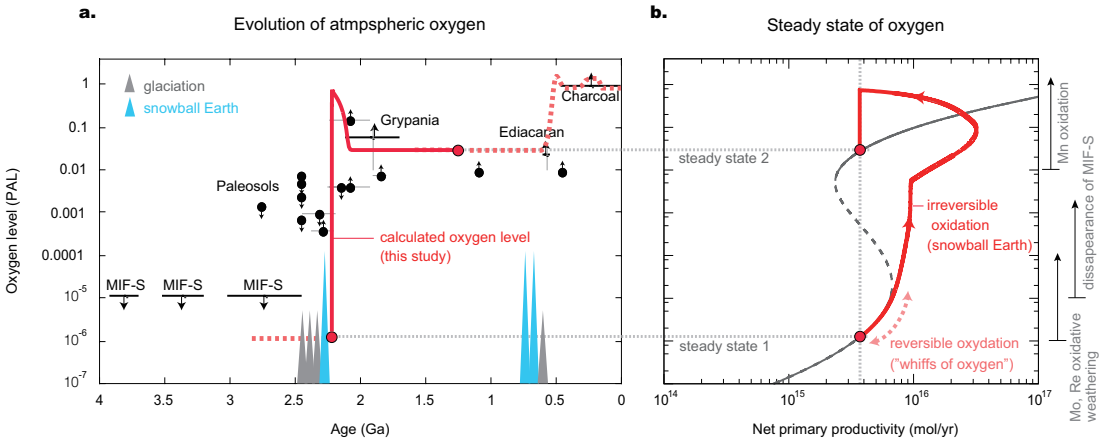

Fig.1.3 Evolution of atmospheric oxygen levels. a, Oxygen evolution for the nominal case which is shown in Fig. 1.2 (solid red line) superimposed on a compilation of geochemical evidence for paleo-oxygen levels (Goldblatt et al., 2006 and references therein) . The dashed line shows a possible evolution of oxygen levels in the Neoproterozoic. Gray dotted lines are proposed stable steady levels of oxygen. Oxygen levels constrained by proxies are also shown (Farquhar et al., 2007; Goto et al., 2013; Klemm, 2000; Pavlov and Kasting, 2002). **b,** Evolutionary track of atmospheric oxygen levels after the snowball glaciation as shown in Fig. 1.2 (red solid curve) superimposed on a bistability diagram between the atmospheric O_2 levels and net primary productivity given by Goldblatt et al. (2006). Solid and dashed gray curves show stable and unstable steady states, respectively.

1.5. Discussion

1.5.1. Interpretation of geological record

The results are in good agreement with stratigraphic evidence for surface oxygenation in the geological records. The Paleoproterozoic sedimentary rocks of the Transvaal Supergroup, South Africa, contain a low-latitude glacial diamictites (Evans et al., 1997; Kirschvink et al., 2000) which is thought to represent the Paleoproterozoic snowball glaciation (Fig. 1.4). In the Transvaal Supergroup, manganese-iron ore deposits (Hotazel Formation; Fig. 1.4) occur between the glacial diamictites (Makganyene Formation; Fig. 1.4) and postglacial cap carbonates (Mooidraai Formation; Fig. 1.4) (Kirschvink et al., 2000). These features are consistent with my results in which a rise of oxygen content in the atmosphere and surface ocean occurs before the deposition of cap carbonate (Fig. 1.2). In addition, I suggest the occurrence of an oxygen overshoot to ~1 PAL for ~10^8 years after glaciation. This may account for the global deep-water oxygenation in 2.1 Ga (Canfield et al., 2013). The O_2 overshoot would have enhanced oxidative weathering of continental sulfides (e.g., Fe_2S) and depositions of ferric iron from the surface oceans (Bekker and Holland, 2012). The oxidative weathering of sulfides might have increased the sulfate (SO_4^{2-}) reservoir in the oceans to levels sufficient for the precipitation of sulfate minerals. This may explain global sulfate depositions at 2.2–2.1 Ga, including sulfate evaporates (Lucknow Formation; Fig 1.4) found above the cap carbonate unit in the Transvaal Supergroup (Schröder et al., 2008).

Weak oxygenation of the early atmosphere and surface ocean would have pre-dated the Paleoproterozoic snowball Earth glaciation (Anbar et al., 2007; Farquhar et al., 2007; Goto et al., 2013; Kendall et al., 2010; Papineau et al., 2007). Geochemical evidence of oxidative weathering suggests an appearance of a mildly oxidizing atmosphere (10^{-8}–10^{-5} PAL) in the late Archean and early Paleoproterozoic (Anbar et al., 2007; Goto et al., 2013; Kendall et al., 2010). Such ‘whiffs’ of oxygen may be interpreted as records of probably reversible fluctuations in O_2 levels in a low hysteresis branch, due to small changes in marine primary production (Figs. 1.3b and 1.8). Previous studies have shown that a large degree of mass-independent

fractionation of sulfur isotopes (MIF-S) disappeared during repeated glaciations pre-dating the snowball Earth event (Farquhar et al., 2007; Papineau et al., 2007). However, numerical modeling has shown that the decrease in MIF-S signatures is not only associated with a rise in O_2 but also with a collapse in atmospheric CH_4 (Zahnle et al., 2006), hence, low levels of atmospheric CH_4 at the time of deposition are an alternative interpretation for the lack of MIF-S during the repeated glaciations pre-dating the snowball glaciation (Zahnle et al., 2006).

By contrast, manganese can only be oxidized by O_2 or nitric acid within marine environments (Kirschvink et al., 2000; Kopp et al., 2005), indicating that the deposition of manganese oxides within ocean settings would require large quantities of O_2 (Klemm, 2000). I suggest that the formation of manganese oxides just above the low-latitude glacial diamictites in the Transvaal Supergroup represents a distinct, irreversible O_2 transition occurred immediately after the snowball glaciation (Fig. 1.3b). Large perturbations in biogeochemical cycles induced by the snowball glaciation should be, thus far, the unique trigger for the GOT.

According to the recent biogeochemical study, the O_2 levels in the Mesoproterozoic would have been as low as 10^{-3} PAL (Planavsky et al., 2014). Although the present study considers $\sim 10^{-2}$ PAL as the high branch of the steady-state O_2 level, this value can vary depending on the model assumptions. For instance, in the model, the steady-state O_2 level is affected by the rate of CH_4 generation in the oceans through the redox balance equations. The rate of CH_4 generation is determined by the decomposition process of organic carbon in the ocean as well as the redox state of the ocean. Although sulfate reduction plays major roles in the decomposition of organic carbon in the modern ocean, it is not considered in the model. This is because there were small amount of sulfate iron in the early Paleoproterozoic oceans. Sulfate ion should have however been accumulated in the ocean on the order of 10^7 years after the snowball glaciation. As a result, this may overestimate the biogenic CH_4 flux in my model, and hence lower the steady-state O_2 level. Furthermore, I simply divide the ocean into two boxes, whereas multi-box models are usually used to represent the modern ocean [e.g., Ozaki et al, 2011; Ozaki and Tajika, 2013], in which the deep ocean box is oxidized by transport of O_2-rich

water from high-latitude ocean box. As the two-box ocean model would make the deep ocean anoxic compared with a multi-box model for the same atmospheric O_2 level, this again may overestimate the biogenic CH_4 flux and the steady-state O_2 level. In the future work, full descriptions of sulfur cycle in a multiple ocean box model would be necessary to calculate more realistic steady-state O_2 levels.

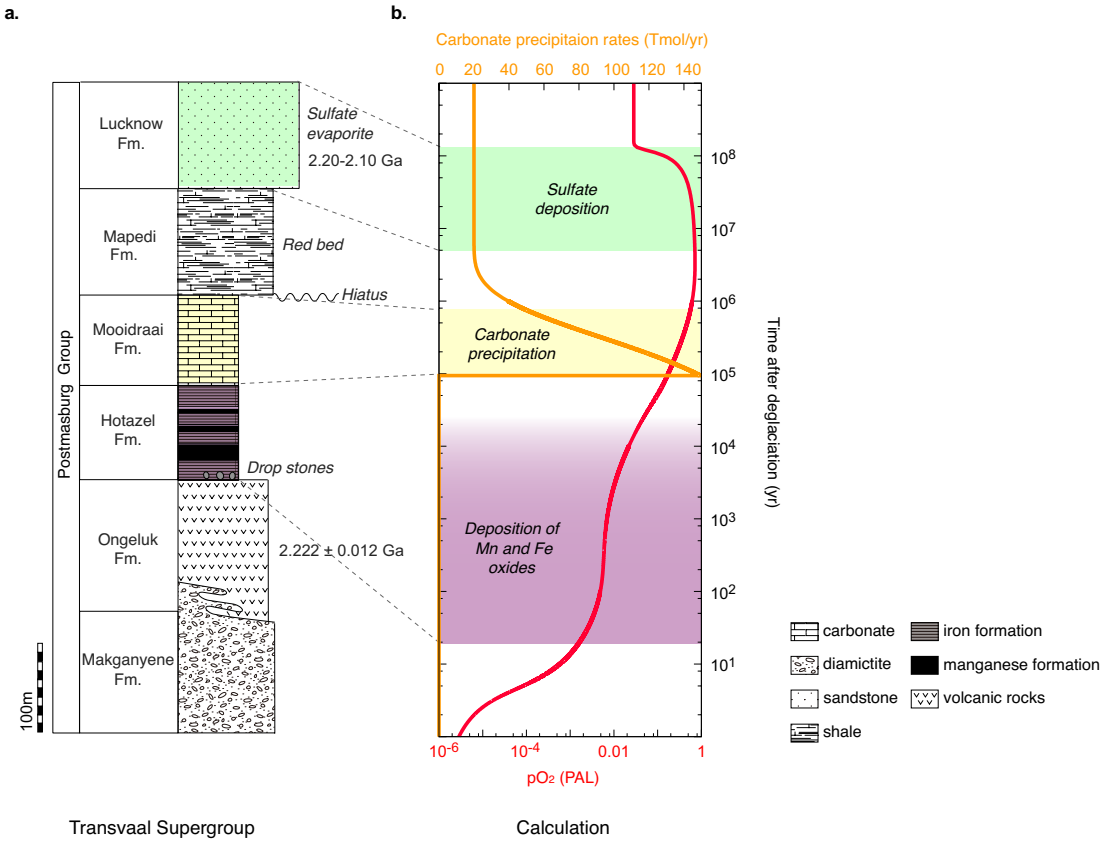

Fig.1.4 Comparison of the model results with geological records. a. Columnar section of Transvaal Supergroup, Griqualand West region of the Northern Cape Province, South Africa (Kirschvink et al., 2000; Schröder et al., 2008). The Paleoproterozoic sedimentary rocks of the Transvaal Supergroup contain a low-latitude glacial diamictite (Makganeye Fm.), manganese and iron formations (Hotazel Fm.), and carbonate (Mooidraai Fm.) (Evans et al., 1997; Kirschvink et al., 2000). Red beds and molds of sulfate evaporate in Mapedi and Lucknow Fms., respectively, are formed after the formation of carbonate (Kirschvink et al., 2000; Schröder et al., 2008). Hiatus exists between Mooidraai and Mapedi formations, and the time gap due to the hiatus would be 10^7–10^8 years or less (Schröder et al., 2008). **b.** Numerical results for the nominal case (as shown in Fig. 1.2). Atmospheric oxygen levels (red) and carbonate precipitation rates (yellow) are shown as a function of time after the glaciation. My calculations show that an increase in atmospheric oxygen level precedes the precipitation of carbonate (also see Fig. 1.2). Long-term oxygen overshoot (> 0.1 PAL over ~10^8 years) also occurs after the carbonate formation, which may result in accumulation of sulphate ions in the oceans, followed by deposition of sulphate minerals.

1.5.2. Correlation with the Lomagundi d^{13}C excursion

The Paleoproterozoic is also marked by large positive shifts of $\delta^{13}C$ value in inorganic carbon deposited between ~2.2–2.1 Ga (the "Lomagundi-Jutali event")(Karhu and Holland, 1996). One interpretation of the Lomagundi event is enhanced organic carbon burial and a rise of O_2 during this period (Karhu and Holland, 1996). I show that the snowball glaciation triggers the transition of O_2 levels due to high rates of organic carbon burial, which would possibly cause a positive excursion in $\delta^{13}C$ recorded in carbonate minerals precipitated immediately after the glaciation. However, if the timescale of $\delta^{13}C$ excursion in the Lomagundi-Jutali event is on the order of ~10^8 years, the snowball glaciation would not be able to explain that timescale because the rate of organic carbon burial falls to a steady state (i.e., the carbon cycle reaches an equilibrium) in 10^7 years after the glaciation in the model (Fig. 1.2). The timescale required to stabilize the carbon cycle could be prolonged if the chemical weathering of the continents is limited by transport of glacial tills rather than kinetics of chemical reactions (Mills et al., 2011). However, sensitivity studies suggest that even under such transport-limited conditions for chemical weathering, the duration of enhanced organic carbon burial becomes only a few times of the nominal case (Fig. 1.7). One possibility to further prolong biological productivity is to take into account the positive feedback mechanism among the rise of O_2 and phosphorus input to the ocean (Bekker and Holland, 2012); that is, when O_2 rises, phosphorus input to the ocean might be enhanced owing to effective weathering of apatite on the continents by oxidative weathering of sulfides, which produces sulfuric acid, leading to prolonged, high levels of biological productivity (Bekker and Holland, 2012). Further investigations on the timescale on this feedback mechanism are required.

1.5.3. Sensitivity studies

Temporal variations of the rise of O_2 (i.e., the timing of the O_2 onset and magnitudes and timescale of the overshoot) depend on the phosphate accumulation

in the oceans after the deglaciation (Fig. 1.2d). Phosphate accumulation, in turn, is controlled by the initial atmospheric CO_2 concentration and oceanic phosphate concentration, phosphorus cycle, and weathering efficiency. Sensitivity studies were performed regarding the uncertain parameter in these initial and boundary conditions (Fig. 1.2 and Figs. 1.5-1.8). The results show that the assumption for the initial oceanic phosphorus concentration, phosphorus cycle, and weathering efficiency does not significantly affect the conclusions of the transition of oxygen levels within 10^4 years and occurrence of oxygen overshoot (Fig. 1.2 and Fig. 1.5-1.7). However, on the contrary, the temporal variations of the rise of O_2 are affected greatly by the initial atmospheric CO_2 concentration (Fig. 1.8). Under high initial CO_2 conditions (e.g., 0.7 and 0.3 atm), atmospheric oxygen level increases rapidly and irreversibly, leading to an oxygen overshoot (0.1–1PAL). In contrast, a weak and reversible oxygenation (10^{-6}–10^{-5} PAL) occurs in response to a small increase in atmospheric CO_2 level (e.g., initial $CO_2 < 0.086$ atm) (Fig. 1.8).

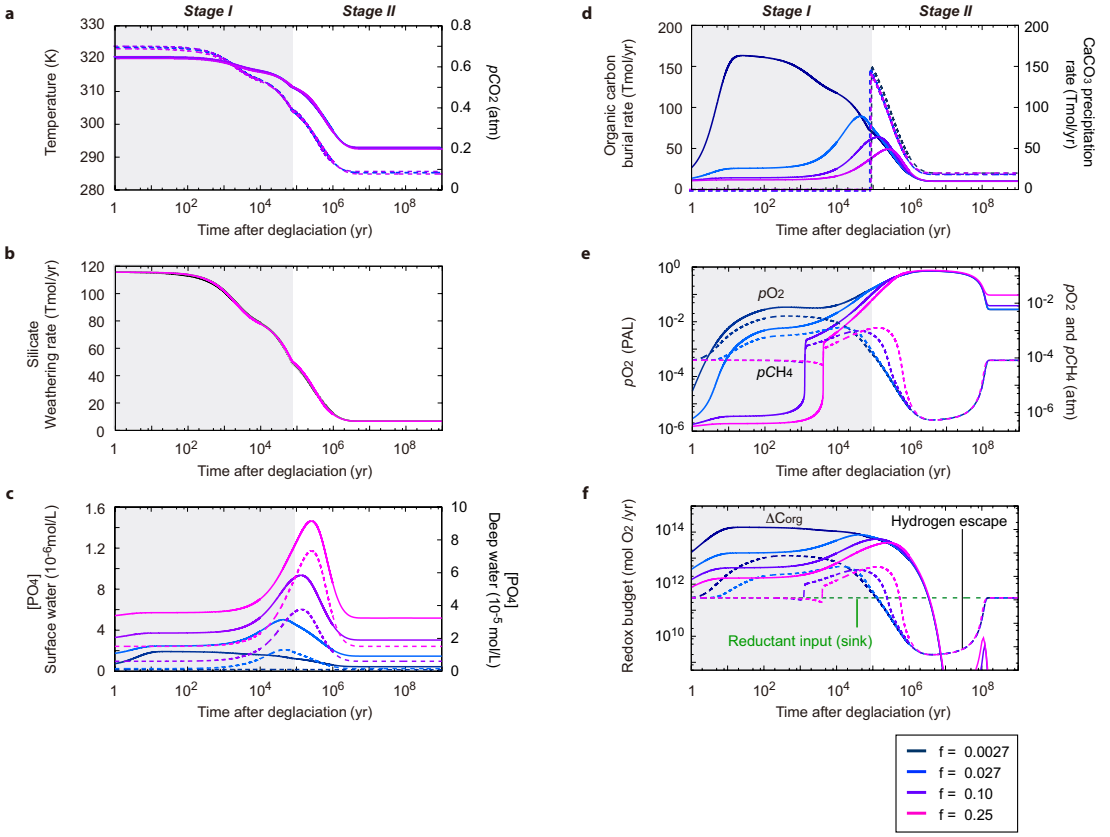

Fig.1.5 Sensitivity to phosphorus cycle: The present-day *f* value is suggested to be ~0.2. Smaller *f* values mean that more organic matter produced by photosynthesis is decomposed in the surface ocean. Given smaller size of life without any skeletons in the surface oceans in the Precambrian periods, the *f* value in Proterozoic would be much smaller than that of today. In the case of small *f*, recycling of phosphorus through organic matter decomposition occurs effectively in the surface ocean, leading to a rapid increase in productivity and atmospheric oxygen. For $f = 0.0027$, almost all of organic matter is decomposed in the surface ocean. Accordingly, a further decline in *f* does not change the results significantly. Under larger *f* conditions, in contrast, organic matter is more efficiently exported to the deep ocean, similar to the situations in the present-day oceans. Remineralization of organic matter in the deep ocean leads to growth of a deep ocean phosphorus reservoir, and biological productivity in the surface ocean is then limited by a phosphorus input via upwelling. The results show that it takes longer time to increase productivity and atmospheric oxygen for larger *f* values. However, in any cases, timescales of the rise of oxygen are less than ~10^4 years after the termination of a snowball glaciation. Thus, I suggest that the conclusion of rapid oxygenation (<~10^4 years) does not change significantly with respect to the uncertainty in phosphorus cycle in Paleoproterozoic.

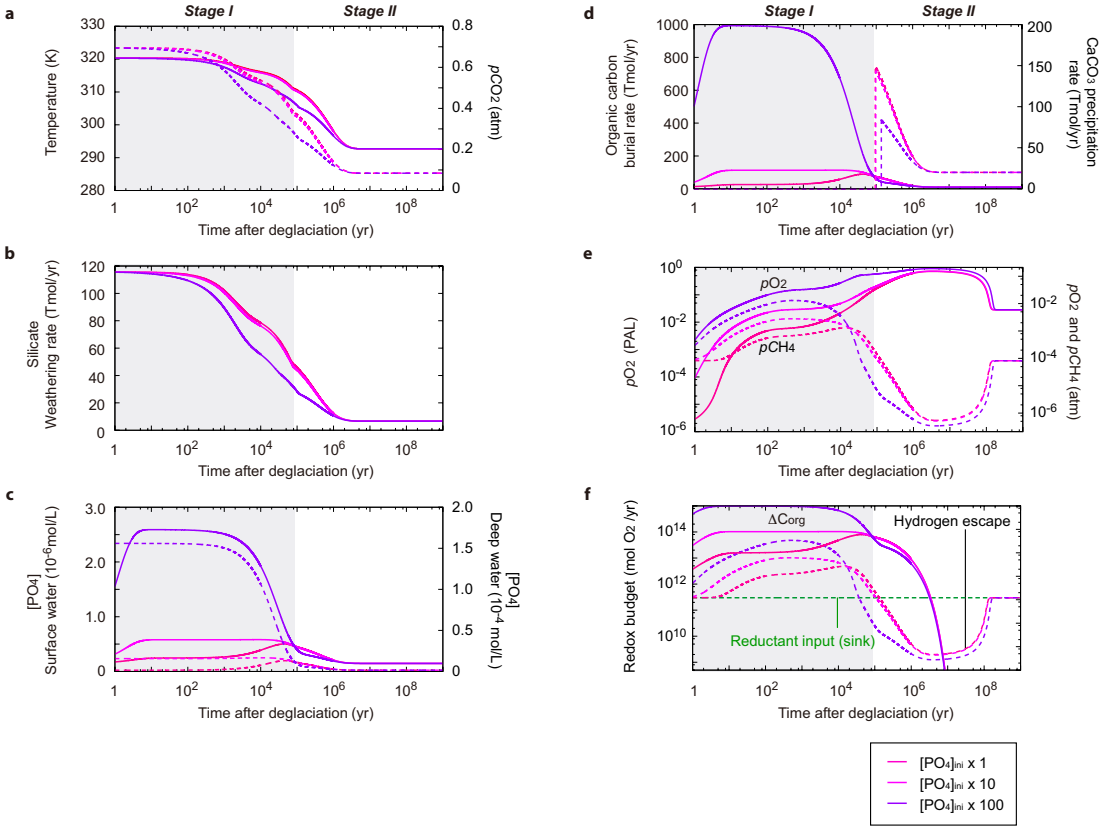

Fig.1.6 Sensitivity to the initial phosphate concentration: Given the possibility of accumulation of dissolved species/ions in the oceans during a snowball Earth glaciation (Hoffman and Schrag, 2002; Kirschvink et al., 2000), there is a large uncertainty in the initial phosphate concentration in our calculations. Assuming that phosphate can accumulate in the oceans until the oceans become supersaturated (the degree of saturation: S = 1.7) with respect to octacalcium phosphate (Gunnars et al., 2004), and that the oceans are isolated from the atmosphere during the snowball glaciation (pH = 7–8; Le Hir et al., 2008), the maximum phosphate concentration accumulated over the glaciation could be 1–100 times the phosphate concentration in the present-day oceans. In the case of higher initial phosphate concentrations (e.g., 10 and 100 time the present-day value), burial rate of organic carbon increases more rapidly, leading to a more rapid rise of oxygen ($<10^5$ years to reach ~1 PAL). However, in long-term evolution ($>10^4$–10^5 years after the glaciation), the total amount of phosphate provided via weathering would dominate or be comparable to the initial phosphorus concentration in the deep ocean. Thus, the uncertainty in initial phosphorus concentration does not affect my conclusions of the transition of oxygen levels within 10^4 years and occurrence of oxygen overshoot significantly.

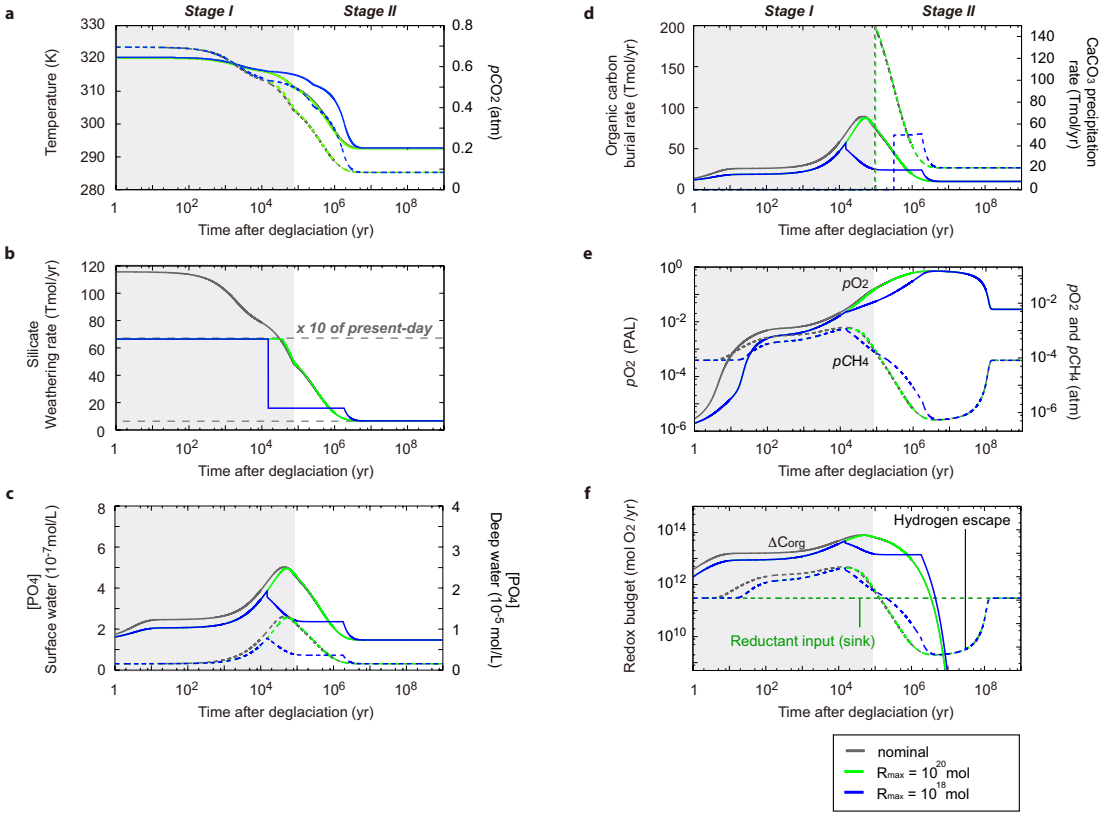

Fig.1.7 Sensitivity to the formulation of chemical weathering: The weathering can be limited by the transport (i.e., physical erosion) of glacial tills rather than kinetics, which may affect biogeochemical responses after snowball glaciations (Mills et al., 2011). Under such transport-limited conditions, there is an upper limit on the weathering rate, which is suggested to be the same as the proposed values for the Phanerozoic physical erosion rate (2.4 times of the present-day weathering rate) (Mills et al., 2011). Under kinetically-limited conditions, on the other hand, the upper limit of weathering rates is suggested to be 10 times of the present-day value (Mills et al., 2011). As a sensitivity study of the effect of transport limitation, Iconsider that there is a limitation of the amount of fresh glacial tills (R_{max}), and vary it from 10^{18} mol to 10^{20} mol of silicates (Mills et al., 2011). After weathering of these amounts of tills, I consider that the limiting factor switches to transport processes (Mills et al., 2011). In the nominal case, I do not consider the limitation for the amount of glacial tills. The results show that the weathering reaches transport limitation in ~10^4 years for R_{max} = 10^{18} mol. Due to the transport limitation, the magnitude of the weathering and organic carbon burial rates after the snowball glaciation is dampened compared to those in the case of kinetic limitation. However, the duration of high levels of the weathering and organic carbon burial rates is prolonged due to the transport limitation, and a transition of oxygen steady states, overshoot of oxygen, and massive deposition of carbonate occur regardless of the limiting factor of weathering.

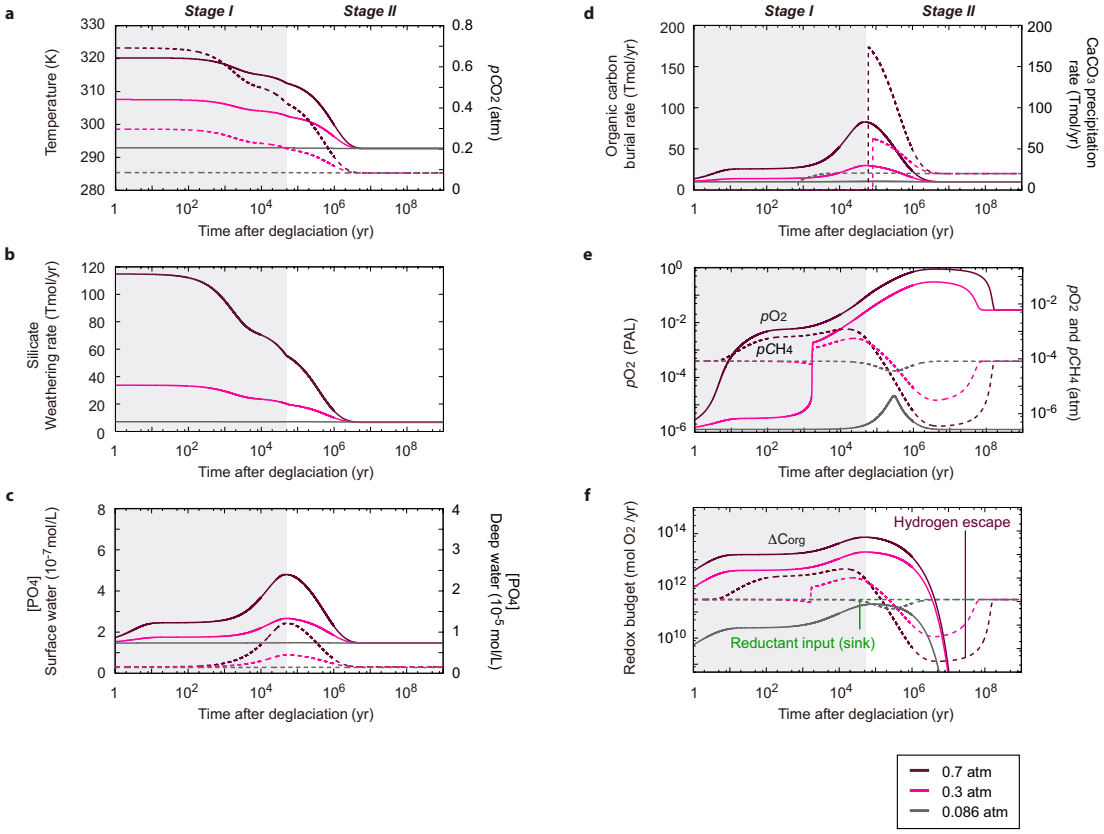

Fig.1.8 Sensitivity to the initial atmospheric CO_2: The sensitivity study suggests that timescales of oxygenation and amplitudes of oxygen overshoot depend on the initial conditions of atmospheric CO_2. Under high initial CO_2 conditions (e.g., 0.7 and 0.3 atm), atmospheric oxygen increases rapidly and irreversibly, leading to an oxygen overshoot (0.1–1PAL). After a rise in oxygen, massive carbonate precipitates in the oceans (see main text). In contrast, a weak and reversible oxygenation (10^{-6}–10^{-5} PAL) occurs in response to a small increase in atmospheric CO_2 (e.g., initial CO_2 = 0.086 atm). In this case, massive carbonate precipitation does not occur. Because high atmospheric CO_2 levels (~0.7 atm) are needed to escape from the Paleoproterozoic snowball glaciation (Tajika, 2003), the former case of high the initial CO_2 is considered to correspond to the aftermath of the snowball glaciation. My results show that oxygen overshoot and formation of cap carbonate occur even if initial CO_2 levels vary from 0.7 atm within a factor of two. The latter case of a weak and reversible oxygen increase may be consistent with the scenario of 'whiffs of oxygen' in the late Archean proposed by recent geochemical studies (Anbar et al., 2007; Goto et al., 2013; Kendall et al., 2010)

1.5.4. Constraining the magnitude of O_2 overshoot: calculation using one-dimensional ocean model

The sensitivity study shows that the magnitude of O_2 overshoot is highly dependent on the initial atmospheric CO_2 concentration (Fig. 1.8). If we assume conventional "hard snowball Earth" scenario, high atmospheric CO_2 levels (~0.7 atm) are required to escape from the Paleoproterozoic snowball Earth (Tajika, 2003). In such a case, deglaciation triggers the rise of O_2 with an extensive overshoot to ~1 PAL, regardless of uncertainties in other parameters (Fig. 1.2 and Figs. 1.5-1.7). However, the amount of CO_2 required for the deglaciation can be smaller than ~0.7 atm if we assume smaller ice coverage than the typical "hard snowball Earth" and/or consider the effect of cloud (Hyde et al. 2000; Abbot et al. 2012). Further, even under the "hard snowball Earth" assumption, the atmospheric CO_2 levels required to escape from the glaciation can vary among climatic models. Accordingly, although my calculation results suggest that the Paleoproterozoic snowball Earth event caused the O_2 transition with an overshoot, the O_2 level during the overshoot is still unclear. In order to constrain the magnitude of the O_2 overshoot, I perform additional sensitivity study using a detailed one-dimensional ocean model. By imposing three different temporal variations of atmospheric O_2 (i.e., a rise of O_2 with ~1 PAL overshoot and 0.1 PAL overshoot, and a rise of O_2 without overshoot) obtained from the box model in Section 1.5.3 into the ocean model as a boundary condition, I calculate the responses in the ocean with regards to concentrations of dissolved sulfate (SO_4) and O_2 and compare the results with geological records of O_2 overshoot (i.e., deposition of sulphate minerals and deep water oxygenation).

The model is developed based on a previous work by Ozaki and Tajika (2013). In this model, the deep ocean is divided into 60 layers, and mass balance of dissolved components including O_2, SO_4, NO_3, PO_4, Ca, H_2S, NH_4, Alk, DIC are calculated, considering diffusion, advection, biogeochemical processes and abiotic chemical reactions. This model considers several organic matter decomposition processes depending on redox conditions in the oceans (i.e., aerobic respiration, denitrification, and sulfate reduction). The organic matter decomposition is modeled such that the marine organic matter is oxidized by oxidant that yields the greatest

free energy change per mole of organic carbon oxidized, hence enable the models to simulate biogeochemical processes under very wade range of redox environments. Thus, the model can simulate dissolved O_2 and SO_4 concentrations in the oceans under wade range of atmospheric O_2 levels, with high vertical resolution.

As this model is originally developed for the calculation of environmental changes (such as Ocean Anoxic events) in Phanerozoic, I add some modification in the aim of applying the model to severely anoxic condition in the Paleoproterozoic. First, I model the sulfur cycle under low atmospheric O_2 levels presumed in the Paleoproterozoic. Influx of SO_4 to the oceans via oxidative weathering of continental sulfides is expressed as follows:

$$F_{wp} = \left(\frac{pO_2}{pO_2^*} \right)^{0.5} F_{wp}^*$$

where F_{wp} represents a weathering rate of sulfide minerals in sedimentary rocks exposed on the continents, and F_{wp}^* represents the weathering rate at present. pO_2 is the atmospheric O_2 levels, while pO_2^* represents the present-day level of the atmospheric O_2. The dependence on atmospheric O_2 levels is obtained from weathering experiments (Williamson and Rimstidt, 1994). I assume 2.0 x 10^{12} mol/year for the value of F_{wp}^* based on the estimate by Emerson et al. (2009). Dissolved SO_4 are converted to sulfide (H_2S) through sulfate reduction, depending on the oxygen concentration in the ocean. Sulfur in the atmosphere-ocean system is removed via deposition of sulfate minerals and sulphide minerals (mainly as pyrite) into the sediments, whose rate is proportional to the concentrations of SO_4 and H_2S, respectively. Second, considering that the oceans can be depleted in sulfate under low O_2 conditions, I add methanogensis into the decomposition processes of organic matter, so that if the oceans are depleted in sulfate ions, the decomposition proceeds via methane fermentation.

The calculation results of the time evolution of dissolved O_2 and SO_4 concentration in the oceans under three different temporal variations of atmospheric O_2 (i.e., a rise of O_2 with ~1 PAL overshoot and 0.1 PAL overshoot, and a rise of O_2 without overshoot) are shown in Fig.1.9 (Figs. 1.9A-2 and 3, 1.9B-2 and 3, and 1.9C-2 and 3). The results show that the ~1 PAL overshoot of atmospheric oxygen causes oxygenation of continental shelf and the deep-water in the ocean (Fig.1.9A-2), which might account for the evidence of deep-water oxygenation in the 2.1 Ga reported from the section in the Republic of Gabon (Canfield et al., 2013). The overshoot of oxygen also causes drastic changes in the sulfur cycle in the atmosphere and ocean system. Sulfate input to the ocean from the continents is enhanced during the overshoot of atmospheric oxygen levels, and result in the accumulation of sulfate ions in the ocean (Fig. 1.9A-3). The level of accumulation is greater than the level required for the deposition of sulfate minerals (>2.5 mM; Schröder et al., 2008). The results show that the depositional rate of calcium sulfate increases during the sulfate accumulation (Fig. 1.9A-4), which is consistent with the global deposition of sulfate mineral during 2.22-2.08 Ga. However, under low levels of overshoot (~0.1 PAL) or the absence of overshoot, such responses in dissolved O_2 and SO_4 might not occur (Fig.1.9 B-2 and 3, C-2 and 3). Accordingly, I suggest that the oxygen transition in the Paleoproterozoic was accompanied with an extensive overshoot reaches ~ 1 PAL and that the snowball glaciation would be a strong candidate as the trigger for the rise of oxygen.

It should be noted that SO_4 could be consumed by reacting with CH_4 (AOM: Anaerobic Oxidation of Methane), a process which is not included in the current model. However, a numerical calculation using a biogeochemical cycle model including AOM suggest that AOM occurs in O_2 levels much lower than ~0.01 PAL (K. Ozaki, personal communication). The results of my study suggest that the O_2 levels exceeds ~0.01 PAL within a very short timescale (<~10^4 years after the snowball deglaciation). On the other hand, due to the long residence time of sulfur in the ocean, the accumulation of SO_4 occurs ~10^7 years after the snowball deglaciation, under high O_2 levels (>~0.01 PAL) where AOM may not occur. Thus, although AOM is not included in the current model, it does not significantly change the conclusion.

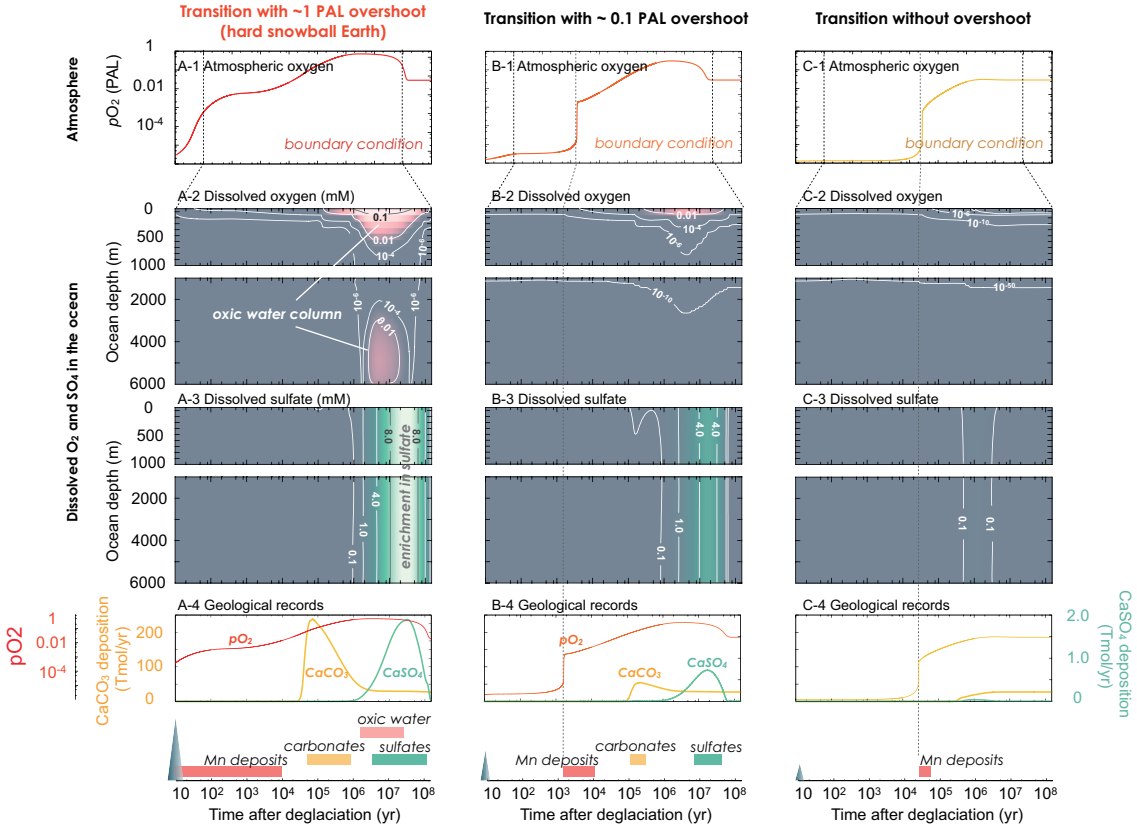

Fig. 1.9 Changes in dissolved O_2 and SO_4 levels in the ocean in responses to the rise of oxygen. A-1, B-1, and C-1, temporal variation in the atmospheric O_2 levels as a boundary condition (rise of O_2 with ~ 1 PAL overshoot, 0.1 PAL overshoot, and without overshoot, respectively). **A-2, B-2, and C-2,** temporal variation in oceanic dissolved O_2 concentration in response to the rise of O_2. **A-3, B-3, and C-3,** temporal variation in oceanic dissolved SO_4 concentration in response to the rise of O_2. **A-4, B-4, and C-4,** possible geological records suggested by calculations.

1.6. Summary of Part I

I evaluated the timescale and magnitudes of a rise of O_2 levels induced by the Paleoproterozoic snowball glaciation. I examined biogeochemical responses to the climate transition at the termination of the snowball glaciation using a biogeochemical cycle model. During the climate recovery from the snowball glaciation, the rates of chemical weathering and nutrient input to the oceans are greatly enhanced under the transient super-greenhouse conditions, which causes elevated biological productivity in the oceans. This results in both a rapid transition ($<10^4$ years) of atmospheric O_2 from a low steady state branch ($< 10^{-5}$ PAL) to a high branch (~0.01 PAL or greater) and an accumulation of massive O_2 up to 1 PAL (i.e., overshoot) after the deglaciation. I show that the intense overshoot of O_2 level persists for $\sim 10^8$ years due to slow input of reductant into the atmosphere-ocean system. These results are in good agreement with the geological records (deposition of manganese oxides and sulfate minerals, and deep-ocean oxygenation) after the Paleoproterozoic snowball glaciation. Despite an uncertainty in the interpretation of the Lomagundi-Jutali event, I thus far conclude that the snowball glaciation would have been the oxidative forcing sufficient to trigger the observed dynamic transition of O_2 levels (i.e., GOT) in the Paleoproterozoic.

Snowball Earth events cause an accumulation of CO_2, which results in a strong disequilibrium in the atmosphere–ocean system when ice melts. i show that this disequilibrium would be the driving force towards a high steady-state level of O_2. Given the occurrence of snowball Earth events at ~2.2, 0.72 and 0.64 Ga (Evans et al., 1997; Hoffman and Schrag, 2002; Kirschvink et al., 2000), phosphate accumulations and massive releases of O_2 would have occurred at both the beginning and end of the Proterozoic (Planavsky et al., 2010; Sahoo et al., 2012). If so, snowball glaciations may have played an essential role in the phase changes of both environmental redox conditions and biological evolution during Earth's history.

Part II: Rise of oxygen and evolution of DNA sequences of the promoters in cyanobacteria

2.1. Consequence of the rise of oxygen to the biological evolution

The Paleoproterozoic rise of O_2 was a transition from low O_2 steady state (< 10^{-5} PAL) to high O_2 steady state (> 10^{-2} PAL) with an extensive overshoot to ~1 PAL (Chapter 2). Such major changes in the environmental O_2 level must have been a severe stress to the biosphere that has been long adapted to the reducing environments. The environmental stress would have caused the adaptive evolution of life and/or the changes in ecosystems. Indeed, fossil records suggest that the rise of O_2 roughly coincided with the biological innovations: a large marine organic fossil considered as eukaryotes, *Grypania spiralis*, first appears in the 2.1-1.9 Ga Negaunee Iron Formation, northern Michigan, USA (Han and Runnegar, 1992). From the compilation of the maximum size of known fossil organisms, it has been suggested that the size of organisms has largely increased at this age (Payne et al., 2009). Further, large fossils of multicellular-like organisms have been found in the ~2.1 Ga black shales in the Francevillian Supergroup, the Republic of Gabon (El

Albani et al., 2010; Canfield et al., 2013). In addition to the paleontological studies, molecular clock analysis has suggested that the last common ancestor of extent eukaryotes appeared sometime between 1.866 and 1.679 Ga (Parfrey et al., 2011). Although these geochemical and biological studies suggest the linkage between the rise of O_2 and the biological evolution, how the changes in environmental O_2 levels affect the biological evolution has been poorly understood. This may be owing to the lack of direct evidence which shows the effect of environmental redox changes to the biosphere.

2.2. Evolution of Cyanobacteria

Cyanobacteria would be one of the organisms which should have been greatly affected by the changes in the atmospheric O_2 levels, because they are photosynthetic bacteria and live in the euphotic zone of the oceans (the uppermost 0-200 m of the surface oceans). The origin of cyanobacteria is not fully understood. However, cyanobacteria must have originated before the GOE, considering that the oxygenic photosynthesis by cyanobacteria was the only major source of the O_2 in the Paleoproterozoic. Moreover, the occurrences of small and episodic oxidation events called “whiffs of oxygen” before the GOE (2.6-2.5 Ga) (Anbar et al., 2007; Goto et al., 2013; Kendall et al., 2010) suggest that the O_2 production by cyanobacteria might have preceded the GOE. Therefore, cyanobacteria appeared in the reducing conditions and caused the GOE, and, then, survived severe environmental stress due to the elevated levels of O_2 in the atmosphere and oceans. Thus, studying the evolution of cyanobacteria will enable us to track the possible adaptive evolution of life to the rise of O_2 during the GOE.

2.2.1. Fossil record

Direct evidence that shows the evolution of cyanobacteria would be cellular microfossils, which have morphological counterparts among extant cyanobacteria. Extant cyanobacteria are diverse in morphology, classified into five subsections

(Rippka et al., 1979) (Table 2.1): a group of unicellular coccoids divide by binary fission (Subsection I, formely Chroococcales), a group of unicellular colonial coccoids divide by multiple fission, via division of mother cells into small daughter cells called baeocysyts (Subsection II, Pleurocapsales), a group of filamentous cyanobacteria (Subsection III, Oscillatoriales), a group of filamentous cyanobacteria that have cells specialize in nitrogen fixation called heterocysts, or have resting cells to survive environmental stresses called akinetes (Subsection IV, Nostocales), and a group of filamentous cyanobacteria that have true branching in addition to heterocysts and akinets (Subsection V, Stigonemales). The identification of cyanobacterial microfossils has been relied on such a variety in morphology.

Table 2.1 *Major groups of cyanobacteria defined by Rippka et al. (1979)*

<table>
<tr><td rowspan="2">Unicellular</td><td>Reproduction by binary fission</td><td>Subsection I</td></tr>
<tr><td>Reproduction by multiple fission giving rise to small daughter cells (baeocytes), or by bothmultiple fission and binary fission</td><td>Subsection II
Pleurocapsales</td></tr>
<tr><td rowspan="3">Filamentous</td><td>Trichome always composed only of vegetativecells</td><td>Division in only one plane
Subsection III
Oscillatoriales</td></tr>
<tr><td rowspan="2">In the absence of combined nitrogen, trichome contains heterocysts; some also produce akinetes</td><td>Division in only one plane
Subsection IV
Nostocales</td></tr>
<tr><td>Division in more than one plane
Subsection V
Stigonemales</td></tr>
</table>

Fossil records of cyanobacteria are summarised in Table 2.2. The oldest well-accepted microfossils of cyanobacteria would be fossilised akinets, *Archaeosllipsoides*, found in the ~2.1 Ga black shales in the Francevillian Supergroup, the Republic of Gabon (Tomitani et al., 2006). Although relatively poorly preserved compared to younger fossils (e.g., *Archaeosllipsoides* fossils in 1.65-Ga Amelia Dolomite, Australia and in 1.5-Ga cherts from Billyakh Group, Russia;Golubic et al., 1995), the fossile of 2.1 Ga exhibits morphological features similar to the akinetes of extant nostocalean genus *Anabaena* (Subsection IV) (Tomitani et al., 2006). The fossils of colonial coccoids of 2.0 Ga are found in the Belcher Supergroup, Canada, which are also recognized as fossilised cyanobacteria (*Entophysalis*) (Golubic and Seong-Joo, 1999; Hofmann, 1976), although taxonomic affinity to extant cyanobacteria is uncertain. Fossils of ellipsoids of 2.0 Ga are also found in the same formation in the Belcher Supergroup, the taxonomy of which is identified as extant unicellular cyanobacteria, *Gloeobacter* (Subsection I) (Golubic and Seong-Joo, 1999; Hofmann, 1976). Thereafter, several filamentous and coccoid microfossils (Subsections I and III) became common in the Gunflint Iron Formation (1.9 Ga) in Ontario, Canada (Golubic and Seong-Joo, 1999). In the Duck Creek Dolomite (1.8 Ga), Australia, several types of filamentous and coccoid microfossils resemble extant cyanobacteria have also been reported (Knoll et al., 1988). The earliest microfossil of Pleurocapsa (Subsection II) has been reported from the Dahongyu Formation (1.7 Ga), China (Zhang and Golubic, 1987). In the Gaoyuzhuang Formation (1.4-1.5 Ga), China, several well-identified microfossils have been reported: multi-trichomous filamentous microfossil similar to *Microcoleus* (belongs to Subsection III), coccoids resemble *Chamaesiphon* (Subsection I), and filamentous microfossils correspond to *Calothrix* and *Aphampthece* (Subsection IV) (Golubic and Seong-Joo, 1999).

These fossil records suggest that almost all morphological groups of extant cyanobacteria appeared before Mesoproterozoic (~1.4 Ga). On the other hand, microfossils of cyanobacteria older than 2.1 Ga are absent, despite that cyanobacteria are considered to have emerged before the GOE (2.45−2.22 Ga). This may be partly because there are very few chances to preserve microfossils of cyanobacteria in older rocks. Smaller cellular sizes at the origin of cyanobacteria might be responsible for

the poor preservation (Blank and Sánchez-Baracaldo, 2010). Thus, fossil record must be regarded as a minimum constraint when discussing the evolution of cyanobacteria.

Table 2.2 *Fossil records of cyanobacteria*

Age (Ga)	**Fossils**	Source rocks	**References**
2.1	Fossilised akinets, *Archaeosllipsoides* (IV)	Francevillian Supergroup, the Republic of Gabon	Tomitani et al. (2006)
2.0	Coccoid cyanobacterium *Eoentophysalis belcherensis* and forms similar to *Gloeobacter* (I)	Belcher Supergroup, Canada	Hoffman (1976); Golubic and Seong-Joo (1999)
1.9	Filamentous and coccoid microfossils (I and III)	Gunflint Iron Formation, Canada	Golubic and Seong-Joo (1999)
1.8	Filamentous and coccoid microfossils (I and III)	Duck Creek Dolomite, Australia	Knoll et al. (1988)
1.7	Pleurocapsa (II)	Dahongyu Formation, China	Zhang and Golubic (1987)
1.65	*Archaeosllipsoides* (IV)	Amelia Dolomite, Australia	Golubic et al. (1995)
1.5	*Archaeosllipsoide* (IV)	Billyakh Group, Russia	Page et al. (2000)
1.4	Coccoids resemble *Chamaesiphon* (I), filamentous microfossil similar to *Microcoleus* (III), and filamentous microfossils correspond to *Calothrix* and *Aphanopthece* (IV)	Gaoyuzhuang Formation, China	Golubic and Seong-Joo (1999)
0.8	Coccoid form resembles *Chroococcus* (I)	Bitter Springs Formation, Australia	Knoll and Golubic (1979)

2.2.2. Phylogeny

Phylogenetic analysis is a powerful tool that compensates for the limitation of fossil records. The phylogeny of cyanobacteria has been well studied by several groups (e.g., Blank and Sánchez-Baracaldo, 2010; Sánchez-Baracaldo et al., 2014, 2005; Schirrmeister et al., 2015, 2013; Shih et al., 2013; Tomitani et al., 2006). The previous works have shown common tree topology, suggesting that the majority of extant cyanobacteria can be divided into six to five major clades, which is consistent with the results from fossil analyses. The evolutionary relationships do not always match the morphological classification (major phylogenetic clades of cyanobacteria suggested by the previous works, and their relationships to morphological classification are summarized in Table 2.3).

The diversification age of each clade has been studied by fossil records and the molecular clock analysis (e.g., Tomitani et al., 2006; Blank and Sánchez-Baracaldo, 2010; Sánchez-Baracaldo et al., 2014; Schirrmeister et al., 2013, 2015). Although the age of diversification estimated from the molecular clock studies may have large uncertainty, the molecular clock studies consistently suggest the origin of cyanobacteria well before the GOE (> 2.4-2.3 Ga), which is obtained independently from the datasets or of the age calibration points. They also show that the diversification of the ancestor of three major lineages of extant cyanobacteria roughly overlaps the GOE (2.3-2.0 Ga) and small diameter marine cyanobacteria (alpha-cyanobacteria) diverged later at 1.0-0.6 Ga (Table 2.3) (Blank and Sánchez-Baracaldo, 2010; Sánchez-Baracaldo et al., 2014; Schirrmeister et al., 2013, 2015). Based on the first occurrence of fossil akinetes at ~2.1 Ga, combined with the results of phylogenetic analysis, groups IV and V of cyanobacteria are suggested to have diverged during the GOE (Tomitani et al., 2006; Blank and Sánchez-Baracaldo, 2010; Sánchez-Baracaldo et al., 2014; Schirrmeister et al., 2013), possibly during the period of O_2 overshoot.

Although the phylogenetic and molecular clock results have contributed greatly to our understanding of the phylogeny and the timing of cyanobacterial diversification, still little is known about a linkage between the rise of O_2 and the evolution of cyanobacteria. There have been some studies suggesting that the

morphological and/or ecological evolution of cyanobacteria caused the rise of O_2 (Sanchez-Barakaldo et al., 2010; Schirrmeister et al., 2013, 2015). For instance, Blank and Sanchez-Baracaldo (2010) suggest that the changes in the habitat of cyanobacteria from fresh water to marine environments caused the GOE. Schirremeister et al. (2013) suggests that the emergence of filamentous cyanobacteria might have contributed to the rise of O_2. On the other hand, however, there have been no previous studies that investigated the effect of the O_2 rise to the evolution of cyanobacteria. Moreover, previous works have only focused on the morphology and habitat of cyanobacteria, the characteristics that might not directly reflect the environmental O_2 levels. It is still difficult to discuss the effect of rise of environmental O_2 levels to the evolution of cyanobacteria. Thus, phylogenetic analysis of cyanobacteria using an indicator that directly reflects the environmental O_2 levels will be required.

Table 2.3 *Major phylogenetic clades of cyanobacteria*

<table>
<tr><th colspan="7">Clade</th><th>Study</th></tr>
<tr><td>NA</td><td>Clade 1</td><td>Clade 2</td><td>Clade 3</td><td>Clade 4</td><td>Clade 5</td><td>Clade 6</td><td>Schirrmeister et al. (2015)</td></tr>
<tr><td>Clade CR</td><td>Clade F</td><td>Clade E</td><td>Clade C</td><td>Clade A</td><td colspan="2">Clade B</td><td>Shih et al. (2013)</td></tr>
<tr><td>LPP</td><td>NA</td><td>No name</td><td>SynPro</td><td colspan="2">PNT</td><td>SPM</td><td>Sanchez-Baracaldo et al. (2014)</td></tr>
<tr><td>I and III</td><td>III</td><td>I</td><td>I</td><td>III</td><td>IV and V</td><td>I, II, and III</td><td>Morphology
Rippka (1979)</td></tr>
<tr><td colspan="3">Early branching lineages
> ~2.3 Ga</td><td>Alpha-cyanobacteria
1.0-0.6 Ga</td><td colspan="3">Major three lineages of extant cyanobacteria
2.3-2.0 Ga</td><td>Age of diversification
Sanchez-Baracaldo et al. (2014)</td></tr>
</table>

2.3. Evolution of the promoters for O_2 catalysing enzymes

In this study, I focused on the evolution of two enzymes that relate to the metabolisms using O_2 as a substrate: Fe-SOD (Fe-superoxide dismutase) and RubsiCO (ribulose 1,5-bisphosphate carboxylase/oxygenase). I hypothesized that changes in the levels of gene expression (e.g., the amount of enzymes synthesised within cells) of these enzymes might reflect the changes in O_2 levels in the environments, hence, can be used as indicators that record the adaptive evolution of cyanobacteria to the rise of O_2. Below, I describe possible consequences of the GOE to the evolution of biochemical characteristics of Fe-SOD and RubisCO.

2.3.1. Fe-SOD

The rise in O_2 concentration in the environments causes the rise in O_2 concentration in the cells via diffusion. The reduction of O_2 molecules in cells generates various highly reactive intermediates called reactive oxygen species (ROS) including the superoxide anion ($O_2^{\cdot-}$), hydrogen peroxide (H_2O_2), and hydroxyl radical ($HO^{\cdot}$) through the following sequences (e.g., Latifi et al., 2009; Sheng et al., 2014).

$$O_2 + e^- \rightarrow O_2^{\cdot-}$$

$$O_2^{\cdot-} + 2H^+ + e^- \rightarrow H_2O_2$$

$$H_2O_2 + 2H^+ + e^- \rightarrow H_2O + HO^{\cdot}$$

$$HO^{\cdot} + H^+ + e^- \rightarrow H_2O$$

The ROS react with several biomolecules (e.g., DNA, lipids, and proteins), and damage the living organisms. Thus, in order to protect themselves from the toxicity of ROS, organisms have developed various systems to scavenge the intercellular concentrations of ROS. The SOD is the enzyme that is widely distributed among living aerobic organisms including cyanobacteria and is known to play a major role

in the detoxification of O_2^- by catalysing the following chemical reaction (Latifi et al., 2009):

$$2O_2^- + 2H^+ \rightarrow O_2 + H_2O_2$$

Although H_2O_2 generated through the reaction can still cause damage, it is rapidly reduced into harmless H_2O by a chemical reaction catalysed by catalase or peroxidase enzymes (Latifi et al., 2009). Considering that the concentrations of the ROS in the cells of cyanobacteria will rise under O_2-rich conditions, cyanobacteria must have been forced to cope with severe oxidative damage at the time of the GOE. One possible way to adapt to the rise of O_2 would be to increase the level of gene expression of SOD.

It has been known that there are several different types of SOD, classified according to their metal redox-active centre: Fe-SOD [Fe(III) is used at the active site], Cu/Zn-SOD [Cu(II) and Zn(II)], Mn-SOD [Mn(III)], and Ni-SOD [Ni(II/III)] (Priya et al., 2010). Each type of SOD locates in specific regions in cells, such as cytosol and thylakoid membrane (Mn-SOD), cytosol (Fe-SOD and Ni-SOD), and periplasma (Cu/Zn-SOD)(Sheng et al., 2014). All of the four types of SODs have been observed in cyanobacteria, and most of the species possess multiple forms of SODs encoded by more than one gene (Priya et al., 2010). Phylogenetic analysis has shown that Fe-SOD is the most widely distributed type of SOD in cyanobacteria (Priya et al., 2010). Accordingly, among the four types of SODs, Fe-SOD would be the best target to track the adaptive evolution of cyanobacteria to the rise of O_2.

2.3.2. RubisCO

RubsiCO is the enzyme that catalyses the carbon fixation in the photosynthesis, adding carbon dioxide (CO_2) and H_2O molecules to 1,5-ribulose bisphosphate (RuBP) in the following chemical reaction:

$$\text{RuBP} + H_2O + CO_2 \rightarrow 2 \text{ x 3-phosphoglycerate}$$

The reaction yields two molecules of 3-phosphoglycerate, which are later used in synthesising larger carbohydrate molecules. Howeverm RubisCO is known to have a tendency to confuse its substrate, CO_2, with O_2 under high intercellular O_2/CO_2 conditions (Andrews and Lorimer, 1978). The confusion between O_2 and CO_2 occurs because of the similarities in electrostatic features and molecular sizes between them. The addition of O_2 instead of CO_2 causes unfavourable(?) oxygenation of RuBP, generating one molecule of both 3-phosphoglycerate and 2-phosphoglycolate:

$$\text{RuBP} + H_2O + O_2 \rightarrow \text{3-phosphoglycerate} + \text{2-phosphoglycolate}$$

The reaction is called photorespiration. Retrieve of 2-phosphoglycolate generated through the photorespiration causes the net loss of CO_2, hence reduces the rate of net carbon fixation (Savir et al., 2010; Tcherkez et al., 2006).

During the GOE, the rise in O_2 levels in the environments must have lead to the major increase in intercellular O_2/CO_2 ratio of cyanobacteria, resulting in the prohibition of carbon fixation (Galmés et al., 2014; Tcherkez et al., 2006; Young et al., 2012). Thus, in order to maintain sufficiently high rates of carbon fixation, cyanobacteria might have evolved to increase the gene expression of RubisCO.

2.3.3. Promoters

In prokaryotes, the levels of gene expression are regulated by specific DNA sequences called promoters (Rosenberg and Court, 1979). Promoters are DNA sequences locate just upstream of protein encoding regions. RNA polymerase (RNAP), the enzyme that synthesise mRNA from protein encoding gene, recognises promoters and binds to them. RNAP then initiates the synthesis of mRNA (i.e., RNA transcription), which is later, translated into proteins (Mcclure, 1985; Rosenberg and Court, 1979). The rate of transcription depends on the efficiency of the interaction between RNAP and promoters. “Strong” promoters that efficiently interact with RNAP cause high rate of transcription, which is in turn, lead to high levels of gene expression.

The characteristics of the strong promoters in bacteria are the best studied in *Escherichia coli*. Compilation of the DNA sequences of promoters of several diverse genes in *E. coli* shows that there are highly conserved sequences consist of six bases both in the regions 10 and 35 base pairs upstream of the transcription start site (Rosenberg and Court, 1979). The consensus sequences of these two regions, termed -10 box and -35 box, respectively, are TTGACA and TATAAT (Rosenberg and Court, 1979). In general, promoters that have high similarities to the consensus sequences are considered to enhance the transcription, leading to high levels of expression (Mcclure, 1985). This is based on experimental results: alterations that decrease similarity to the consensus sequence lower the transcription, and mutations that increase similarity to the consensus cause the high rate of transcription (Mcclure, 1985; Rosenberg and Court, 1979). This is also supported by the fact that the semisynthetic promoter which has the precisely the same sequences to the consensus exhibits very high levels of gene expression (Amann et al., 1983; Brosius et al., 1985; Rossi et al., 1983).

All the other eubacteria including cyanobacteria share the same basic principles of promoter recognition, although the difference in actual DNA sequences may exist owing to the difference in RNAPs between organisms (Vogel, 2003). The promoters of cyanobacteria have been systematically studied by Vogel (2003). They have determined experimentally the promoters of 21 different genes of marine cyanobacteria *Prochlorococcus* sp. MED4. Comparison between the promoters showed that there are conserved -10 box that is similar to the consensus -10 box of *E. coli*. Although the number of the data is quite limited, the results suggest that cyanobacteria have promoters similar to those of *E. coli*.

2.4. Objectives

The atmospheric O_2 concentrations have been changed dramatically through the Earth's history, and the gene expression of SOD and RubisCO of cyanobacteria must have been affected by such dynamics of the environmental O_2 levels. The levels of gene expression are controlled by the DNA sequences of promoters, especially of

the sequences in -10 box and -35 box. Thus the promoters might have changed through history, reflecting the changes in the environmental O_2 levels.

It has been suggested that nucleotide and amino acid sequences of extinct ancestors can be statistically estimated if the phylogeny and sequences of extant species are known (e.g., Yang et al., 1995). The methods of ancestral sequence reconstruction have been employed in several previous studies in the field of evolutionary biology. For instance, some studies reconstructed ancestral amino acid sequences and synthesized the proteins of extinct ancestral species from the sequences in laboratory. The biochemical properties of the ancestral proteins were then studied to infer the environments in the deep time (Akanuma et al., 2013; Gaucher et al., 2008).

In this study, I aimed to obtain the ancestral sequences of promoters (i.e., ancestral promoter sequences) of cyanobacterial SOD and RubisCO. From the ancestral promoter sequences, I estimate the changes in the levels of gene expression through history, and discuss the relationships between the changes in the gene expression and atmospheric O_2 levels.

2.5. Methods

In order to obtain the ancestral promoter sequences, I collected the DNA sequences of extant cyanobacteria and determined the promoters of RubisCO and SOD. Then, I constructed the phylogenetic tree of cyanobacteria to identify the phylogenetic relationships of extant cyanobacteria. Finally, using the alignment of extant promoter sequences and the tree topology, the ancestral promoter sequences were calculated.

As describe above, promoter sequences preferred by cyanobacterial RNAP are not necessarily the same as those of *E.coli* (Vogel, 2003). Thus, in order to estimate the gene expression levels from promoter sequences, the sequences of strong promoters of cyanobacteria must be determined. Accordingly, I calculated the ancestral promoters for known highly expressed genes such as rRNA and ribosomal

protein in addition to RubisCO and SOD for comparison. From the similarity between the sequences of ancestral promoters of O_2-related enzymes (ancestral promoters of RubisCO and SOD) and control promoters (ancestral promoters of rRNA and ribosomal protein), I estimated semi-quantitatively the gene expression levels of RubisCO and SOD in the past. Detailed methods are described below.

2.5.1. Determination of extant promoters

DNA sequences of extant cyanobacteria that were expected to cover the region containing -10 box and -35 box were collected from GenBank (http://www.ncbi.nlm.nih.gov). In order to collect the promoter sequences as many as possible, first, the sequences of the target proteins genes (RubisCO, Fe-SOD, rRNA, and ribosomal proteins) were obtained using BLAST. Next, for each sequences of protein and gene, DNA sequences of the regions expected to contain -10 box and -35 box were searched in GenBank. The sequences were collected such that the obtained regions cover > 200-300 base pairs upstream of the start codon of each target protein and gene, including stop codon of genes located just upstream of each target protein and gene. The numbers of collected DNA sequences were, 92 for RubisCO, 78 for Fe-SOD, 115 for rRNA, and 115 for ribosomal protein.

As the binding regions of RNAP, the sequences of -10 box and -35 box are expected to be better conserved than the other regions of DNA, hence, have similarity among species. Thus, in order to determine -10 box and -35 box from the sequence similarity, collected DNA sequences were aligned using MAFFT v.7.017 (Katoh et al., 2002). However, the automatic alignment based only on the similarity between the sequences sometimes causes error in detecting -10 box and -35 box, because it does not concern about the other features of promoters (e.g., gap between the -10 box and -35 box). Thereby, the alignment was manually checked and edited after the MAFFT alignment. There have been several experimental studies that determined the -10 box and -35 box of cyanobacterial RubisCO, Fe-SOD, and rRNA (Chungjatupornchai and Fa-aroonsawat, 2014; Liu et al., 2000; Nierzwicki-bauer and Curtis, 1985; Vogel, 2003). These experimental results were used as guides for the

alignment. Based on the alignment, -10 box and -35 box were determined for each sequence. The alignments of -10 box and -35 box including ~20 base pairs upstream and downstream of the two boxes were exported as FASTA files and used in the calculation of ancestral sequences.

2.5.2. Phylogenetic analysis of cyanobacteria

Phylogenetic tree of cyanobacteria was constructed using a concatenated three-gene data set: small and large subunit ribosomal RNA (SSU and LSU rRNA) and the gene encoding RNAP subunit β' (RpoC1). The sequences are universally present in cyanobacteria taxa and evolutionary conserved (e.g., Blank and Sánchez-Baracaldo, 2010). Sequence data of the three genes were obtained from GenBank. Sequences were aligned using MAFFT v.7.017 (Katoh et al., 2002) and concatenated in Generous v. 7.1.7, then exported as a single PHYLIP file. Sequence positions used for analysis were defined using trimAl v.1.2 (Capella-Gutierrez et al., 2009) such that only alignable position were used in the phylogenetic tree construction. The final data set included 153 sequences and contained 5,115 positions. Tree was constructed using maximum likelihood (ML) method in raxmlGUI (Silvestro and Michalak, 2012). For the DNA evolution model, I chose generalised time-reversible model (Tavare, 1986) with the addition of invariant sites and a gamma distribution of rates across sites (GTR + I + Γ). Given that previous phylogenetic studies consistently have shown *Gloeobacter violaceus* as the earliest lineage of cyanobacteria (Blank and Sánchez-Baracaldo, 2010; Sánchez-Baracaldo et al., 2005; Schirrmeister et al., 2015, 2013; Shi and Falkowski, 2008), recent molecular clock studies have used *Gloeobacter violaceus* to root phylogenetic trees (Sánchez-Baracaldo et al., 2014; Schirrmeister et al., 2015). In this study, I adapted this assumption and treated *Gloeobacter* as outgroup of cyanobacteria.

Once a tree topology was identified, four constraint trees were reconstructed for the calculation of ancestral promoter sequences of four each protein and gene (i.e., RubisCO, Fe-SOD, rRNA, and ribosomal protein). In general, in the calculation of ancestral promoter sequences, species included in phylogenetic analysis and

promoter alignment must be exactly the same. Thus, the constraint trees were built with the set of taxa that is exactly the same as that of each promoter alignment (i.e., alignment of the promotes of RubisCO, Fe-SOD, rRNA, and ribosomal proteins). First, the number of sequences was reduced using MESQUITE v. 3.04 (Maddison and Maddison, 2008) without changing the topology from the reference tree containing 153 sequences. Branch lengths were then recalculated using raxmlGUI with the data set of SSU-LSU-RpoC1 concatenated sequences and GTR + I + Γ model, imposing the tree topology as a constraint. The constraint trees were used to infer the ancestral promoter sequences of respective proteins and genes.

2.5.3. Estimation of ancestral promoters

An ancestral promoter sequence of each interior node was estimated from the given tree topologies and alignments of extant promoter sequences using ML methods (Yang et al., 1995). In ML method, the likelihood of each nucleotide at each position in the sequence is calculated using a statistical model of evolution, taking into account biased substitution rates between nucleotides and branch lengths in the tree. The ancestral sequences are defined such that each nucleotide has the greatest likelihood. In this study, calculations were performed in basml program (Yang et al., 1995) of pamlX package v. 1.3.1, with two different substitution models: HKY85 and TN93.

2.6. Results

2.6.1. Phylogeny of cyanobacteria

Fig. 2.1 shows the obtained results of the phylogenetic tree of cyanobacteria inferred from 153 SSU-LSU-RpoC1 concatenated sequences. The results suggest that cyanobacteria can be divided into six major clades: Clade A-F.

Assuming *Gloeobacter* as outgroup, thermophilic *Synechococcus* [*Synechococcus* sp. JA-2 3B'a(2-13) and JA-3-3Ab] first branches from the rest of

cyanobacteria, which is consistent with the previous studies (e.g., Blank and Sánchez-Baracaldo, 2010; Sánchez-Baracaldo et al., 2014; Schirrmeister et al., 2015). This is followed by the branching of 'Clade A' and 'Clade B'. Clade A includes alpha-cyanobacteria (small diameter marine *Synechococcus* sp. and *Prochlorococcus* sp. and brakish and freshwater *Synechococcus* and *Cyanobacium*), *Synechococcus elongates*, and multicellular *Prochlorothrix hollandica*. Clade B comprises unicellular *Synechococcus* sp. PCC 7336 and 7335 and multicellular *Leptolyngbya* sp.. The branching of 'Clade C', which includes unicellular *Acaryochloris* sp. and *Thermosynechococcus* sp. and multicellular *Pseudanabeana* sp., follows the branching of Clade B. 'Clade D' includes a group of multicellular taxa (morphologically classified into group III, oscillatoriales), such as *Planktothrix agardhii* NIVA-CYA 34, *Arthrospira* sp., *Trichodesmium erythraeum* IMS101, and *Oscillatoria nigro-viridis* PCC 7112. 'Clade E' consists mainly of unicellular cyanobacteria that are morphologically classified into group I (*Synechocystis* sp., *Cyanothece* sp., *Microcystis* sp., *Synechococcus* sp. PCC 7002) and group II (Pleurocapsa), but also includes some of multicellular taxa including *Moorea* sp. and *Microcleus* sp. 'Clade F' contains group IV (Nostocales) and V (Stigonemales), both of which form heterocysts and akinetes.

The early branching of Clade AC followed by the branching of Clade D-F is consistent with the recent phylogenetic analyses (Blank and Sánchez-Baracaldo, 2010; Sánchez-Baracaldo et al., 2014, 2005; Schirrmeister et al., 2015; Shi and Falkowski, 2008). The phylogenetic relationships between Clade A-C and between Clade D-F have been known to differ among studies, depending on data sets and analytical methods. In order to identify well-resolved tree topology with less artefacts, detailed analysis with concatenated core cyanobacterial genes using different sets of taxa, characters, and methods has been performed by Blank and Sánchez-Baracaldo (2010). The consensus tree topology suggested by Blank and Sánchez-Baracaldo (2010) is very similar to the tree topology obtained in this study, with one exception regarding the placement of Clade D: Clade D forms sister clade with Clade F in Blank and Sánchez-Baracaldo (2010), while Clade D branches before Clade E and F in this study. Thus, based on the similarity to the detailed

phylogenomic study, I employ the phylogenetic relationships shown in Fig 2.1 for the estimation of ancestral promoter sequences.

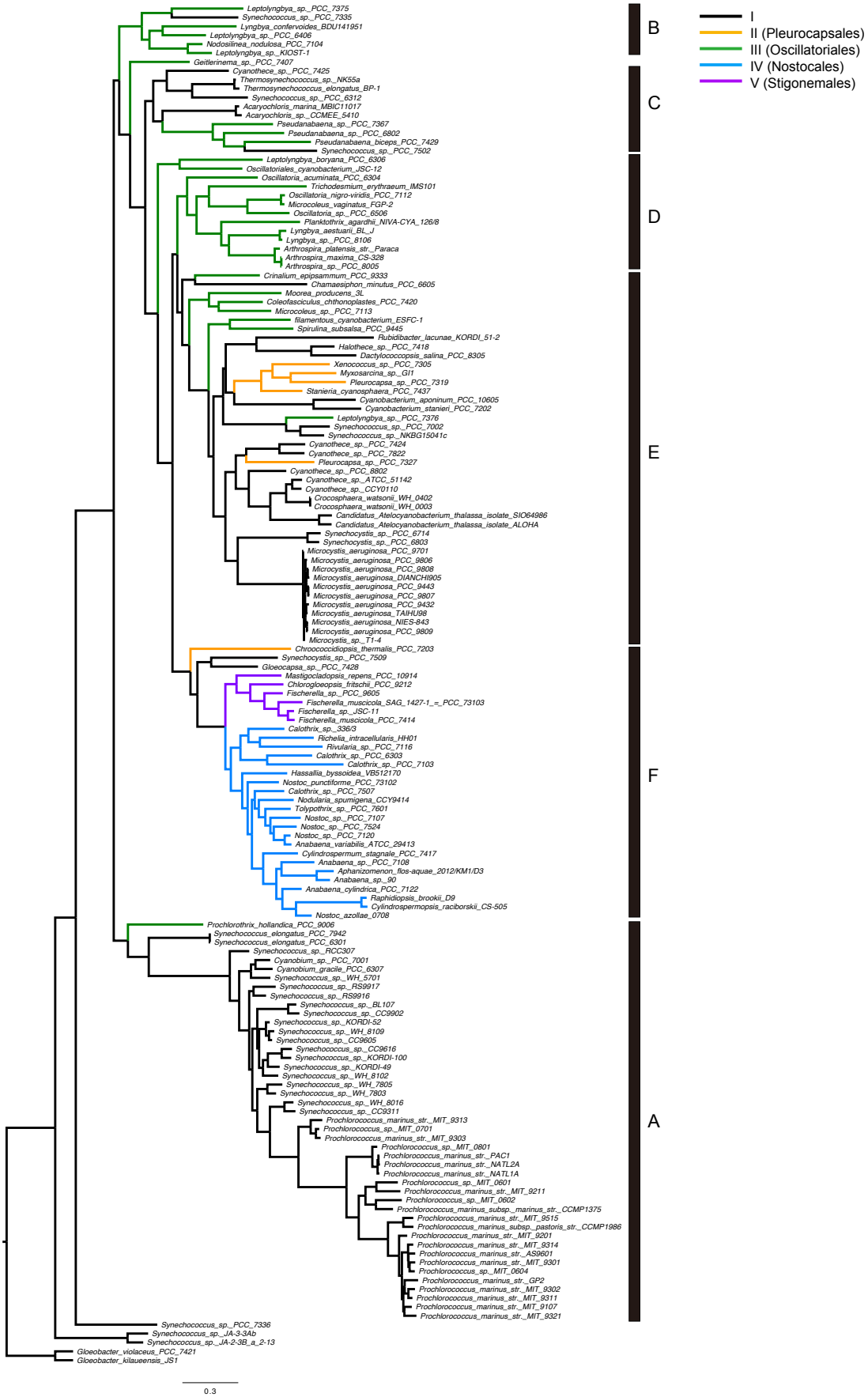
Leptolyngbya_sp._PCC_7375
Synechococcus_sp._PCC_7335
Lyngbya_confervoides_BDU141951
Leptolyngbya_sp._PCC_6406
Nodosilinea_nodulosa_PCC_7104
Leptolyngbya_sp._KIOST-1
Geitlerinema_sp._PCC_7407
Cyanothece_sp._PCC_7425
Thermosynechococcus_sp._NK55a
Thermosynechococcus_elongatus_BP-1
Synechococcus_sp._PCC_6312
Acaryochloris_marina_MBIC11017
Acaryochloris_sp._CCMEE_5410
Pseudanabaena_sp._PCC_7367
Pseudanabaena_sp._PCC_6802
Pseudanabaena_biceps_PCC_7429
Synechococcus_sp._PCC_7502
Leptolyngbya_boryana_PCC_6306
Oscillatoriales_cyanobacterium_JSC-12
Oscillatoria_acuminata_PCC_6304
Trichodesmium_erythraeum_IMS101
Oscillatoria_nigro-viridis_PCC_7112
Microcoleus_vaginatus_FGP-2
Oscillatoria_sp._PCC_6506
Planktothrix_agardhii_NIVA-CYA_126/8
Lyngbya_aestuarii_BL_J
Lyngbya_sp._PCC_8106
Arthrospira_platensis_str._Paraca
Arthrospira_maxima_CS-328
Arthrospira_sp._PCC_8005
Crinalium_epipsammum_PCC_9333
Chamaesiphon_minutus_PCC_6605
Moorea_producens_3L
Coleofasciculus_chthonoplastes_PCC_7420
Microcoleus_sp._PCC_7113
filamentous_cyanobacterium_ESFC-1
Spirulina_subsalsa_PCC_9445
Rubidibacter_lacunae_KORDI_51-2
Halothece_sp._PCC_7418
Dactylococcopsis_salina_PCC_8305
Xenococcus_sp._PCC_7305
Myxosarcina_sp._GI1
Pleurocapsa_sp._PCC_7319
Stanieria_cyanosphaera_PCC_7437
Cyanobacterium_aponinum_PCC_10605
Cyanobacterium_stanieri_PCC_7202
Leptolyngbya_sp._PCC_7376
Synechococcus_sp._PCC_7002
Synechococcus_sp._NKBG15041c
Cyanothece_sp._PCC_7424
Cyanothece_sp._PCC_7822
Pleurocapsa_sp._PCC_7327
Cyanothece_sp._PCC_8802
Cyanothece_sp._ATCC_51142
Cyanothece_sp._CCY0110
Crocosphaera_watsonii_WH_0402
Crocosphaera_watsonii_WH_0003
Candidatus_Atelocyanobacterium_thalassa_isolate_SIO64986
Candidatus_Atelocyanobacterium_thalassa_isolate_ALOHA
Synechocystis_sp._PCC_6714
Synechocystis_sp._PCC_6803
Microcystis_aeruginosa_PCC_9701
Microcystis_aeruginosa_PCC_9806
Microcystis_aeruginosa_PCC_9808
Microcystis_aeruginosa_DIANCHI905
Microcystis_aeruginosa_PCC_9443
Microcystis_aeruginosa_PCC_9807
Microcystis_aeruginosa_PCC_9432
Microcystis_aeruginosa_TAIHU98
Microcystis_aeruginosa_NIES-843
Microcystis_aeruginosa_PCC_9809
Microcystis_sp._T1-4
Chroococcidiopsis_thermalis_PCC_7203
Synechocystis_sp._PCC_7509
Gloeocapsa_sp._PCC_7428
Mastigocladopsis_repens_PCC_10914
Chlorogloeopsis_fritschii_PCC_9212
Fischerella_sp._PCC_9605
Fischerella_muscicola_SAG_1427-1_=_PCC_73103
Fischerella_sp._JSC-11
Fischerella_muscicola_PCC_7414
Calothrix_sp._9363
Richelia_intracellularis_HH01
Rivularia_sp._PCC_7116
Calothrix_sp._PCC_6303
Calothrix_sp._PCC_7103
Hassallia_byssoidea_VB512170
Nostoc_punctiforme_PCC_73102
Calothrix_sp._PCC_7507
Nodularia_spumigena_CCY9414
Tolypothrix_sp._PCC_7601
Nostoc_sp._PCC_7107
Nostoc_sp._PCC_7524
Nostoc_sp._PCC_7120
Anabaena_variabilis_ATCC_29413
Cylindrospermum_stagnale_PCC_7417
Anabaena_sp._PCC_7108
Aphanizomenon_flos-aquae_2012/KM1/D3
Anabaena_sp._90
Anabaena_cylindrica_PCC_7122
Raphidiopsis_brookii_D9
Cylindrospermopsis_raciborskii_CS-505
Nostoc_azollae_0708
Prochlorothrix_hollandica_PCC_9006
Synechococcus_elongatus_PCC_7942
Synechococcus_elongatus_PCC_6301
Synechococcus_sp._RCC307
Cyanobium_sp._PCC_7001
Cyanobium_gracile_PCC_6307
Synechococcus_sp._WH_5701
Synechococcus_sp._RS9917
Synechococcus_sp._RS9916
Synechococcus_sp._BL107
Synechococcus_sp._CC9902
Synechococcus_sp._KORDI-52
Synechococcus_sp._WH_8109
Synechococcus_sp._CC9605
Synechococcus_sp._CC9616
Synechococcus_sp._KORDI-100
Synechococcus_sp._KORDI-49
Synechococcus_sp._WH_8102
Synechococcus_sp._WH_7805
Synechococcus_sp._WH_7803
Synechococcus_sp._WH_8016
Synechococcus_sp._CC9311
Prochlorococcus_marinus_str._MIT_9313
Prochlorococcus_sp._MIT_0701
Prochlorococcus_marinus_str._MIT_9303
Prochlorococcus_sp._MIT_0801
Prochlorococcus_marinus_str._PAC1
Prochlorococcus_marinus_str._NATL2A
Prochlorococcus_marinus_str._NATL1A
Prochlorococcus_sp._MIT_0601
Prochlorococcus_marinus_str._MIT_9211
Prochlorococcus_sp._MIT_0602
Prochlorococcus_marinus_subsp._marinus_str._CCMP1375
Prochlorococcus_marinus_str._MIT_9515
Prochlorococcus_marinus_subsp._pastoris_str._CCMP1986
Prochlorococcus_marinus_str._MIT_9201
Prochlorococcus_marinus_str._MIT_9314
Prochlorococcus_marinus_str._AS9601
Prochlorococcus_marinus_str._MIT_9301
Prochlorococcus_sp._MIT_0604
Prochlorococcus_marinus_str._GP2
Prochlorococcus_marinus_str._MIT_9302
Prochlorococcus_marinus_str._MIT_9311
Prochlorococcus_marinus_str._MIT_9107
Prochlorococcus_marinus_str._MIT_9321
Synechococcus_sp._PCC_7336
Synechococcus_sp._JA-3-3Ab
Synechococcus_sp._JA-2-3B_a_2-13
Gloeobacter_violaceus_PCC_7421
Gloeobacter_kilaueensis_JS1
0.3
B
C
D
E
F
A
I
II (Pleurocapsales)
III (Oscillatoriales)
IV (Nostocales)
V (Stigonemales)

Fig 2.1 Phylogenetic tree of cyanobacteria. ML phylogeny of cyanobacteria calculated using 153 sequences of concatenated SSU-LSU-RpoC1 gene. Branches are coloured according to the morphological subsections (I-V). Phylogenetic clades are grouped into six major groups (A–F)

2.6.2. Extant promoters of highly expressed genes

The alignment of 115 rRNA promoter sequences is shown in Fig.2.2. The results show that, in the almost all clades excluding alpha-cyanobacteria, there are well conserved -10 and -35 boxes, whose sequences are similar to those of *E. coli* (Rosenberg and Court, 1979). The promoters of *Synechococcus sp*. PCC 7942 have been experimentally determined by a previous work (Chungjatupornchai and Faaroonsawat, 2014), which is consistent with the conserved -10 box and -35 box-like sequences in the alignment. Accordingly, for the species except for alpha-cyanobacteria, the conserved two regions were identified as -10 box and -35 box (Fig.2.2). In alpha-cyanobacteria, although there are conserved sequences among species, similarities to the promoters of other clades were considerably low. For the species belonging to alpha-cyanobacteria, sequences that have the best similarities to the promoters of other clades were manually selected and estimated as -10 box and -35 box.

Promoter sequences of ribosomal proteins (115 sequences) are also well conserved in almost all clades (Fig.2.3). In the same manner as rRNA promoters, two conserved regions in the alignment were identified as -10 box and -35 box. Although there are no experimental supports, the conservation of the sequences and their high similarity to the promoters of *E. coli* (Rosenberg and Court, 1979) suggest that the conserved regions are highly likely to be the -10 and -35 boxes of ribosomal proteins. Contrary to rRNA promoters, *E. coli*-like promoters are also conserved in some of the alpha-cyanobacteria (e.g., some of *Prochlorococcus* sp.). However, similarly to the rRNA promoters, the ribosomal protein promoters of other alpha-cyanobacteria such as marine and brackish *Synechococcus* and *Cynobium* groups do not resemble the promoter sequences of other cyanobacteria.

The conservation of the promoters suggests the high expression of the genes. Thus the results imply that, as expected, rRNA and ribosomal proteins are highly expressed in almost all clades of cyanobacteria, hence, the promoters of rRNA and ribosomal proteins can be used as controls. The poor conservation of the promoters of rRNA and ribosomal proteins in alpha-cyanobacteria can be explained either of the differences in RNAP or low levels of gene expression due to slow growth rate of

the species. If the latter was the case, in alpha-cyanobacteria, the promoters of rRNA and ribosomal proteins cannot be used as controls. Thus, -10 and -35 boxes of in alpha-cyanobacteria determined from the alignment were only used for the estimation of ancestral sequences and were not used as controls in estimating the levels of gene expression (detail will be described in the section 2.6.4).

2.6.3. Extant promoters of RubisCO and Fe-SOD

The result of 92 RubisCO promoter sequences with -10 and -35 boxes identified from the alignment is shown in Fig.2.4. The sequences of -10 and -35 regions are highly conserved in alpha-cyanobacteria, Clade F (the clade consists of group IV and V), and some of the species belongs to Clade D and E (Fig.2.4) and match well to the experimentally determined promoter sequence (Nierzwicki-bauer and Curtis, 1985; Vogel, 2003). In the other species, the sequences of -10 and -35 boxes are not conserved (Fig.2.4).

The results of the alignment of 74 Fe-SOD sequences and -10 and -35 boxes identified from the alignment are shown in Fig.2.5. There are conserved -10 and -35 boxes of the species belong to Clade F, the sequences being consistent with the experimental results (Liu et al., 2000). In the other clades, sequences of -10 and -35 boxes are not conserved. For four species belong to alpha-cyanobacteria, -10 and -35 boxes could not be identified, because the regions where the promoters expected to exist seem to be too short to have -10 and -35 boxes (results not shown). In alpha-cyanobacteria, promoters are known to overlap sometimes with the ORFs (Open Reading Frames), because of the small genome size. More experimental data will be needed to identify the promoters of alpha-cyanobacteria, which is beyond the scope of this study. Thus, alpha-cyanobacteria are excluded from the analysis of ancestral Fe-SOD promoters.

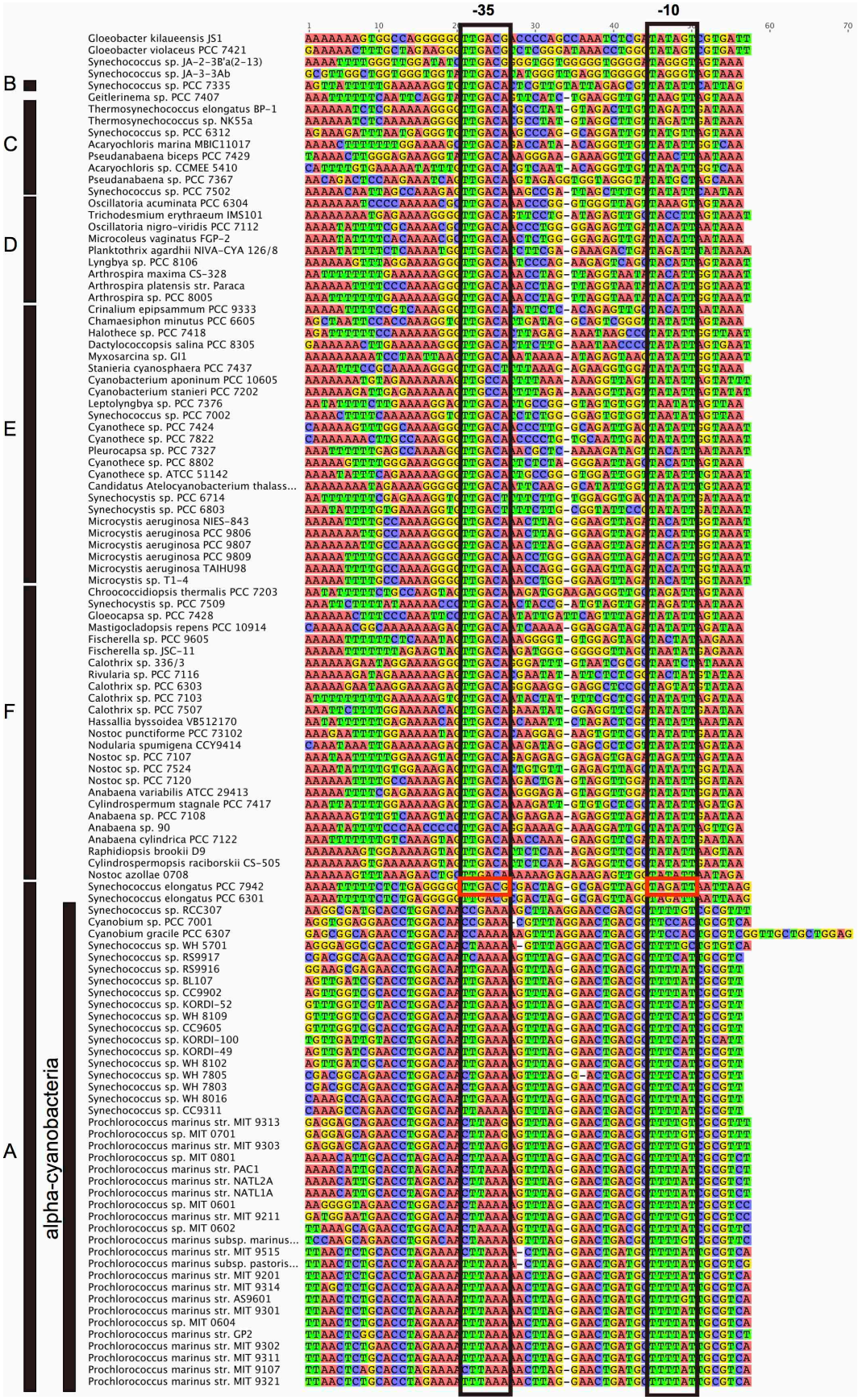

Fig 2.2 Extant promoters of rRNA

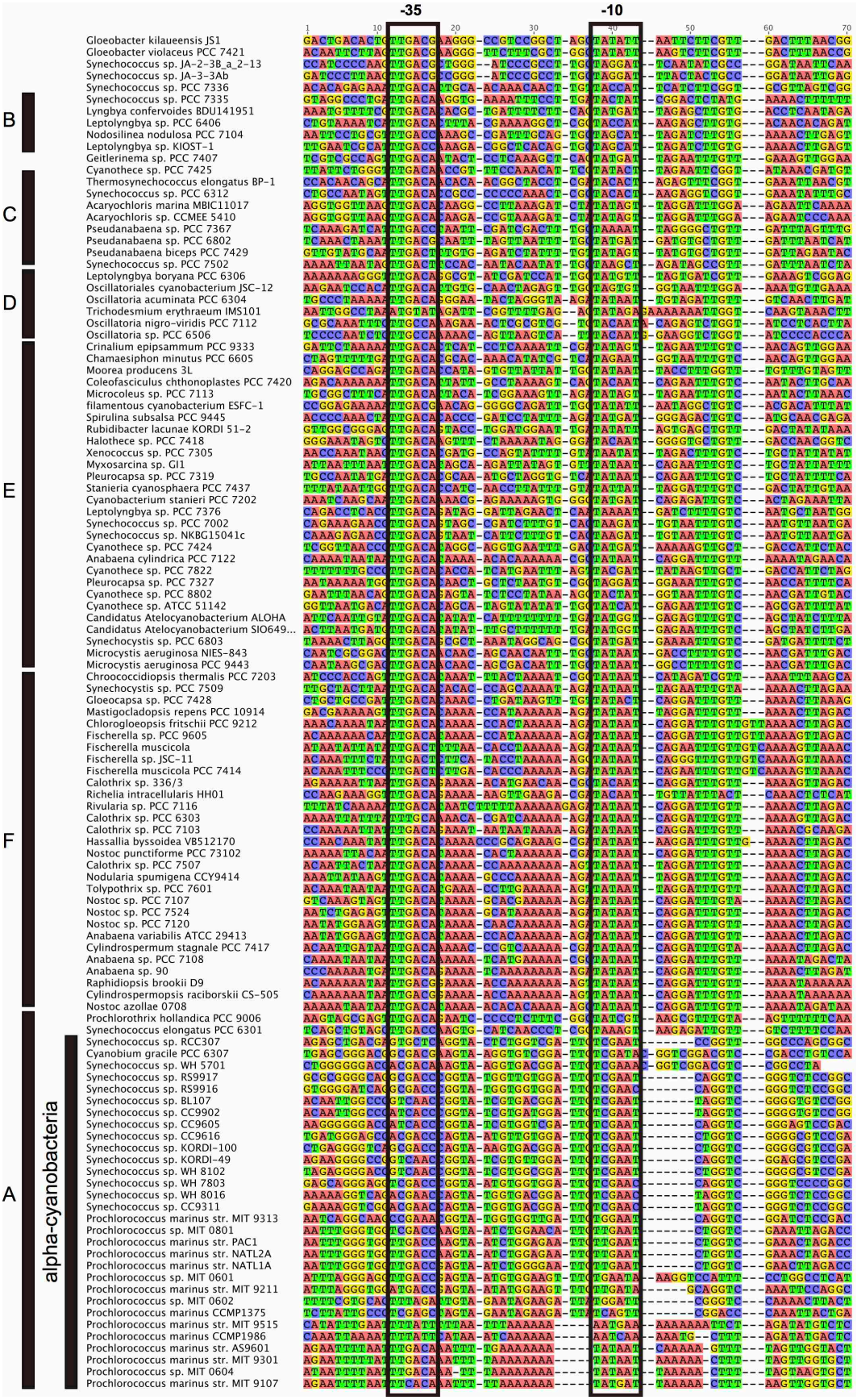

Fig 2.3 Extant promoters of ribosomal protein

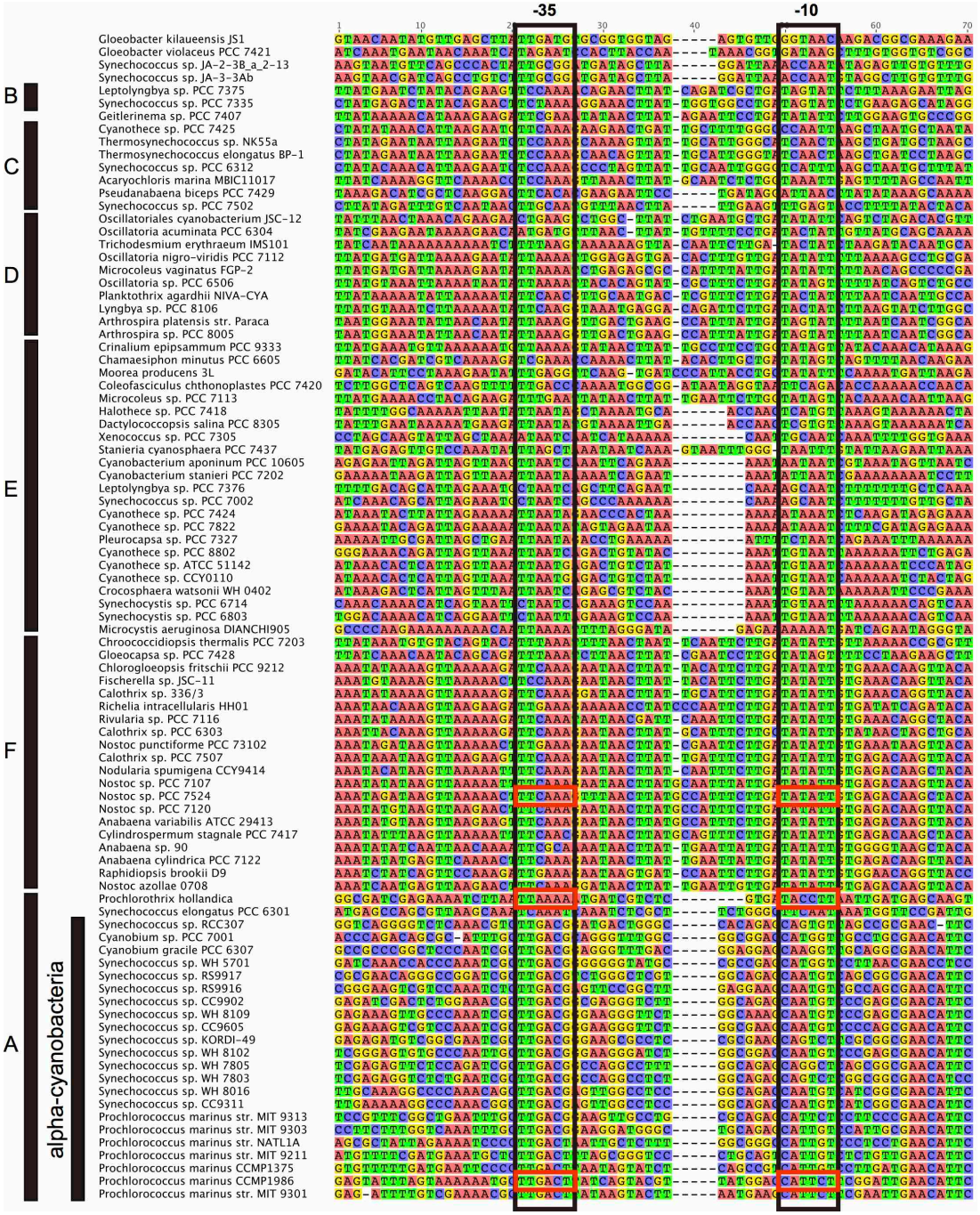

Fig 2.4 Extant promoters of RubisCO

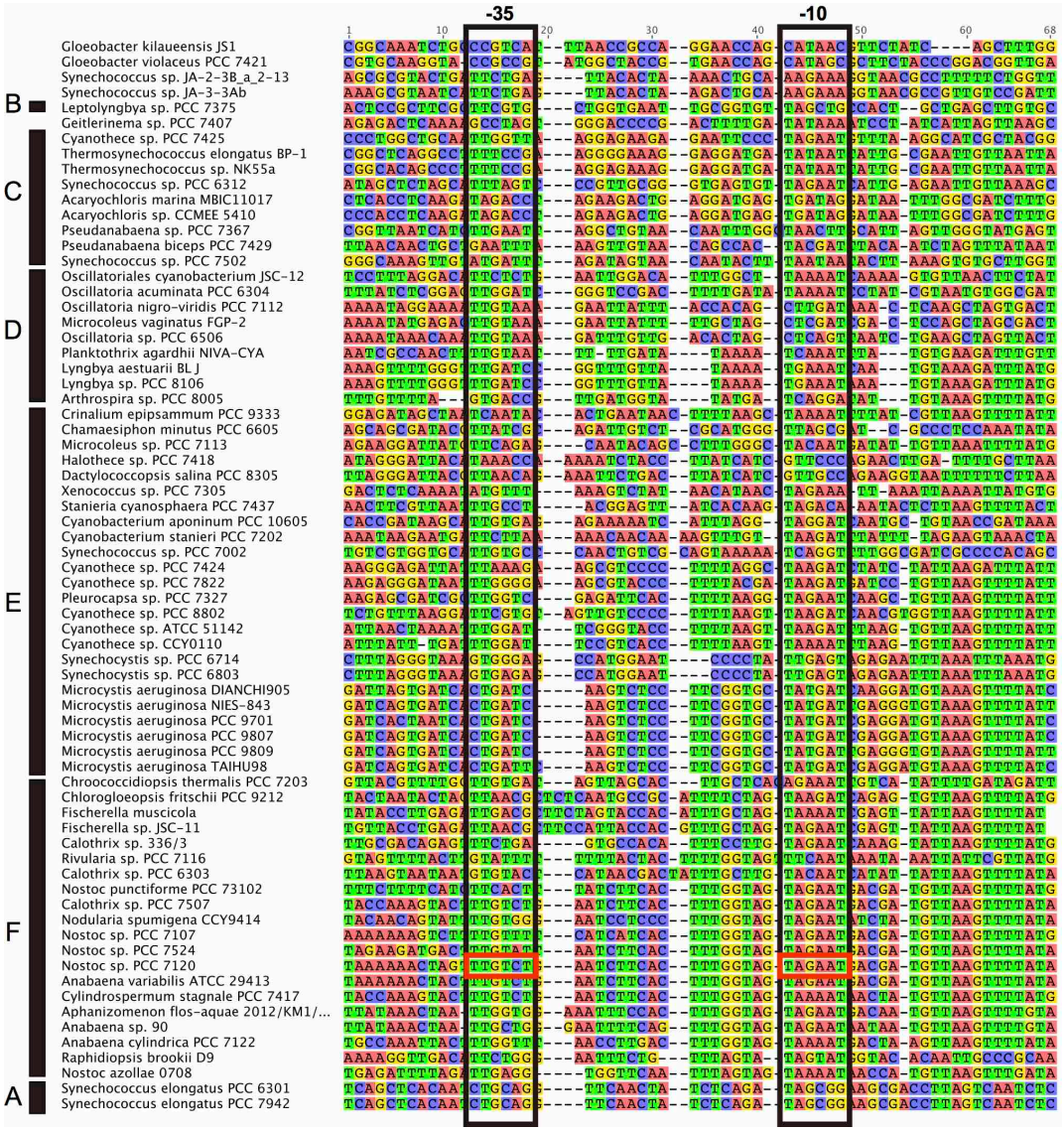

Fig 2.5 Extant promoters of Fe-SOD

Figs. 2.2-2.5 Extant promoters of rRNA, ribosomal protein, RubisCO, ans Fe-SOD. The alignment of -10 box and -35 box with the regions ~20 base pairs upstream and downstream of the two boxes are shown. -10 box and -35 box estimated from the alignment are boxed in black and experimentally determined -10 box and -35 box are boxed in red.

2.6.4. Ancestral promoters

Ancestral promoter sequences of rRNA, ribosomal proteins, RubisCO, and Fe-SOD were estimated from the extant promoter sequences. As the estimation using six different substitution models showed basically identical results, only the results obtained using HKY85 and TN93 models are shown here (Figs.2.6a,b-2.9a,b). Relationships between each branching node and the node number of ancestral sequence are shown in Figs.2.6c-2.9c.

Sequence similarity between ancestral sequences of control promoters (promoters of rRNA, ribosomal proteins) and O_2-related promoters (promoters of RubisCO, and Fe-SOD) at each node were calculated to estimate the gene expression levels. As ancestral promoters of rRNA and ribosomal proteins are similar, I use promoters for ribosomal proteins as controls for simplicity. For example, for the ancestor of Clade F, the ancestral sequences of -10 box and -35 box of each protein or gene were obtained as Table 2.3 as shown below.

Table 2.3 *Ancestral sequences of -10 and -35 boxes of Clade F ancestor*

	-35 box	-10 box
rRNA	TTGACA	TATATT
Ribosomal protein	TTGACA	TATAAT
RubisCO	TTCAAA	TATATT
Fe-SOD	TTGTCT	TAGAAT

In this case, the similarity between RubisCO promoter and ribosomal protein promoter is estimated to be 75%. In the same manner, the similarity between Fe-SOD and ribosomal protein promoter is estimated to be 75%. High homologies suggest the high gene expression levels. The calculations were done for the all nodes where the ancestral sequences were available, and the results are shown in Fig.2.10 for RubisCO and Fig.2.11 for Fe-SOD. Fig.2.10a and Fig.2.11a describe the results

calculated with HKY85 model, and Fig.2.10b and Fig.2.11b show the results calculated with TN93 model.

The results indicate that the sequence similarity between RubisCO and control promoters is high (75-60%) in deep branching nodes including the ancestors of cyanobacteria, the ancestors of Clade A-F, Clade B-F, and Clade C-F (Figs.2.10a, b). The similarity is also high in the nodes corresponding to the later divergence of cyanobacteria, such as the ancestors of Clades D, E, and F (Figs.2.10a, b). In Clade B-E, the similarity decreases with time (into 60-30%), while in the Clade F, the similarity is continuously high (~75%) after the divergence from the ancestor. The results imply that the gene expression levels of RubisCO have been generally high in the deep time, and decreases with time in the almost all clades except for Clade F.

Contrary to RubsiCO, the similarity between Fe-SOD and control promoters is low (60-40%) in the deep branching nodes (Fig.2.11ab). The similarity suddenly increases to ~80% at the time of divergence of the ancestor of Clade B-F, implying the occurrence of transition from low to high gene expression levels at this time (Figs.2.10a, b). The timing of this sudden increase in the gene expression of Fe-SOD coincides with the previously proposed timing of the evolution of marine cyanobacteria (Blank and Sánchez-Baracaldo, 2010); however it precedes the timing of the evolution of filamentous cyanobacteria (Blank and Sánchez-Baracaldo, 2010). The similarity is generally high (75-60%) after the diversification of Clade B-F, although the decreasing trend can be observed in all clades. In some ancestral nodes, similarity decreases to < 50% (Figs.2.11a, b). The results imply that, after the transition from low to high gene expression, the gene expression levels of Fe-SOD have gradually decreased through time.

In order to estimate the changes in levels of gene expression through Earth's history, the similarity was plotted against the divergence time of the each ancestral node (Fig.2.12 and 2.13). The divergence time was obtained from a literature (Blank and Sánchez-Baracaldo, 2010). The results suggest that the gene expression levels of RubsiCO have been generally high since cyanobacteria originated in ~2.7 Ga, and have not been affected by the changes in environmental O_2 levels during the GOE occurred in 2.5-2.0 Ga (Fig.2.12). The levels of gene expression have decreased with

time after the Mesoproterozoic (<1.7 Ga), although some ancestral nodes yield continuously high gene expression levels (Fig.2.12). The levels of gene expression in modern species scatter from very low to high levels (20-80 % in similarity to ribosomal protein promoters), implying the wide range of variation in the ways of evolution to optimize themselves to the habitat. The average of modern gene expression levels is low (similarity to ribosomal protein promoters are calculated as ~54±18 %). Overall, the results show general decreasing trend from the high gene expression levels in the late Archean to the low levels at present.

On the other hand, the levels of gene expression of Fe-SOD would have been low since the emergence of cyanobacteria during the late Archean and have increased in ~2.5-2.0 Ga (Fig.2.13). Considering the uncertainties in both the diversification age and the age of the rise of O_2, the timing of the increase in the gene expression overlaps the time of the GOE (Fig.2.13). Similarly to the results of RubisCO, the gene expression levels gradually decreases from the Mesoproterozoic (< 1.7 Ga) to the present (similarity to ribosomal protein promoters spanning 20-80 %, the average is calculated as ~59±13%) (Fig.2.13).

Fig 2.6.a Ancestral promoters of ribosomal protein (HKY85)

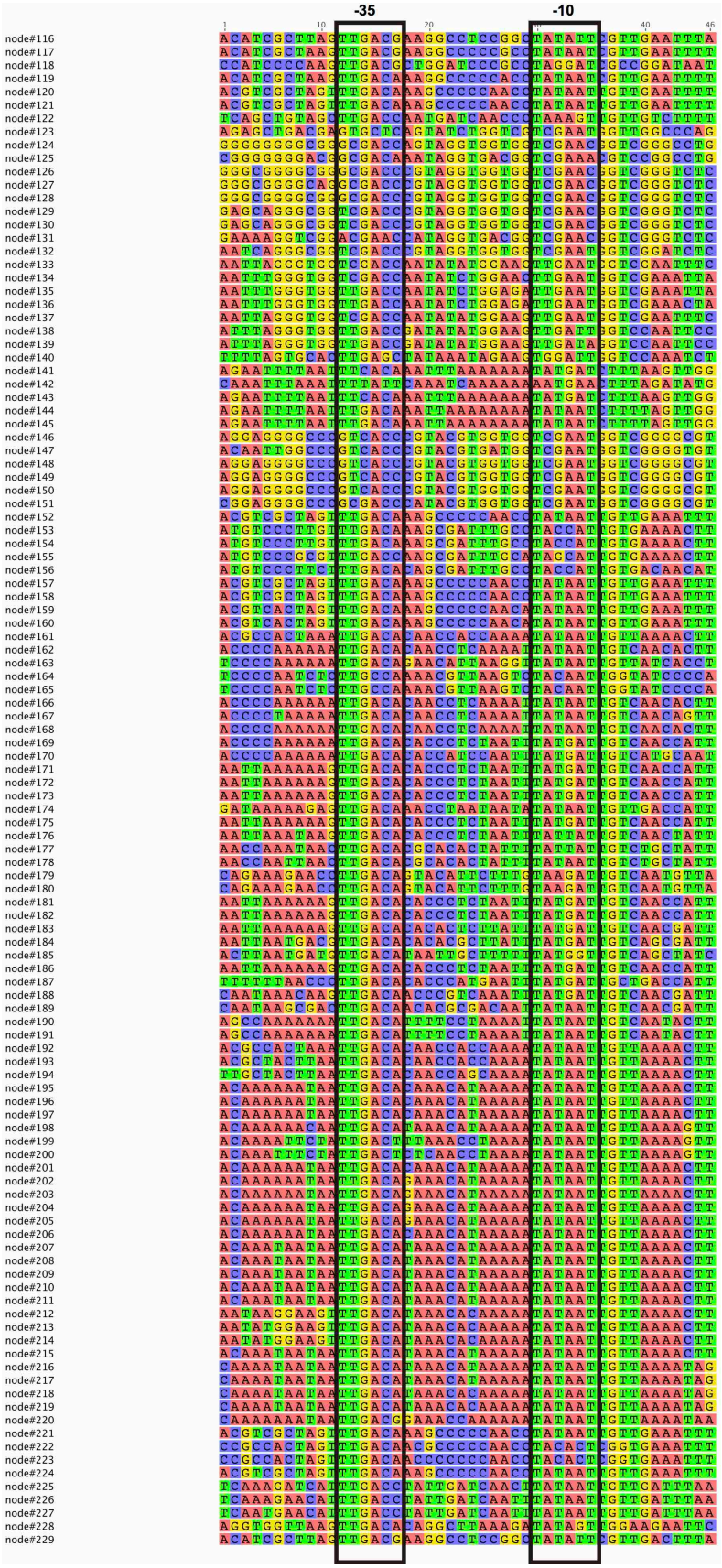

Fig 2.6.b Ancestral promoters of ribosomal protein (TN93)

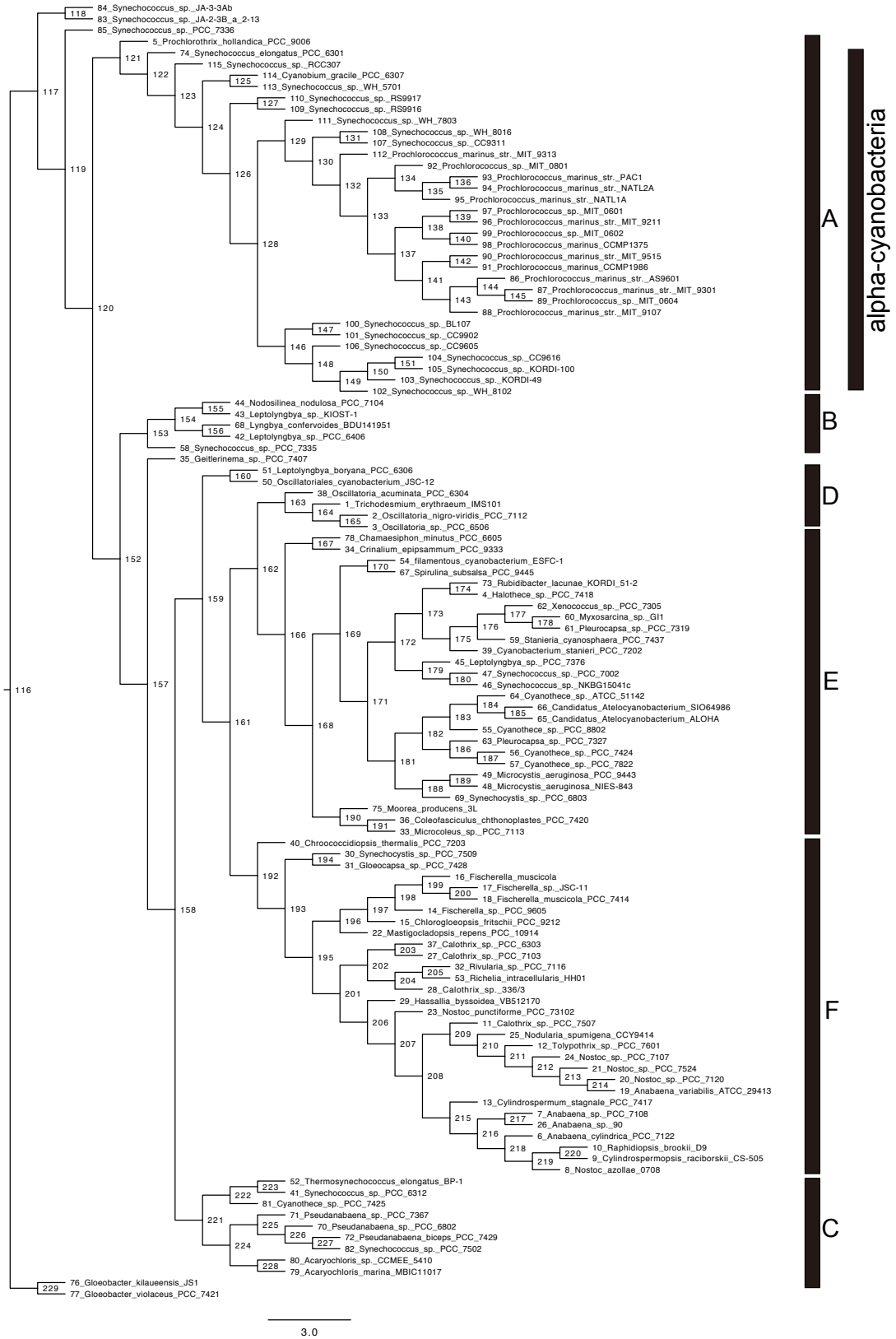

Fig 2.6.c Node numbers of ancestral ribosomal protein promoters

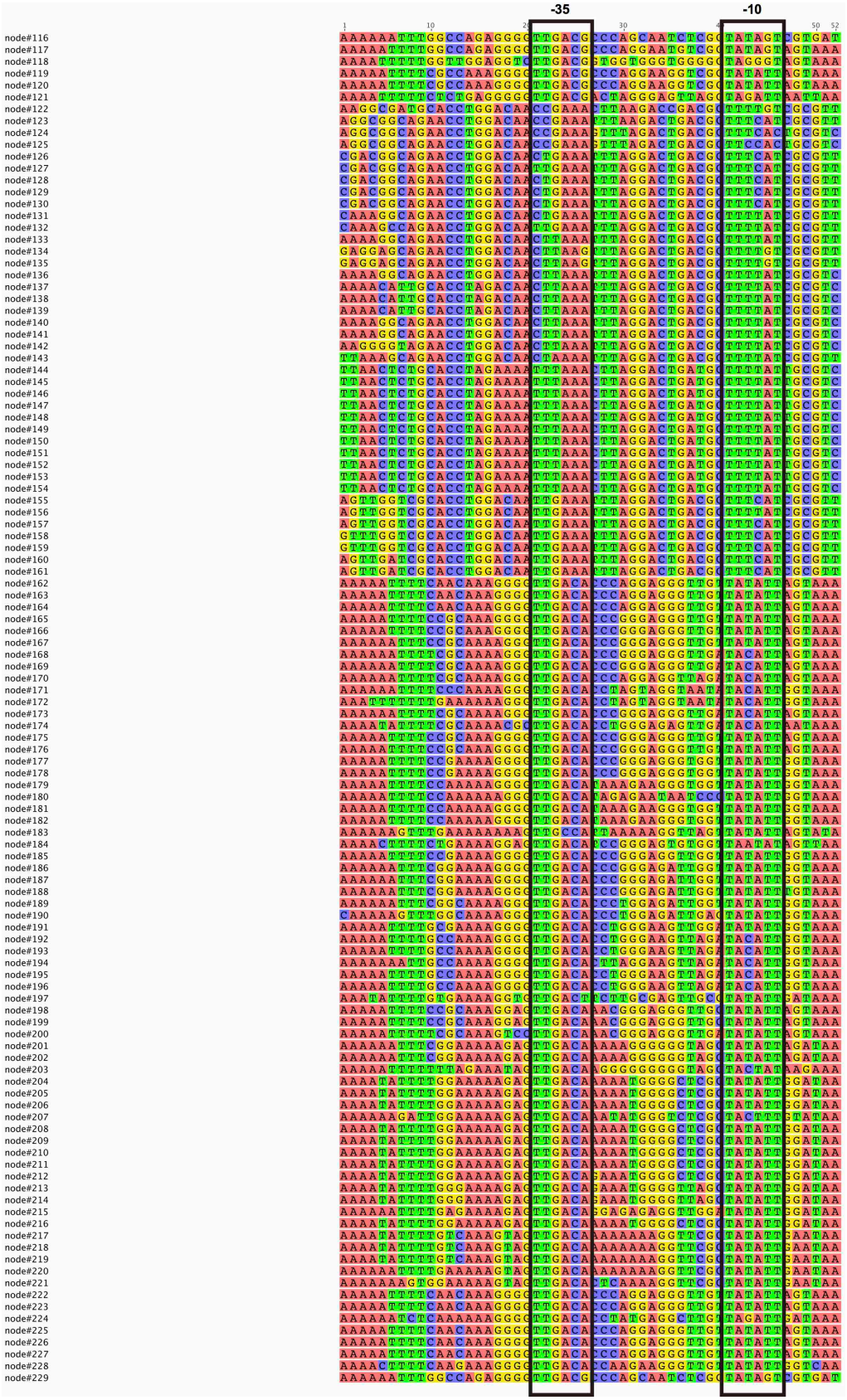

Fig 2.7.a Ancestral promoters of rRNA (HKY85)

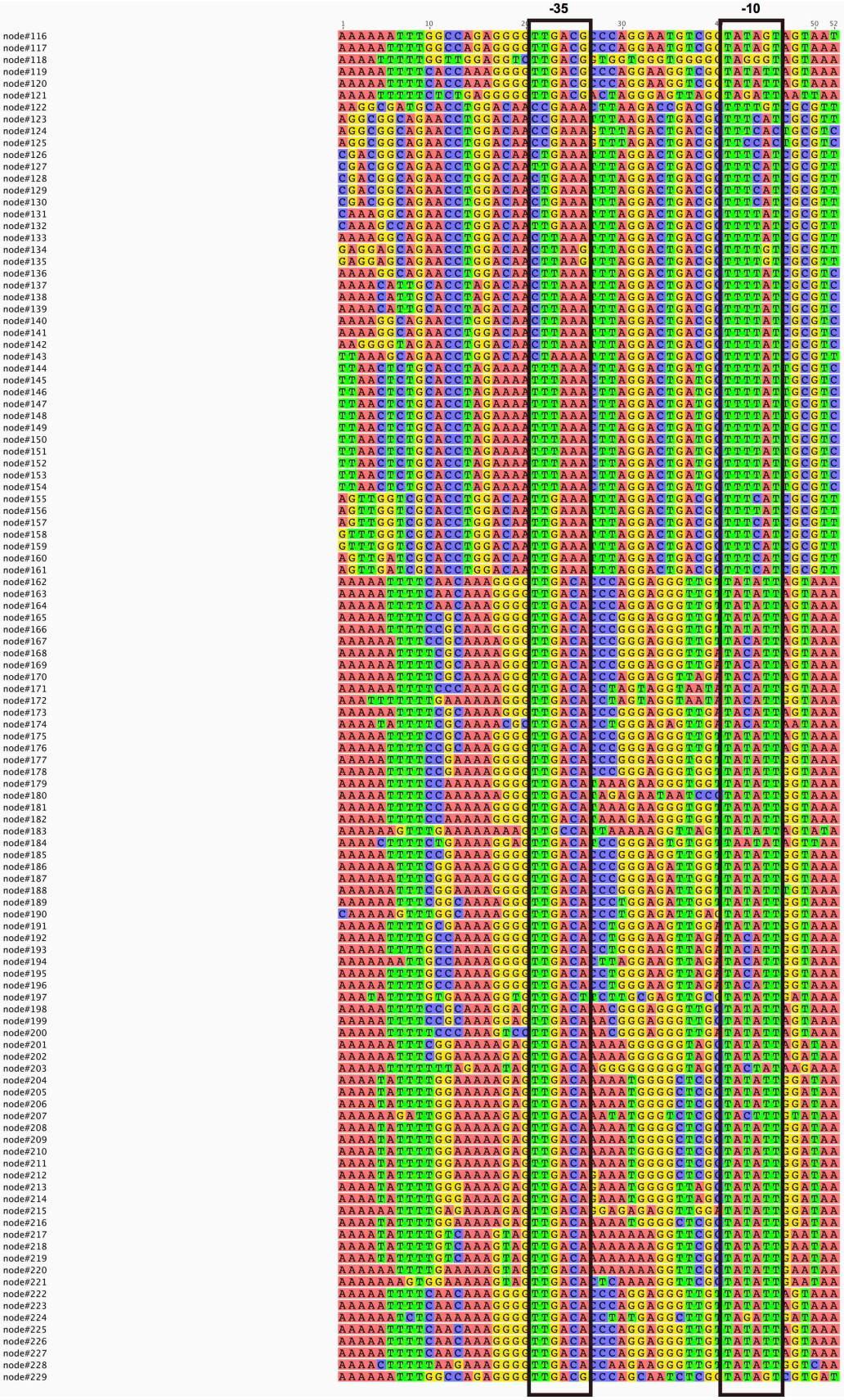

Fig 2.7.a Ancestral promoters of rRNA (TN93)

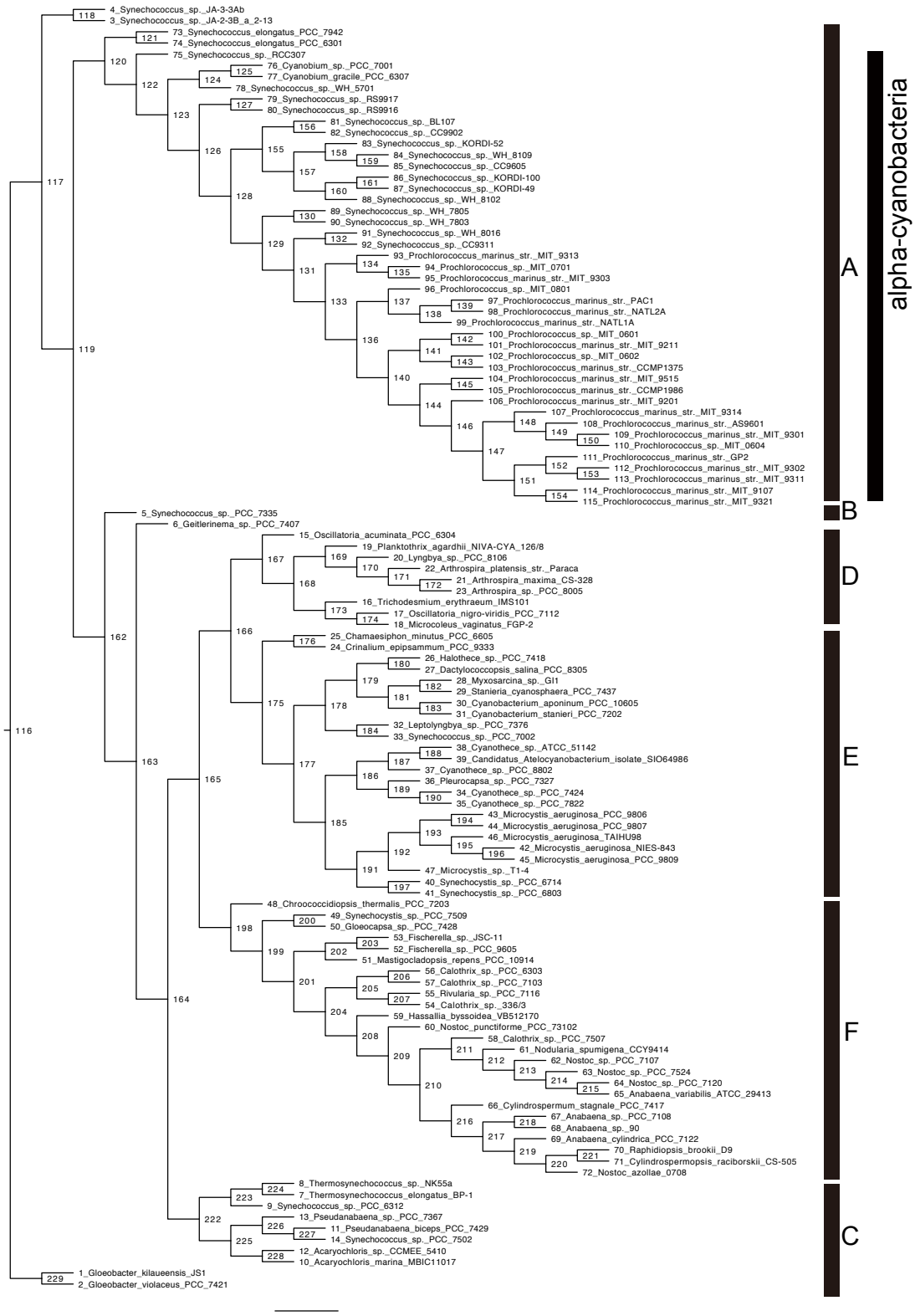

Fig 2.7.c Node numbers of ancestral rRNA

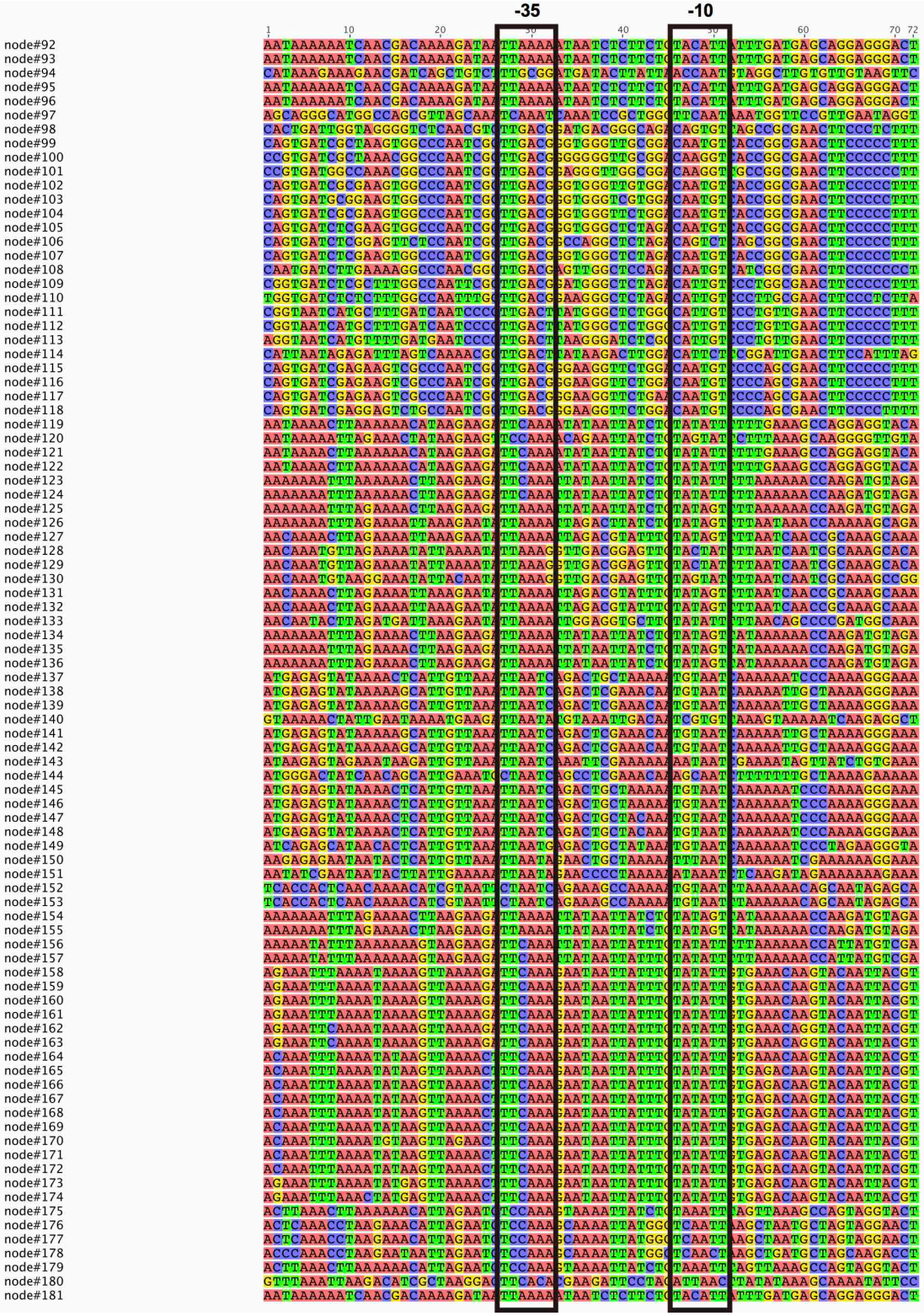

Fig 2.8.a Ancestral promoters of RubisCO (HKY85)

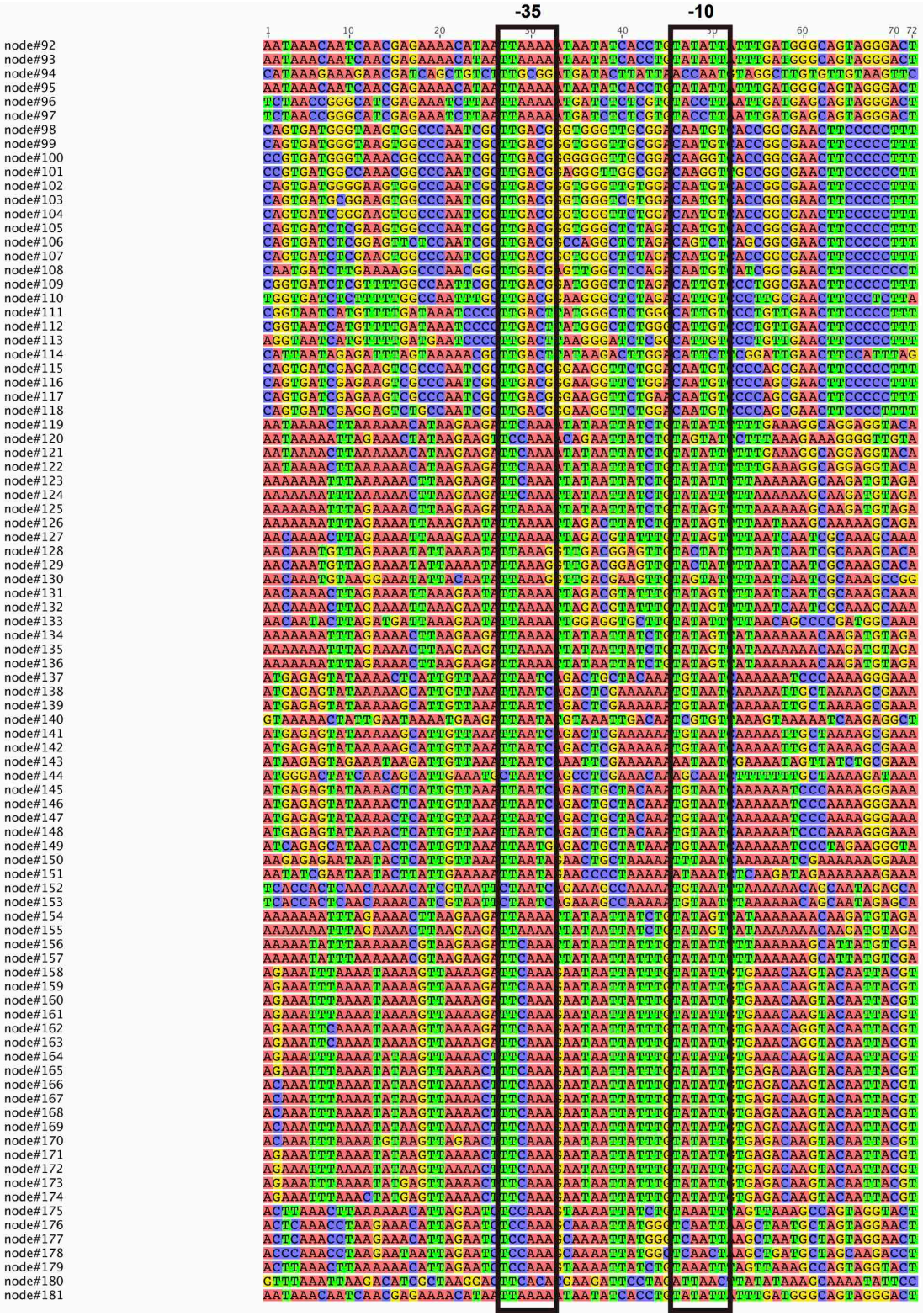

Fig 2.8.b Ancestral promoters of RubisCO (TN93)

Fig 2.8.c Node numbers of ancestral RubisCO promoters

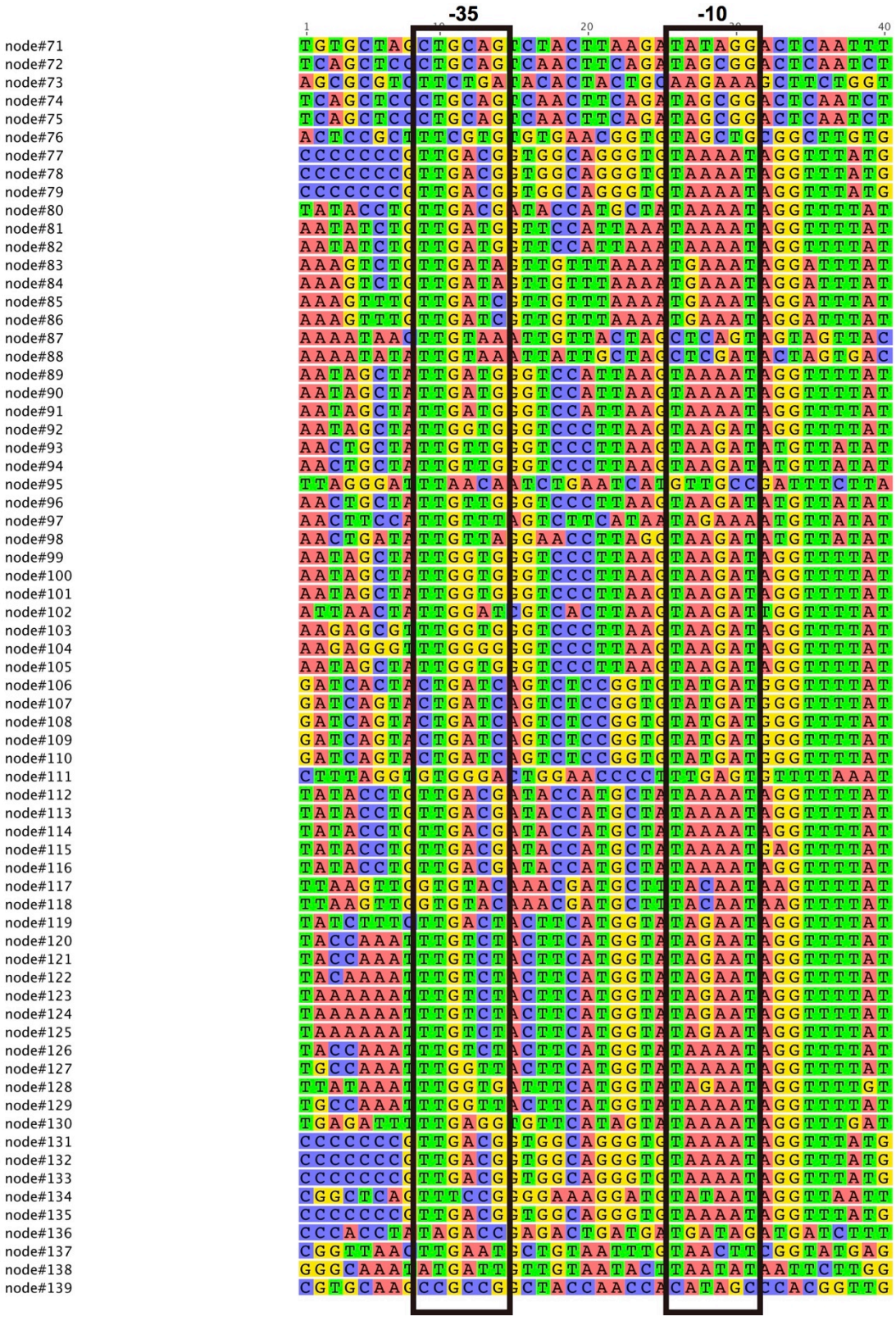

Fig 2.9a Ancestral promoters of Fe-SOD (HKY85)

Fig 2.9a Ancestral promoters of Fe-SOD (TN93)

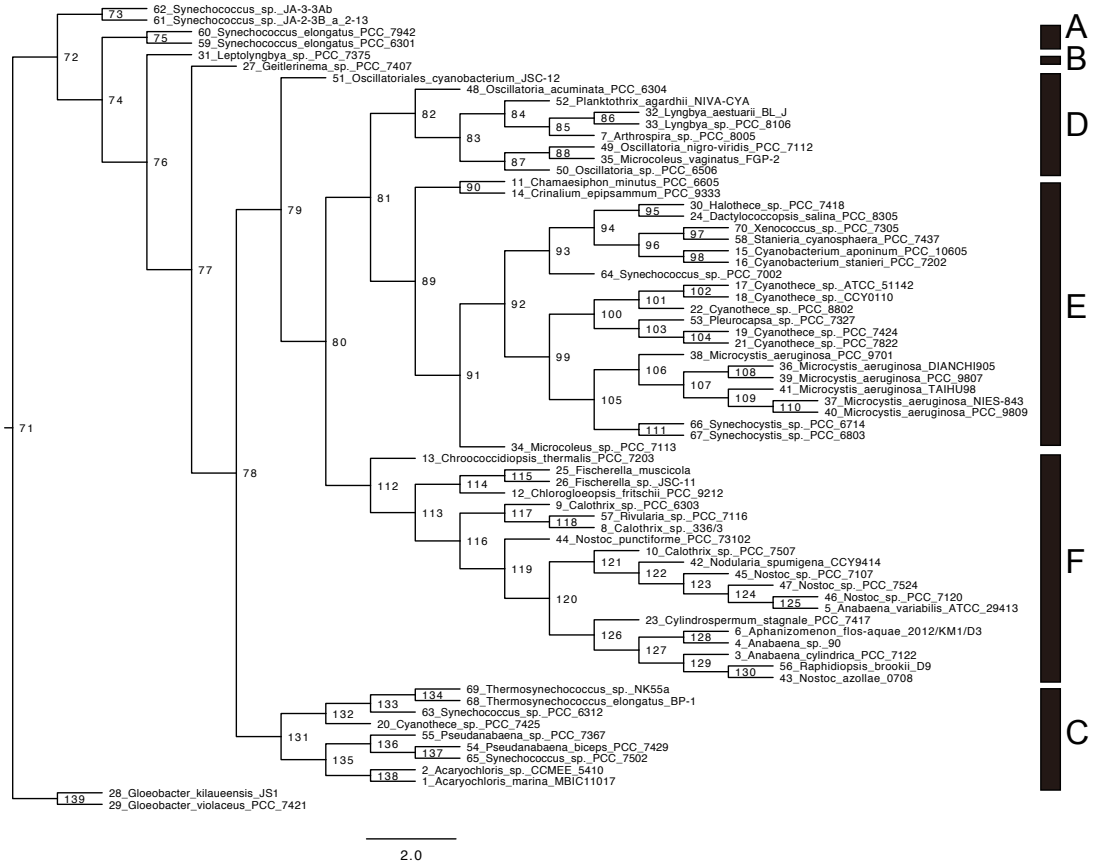

Fig 2.9c Node numbers of ancestral Fe-SOD promoters

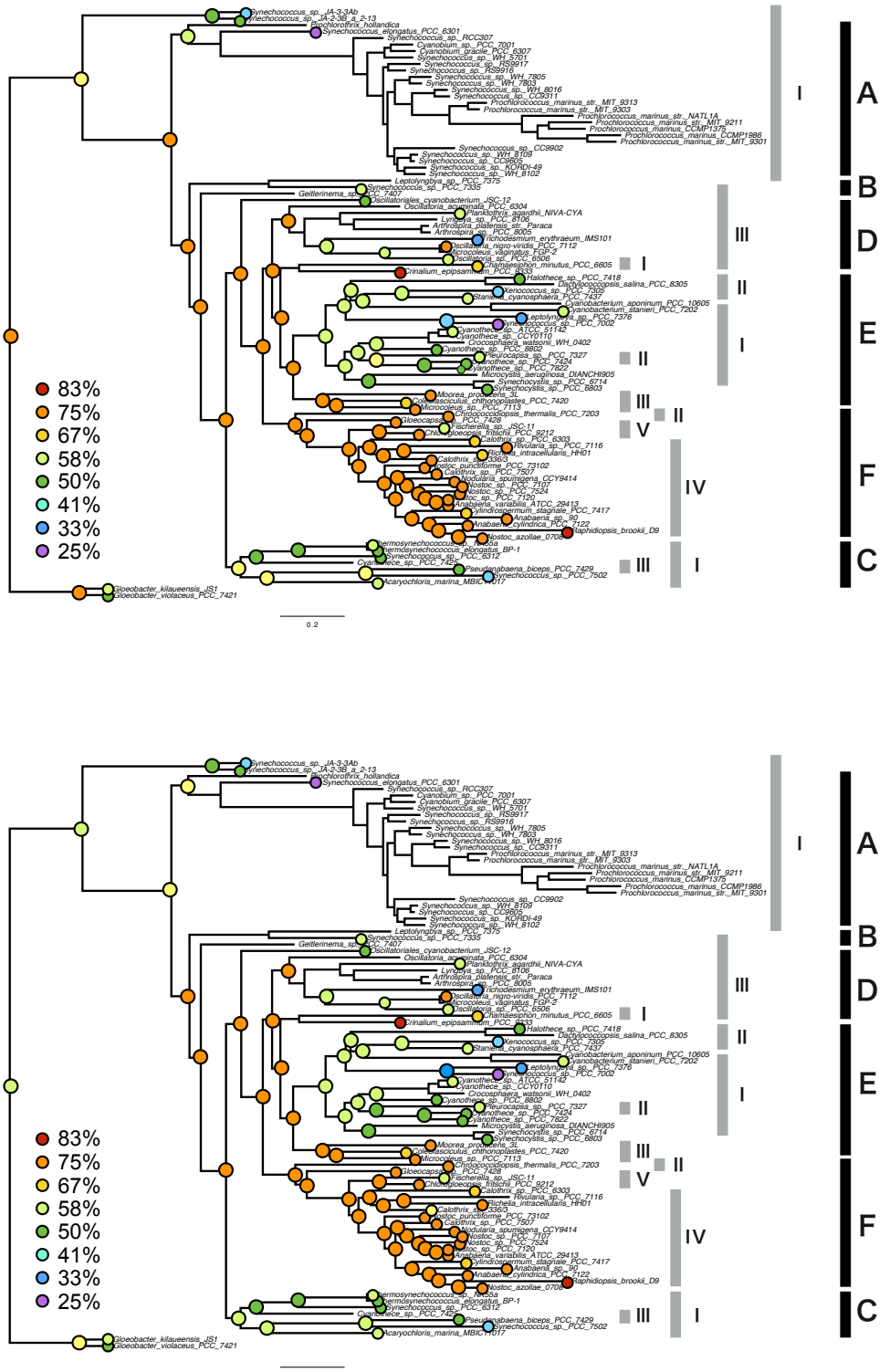

Fig 2.10 Similarity between ancestral promoters of ribosomal protein and RubisCO (a. results obtained by HKY85, b, results obtained by TN93)

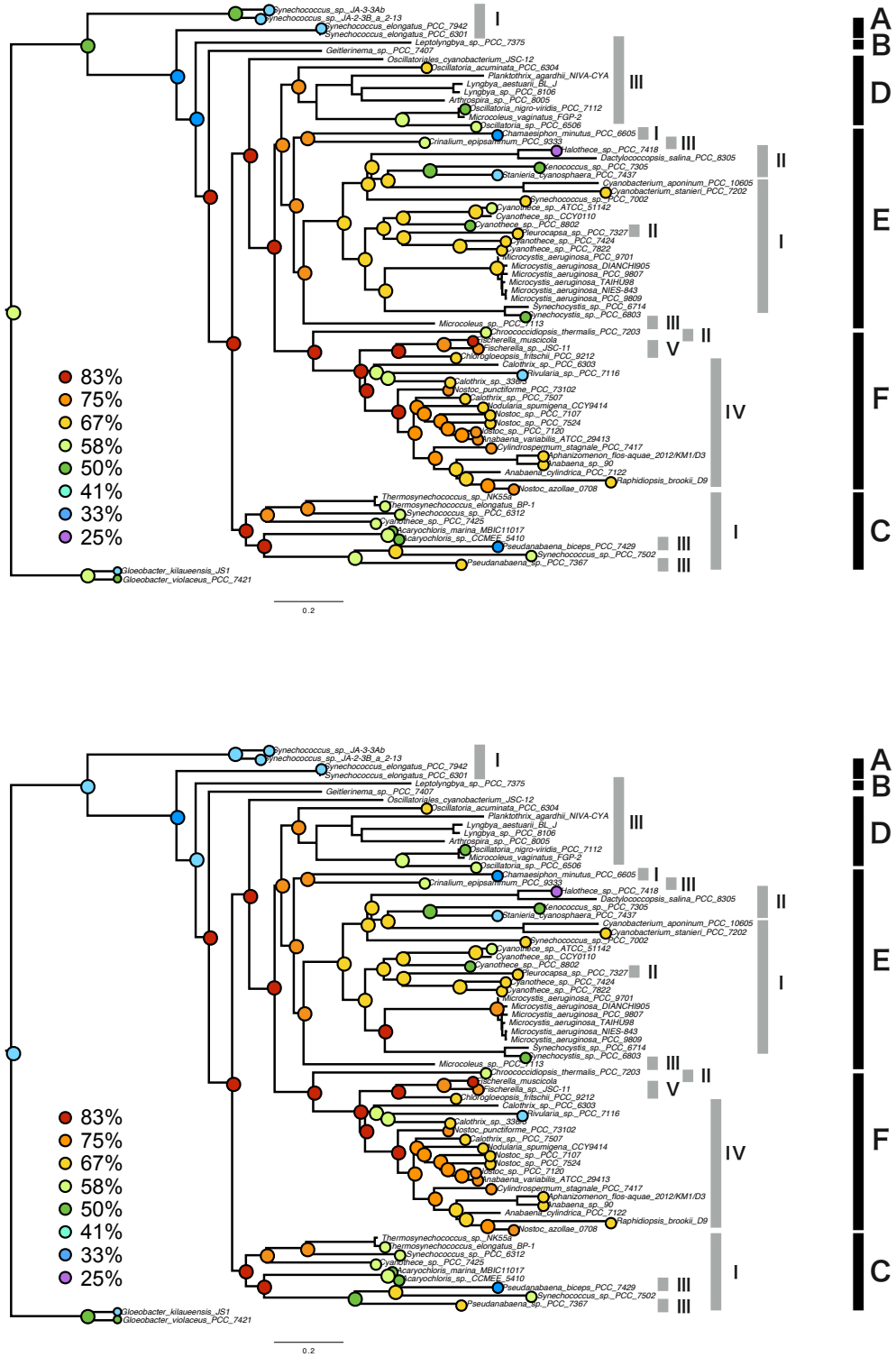

Fig 2.11 Similarity between ancestral promoters of ribosomal protein and Fe-SOD (a. results obtained by HKY85, b, results obtained by TN93)

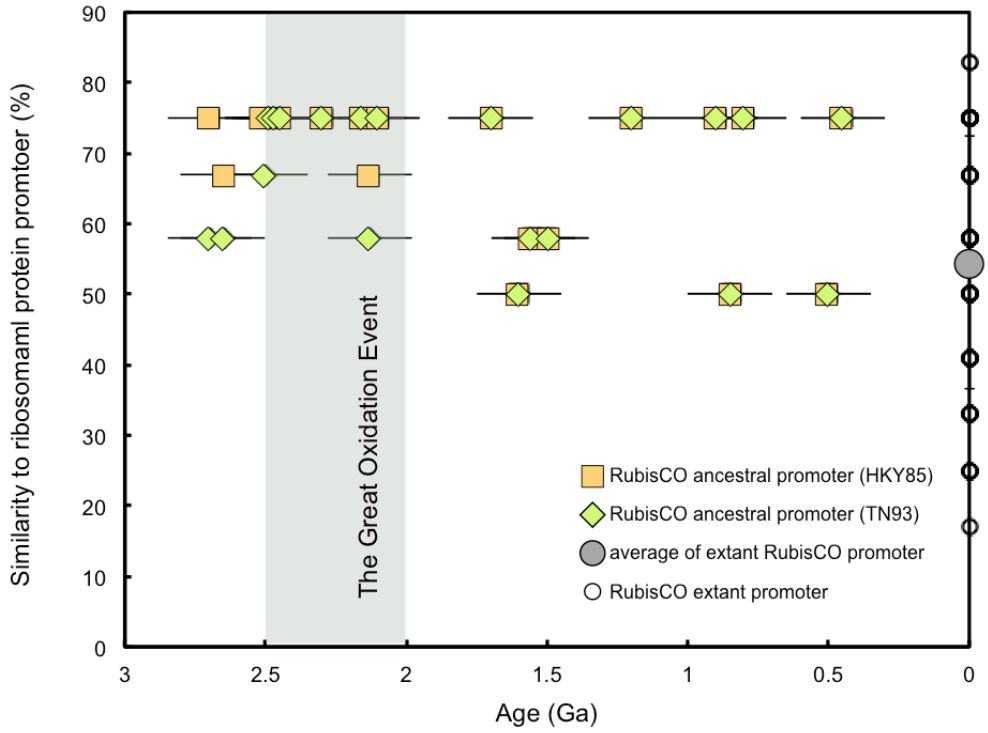

Fig 2.12 Time variation of similarity between ancestral promoters of ribosomal protein and RubisCO

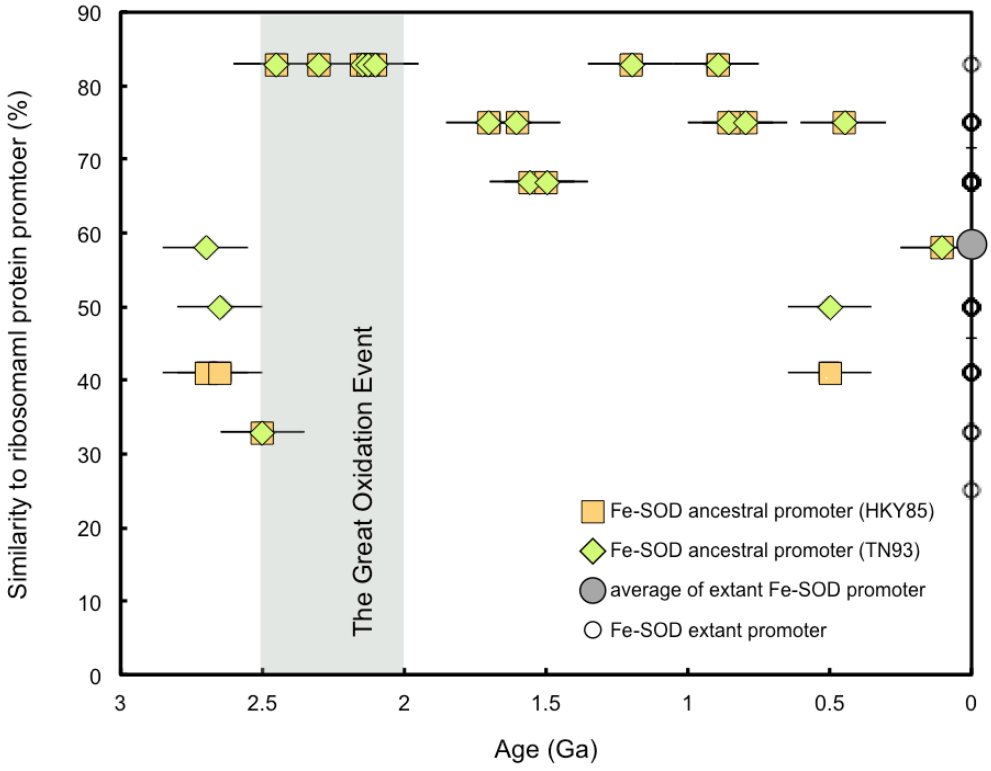

Fig 2.13 Time variation of similarity between ancestral promoters of ribosomal protein and Fe-SOD

2.7. Discussion

2.7.1. Correlation between the rise of oxygen and the gene expression of RubisCO

As mentioned in Section 2.3.2, increases in O_2/CO_2 ratio in the atmosphere might have caused increase in intercellular O_2/CO_2 ratio, resulting in the rise in gene expression levels of RubsiCO. Numerical calculations and geochemical records suggest that, in the Paleoproterozoic, the atmospheric O_2 concentration rapidly increased from low ($< 10^{-5}$ PAL) to high levels, reaching almost the present-day level (~1 PAL) within 10^6 years (Part I). Thereafter, the excess of O_2 in the atmosphere is gradually consumed to decrease O_2 levels to ~0.01 PAL in 10^8 years (Part I). The O_2 levels are considered to have been stable at ~0.01 PAL over the Proterozoic. According to geochemical records, the second major rise of O_2 from ~0.01 PAL to ~1 PAL occurred in the late Neoproterozoic (Figs.0.1 and 1.3). Besides, atmospheric CO_2 levels are considered to have decreased through Earth's history. In accordance with such changes in the atmospheric O_2 and CO_2 levels, environmental O_2/CO_2 ratio would have had a general increasing trend over Earth's history, largely increased in the early Paleoproterozoic and late Neoproterozoic. Nevertheless, the results of ancestral promoter analysis suggest that the gene expression levels of RubisCO have gradually decreased since ~2.7 Ga, lacking any increasing trends reflecting the oxidation events occurred both in the Paleoproterozoic and Neoproterozoic (Fig.2.12). Such discrepancies between the levels of gene expression and atmospheric O_2/CO_2 ratio imply that the gene expression of RubisCO is not simply controlled by the atmospheric composition, but rather affected by other controlling factors.

Possible factors that might affect the gene expression of RubisCO would be habitats or morphologies. For instance, differences in growth rate, which are probably caused by the differences in the morphology and way of fission, might affect the amount of carbon fixed via reaction catalysed by RubisCO. Indeed, Figures. 2.10a, 2.10b, and 2.14 show that the gene expression levels tend to be high in filamentous cyanobacteria (morphologically classified in Subsection III, IV, and V),

while the levels are low in unicellular cyanobacteria (morphologically classified in Subsection I and II). However, there has been an experimental study suggested that the growth rates (i.e., doubling time of cells) of cyanobacteria do not significantly vary between species (Lürling et al., 2013). More physiological studies would be required to discuss the effect of growth rates to the levels of RubisCO gene expression.

Differences in limiting nutrient caused by the variations in the habitats of cyanobacteria might affect the gene expression of RubsiCO as well. It has been suggested that marine cyanobacteria have different system of carbon fixation compared with freshwater species due the difference in limiting nutrients (Badger and Price, 2003). Badger and Price (2003) discussed that marine species, such as *Trichodesmium* (filamentous cyanobacteria included in Clade D), mainly live in oligotrophic waters that are relatively rich in inorganic carbon compared with other nutrients. By contrast, many of freshwater species live in the environments such as microbial mats, estuarine waters, and lakes, where the nutrients other than inorganic carbon are more abundant. In such situations, inorganic carbon tends to become a limiting nutrient (Badger and Price, 2003). Possibly owing to this, freshwater species are known to have various systems of transporting inorganic carbon, which help carbon fixation within cells (Badger and Price, 2003). Although there are some exceptions, unicellular species (morphologically classified in Subsections I and II and included in Clade E) tend to live in marine environments, whereas filamentous species (classified in Subsections III, IV, and V and included in Clades D and F) are more likely to live in freshwaters. Thus, the high gene expression levels in filamentous species shown in the obtained results (Figs.2.10a and 2.10b) might be explained by the differences in habitats.

Relationships between the changes in atmospheric O_2 levels and the levels of gene expression of RubsiCO would be more complicated than expected. Hence, comprehensive and detailed analysis involving habitats and physiology of cyanobacteria would be required for further discussion.

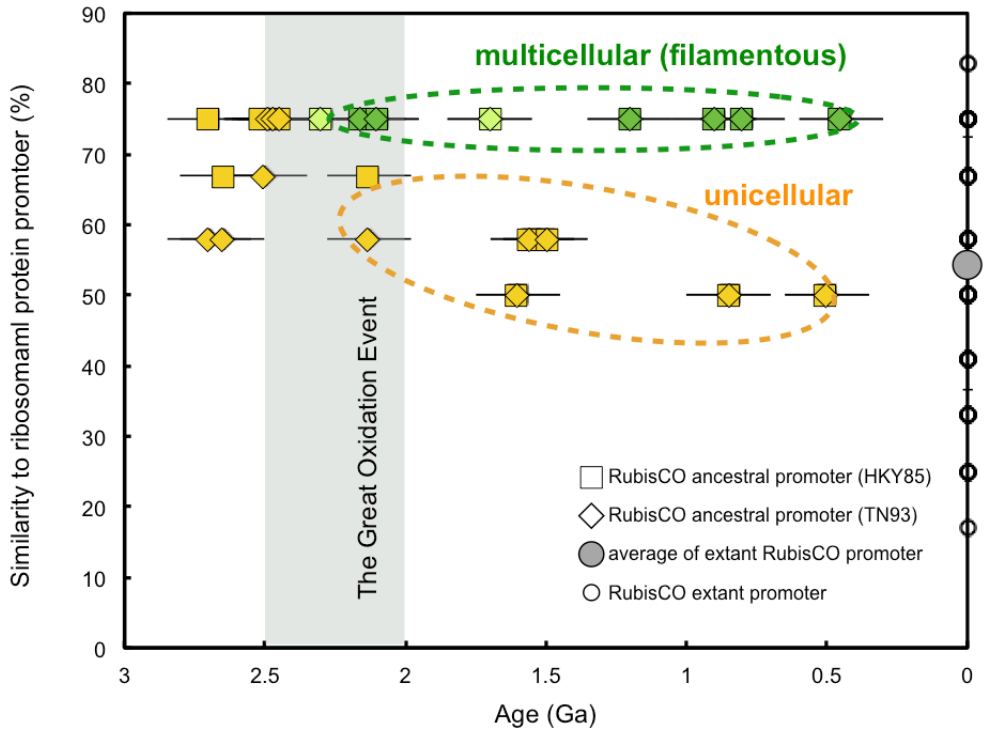

Fig 2.14 Time variation of similarity between ancestral promoters of ribosomal protein and RubisCO- effect of difference in morphologies. Multicellular (filamentous) cyanobacteria (green) and unicellular cyanobacteria (yellow). Ancestral morphologies were obtained from the literature (Blank and Sanchez-Baracaldo, 2010)

2.7.2. Correlation between the rise of oxygen and the gene expression of Fe-SOD

The results of Fig. 2.13 show that the gene expression of Fe-SOD has increased at the onset of the GOE (~2.5 Ga). Morphology and habitat of cyanobacteria, nevertheless, could affect the gene expression levels of Fe-SOD as well as RubisCO (Section 2.7.1). However, my data do not support that the changes in the gene expression levels would have been caused by changes in morphology and/or habitat. First, the gene expression levels of Fe-SOD have increased both for unicellular and multicellular cyanobacteria at the onset of the GOE (Fig. 2.15). This suggests that the difference in morphology of cyanobacteria does not account for the sudden increase in the gene expression at the GOE, although the gene expression after the GOE might have been affected by morphological evolution (Fig. 2.15). Second, my results show no clear relationships between the gene expression levels and possible difference in O_2 levels due to the difference in their habitat. For instance, some non-heterocyst filamentous species classified as Oscillatoriales (Group III, included in Clade D) are known to form microbial mats. Fig. 2.11 shows high gene expression levels of their ancestor at around the GOE (75% in similarity between ancestral promoters of Fe-SOD and ribosomal proteins). On the other hand, most of the unicellular species classified as Group I and included in Clade E live in marine surface water. The species classified in Pleurocapsales (Group II, also included in Clade E) are known to form colony (see Section 2.2.1). The gene expression levels of their ancestor of Clade E at the time of the GOE are as high as that of the ancestor of Group III in Clade D. Despite uncertainties in the habitat of these ancestors (e.g., forming microbial mats or colonies, or living in marine surface water), the above results imply that changes in habitat of cyanobacteria would not have been the major factor that has controlled the increase in the gene expression levels shown in Fig. 2.11. Thus, I suggest that the gene expression of Fe-SOD has increased in response to the O_2 increase at the time of the GOE.

Although the timing of the increase in the gene expression of Fe-SOD coincides with the onset of the GOE, the results of the gene expression do not explain the whole picture of the evolutionary track of the atmospheric O_2 levels.

Some contradictions exist between the changes in the atmospheric O_2 levels and the gene expression levels of Fe-SOD. First, for example, any clear responses to the decrease in O_2 levels at the end of overshoot (~2.0 Ga) are not seen. Rather, the long-term decreases in the gene expression levels are seen over the Proterozoic, the time period when the O_2 levels were relatively stable. Second, although there have been an oxidation event in the late Neoproterozoic, no remarkable increase in the gene expression levels is seen during this period.

Here I discuss the reasons why the increase in the gene expression levels of Fe-SOD has occurred at the onset of the GOE (~2.5 Ga) and why the decrease has not occurred at the end of O_2 overshoot (~2.0 Ga). In general, the environmental changes that have crucial effects on the survival of organisms act as a severe selective pressure, and in turn, result in rapid adaptive evolution of life. On the other hand, the environmental changes that do not directly affect the survival do not necessarily result in rapid evolution of life. At the onset of the GOE, cyanobacteria had to cope with the increasing oxidative stress of ROS. The toxicity of ROS is so critical that it may cause cell death (Latifi et al., 2009), hence forcing cyanobacteria to rapidly adapt to the environments by increasing the gene expression of Fe-SOD. When the atmospheric O_2 levels decreased at the end of overshoot, high levels of gene expression may have been no longer required, rather costing energy to synthesize excess biomolecules. Thus, it might have been advantageous for the survival of cyanobacteria to reduce the levels of gene expression of Fe-SOD. However, in contrast to the oxidative stress by ROS, such a disadvantage caused by the waste of energy may not necessarily affect the evolution of cyanobacteria directly. This may explain the absence of rapid decreasing trend of gene expression after the overshoot. The adaptation to the stable levels of atmospheric O_2 after the GOE (~0.01 PAL) might have occurred gradually over the Proterozoic.

I then discuss possibilities of the absence of a remarkable increase in the gene expression levels of Fe-SOD at the late Neoproterozoic (~0.6 Ga). As a similar increase in the O_2 levels would have occurred at the late Neoproterozoic the discussion on the adaptive evolution of life shown above seems to contradict with the results showing no increase in the gene expression levels of Fe-SOD in the late

Neoproterozoic. One of the possibilities to explain this contradiction is that the gene expression levels of Fe-SOD might have been already enough to protect cell from ROS under the condition of O_2 levels of ~1 PAL. Another possibility is that cyanobacteria might have developed other ways of defence against ROS in order to adapt to the Neoproterozoic rise of O_2. One possible way of defence would be to improve the function of the enzyme itself (i.e., kinetics and/or substrate affinity). Overall efficiency of superoxide detoxification by Fe-SOD can be understood as the multiplication of gene expression levels and performance of each enzyme. Thus, increase in kinetics or substrate affinity of Fe-SOD might have occurred in the Neproterozoic. This hypothesis can be tested in the future by reconstructing ancestral amino acid sequences of Fe-SOD and measuring its biochemical features in the laboratory. In addition, as mentioned in Section 2.3.1, cyanobacteria have multiple forms of SODs (Priya et al., 2010). Increasing gene expression of other forms of SOD (Mn-SOD, Cu/Zn-SOD, and Ni-SOD) might have contributed to the defence against SOD as well. This can be assessed by applying the methods of ancestral promoter reconstruction developed in this study to these enzymes.

Previous works suggest that the rise of O_2 was caused by some evolutionary changes of cyanobacteria that accompanied changes in morphology and/or habitat (e.g., Blank and Sánchez-Baracaldo, 2010; Schirrmeister et al., 2013, 2015). As mentioned in Section 2.6.4, my results suggest that the increase in the gene expression levels of Fe-SOD have coincided with the evolution of marine cyanobacteria and have preceded the emergence of filamentous cyanobacteria. Accordingly, I suggest that there may be no clear relationships between the rise of O_2 and the morphological evolution of cyanobacteria [i.e., the emergence of filamentous cyanobacteria (Schirrmeister et al., 2013, 2015)]. Rather, the rise of O_2 would have caused by the evolution of habitat of cyanobacteria [i.e., the changes in habitat from fresh water to marine environments (Blank and Sánchez-Baracaldo, 2010)] and/or the bloom of cyanobacteria due to large climatic events (Part I).

In order to fully understand the adaptive evolution of life to the rise of O_2, additional works including ancestral protein resurrection experiments and/or ancestral promoter analysis would be required. However, the results of this study

also indicate that, if combined with these approaches, the ancestral promoters can act as a novel proxy that records the adaptive evolution of life. This enables us to further discuss the cause and consequence of the rise of O_2, and their relationships to the biological evolution.

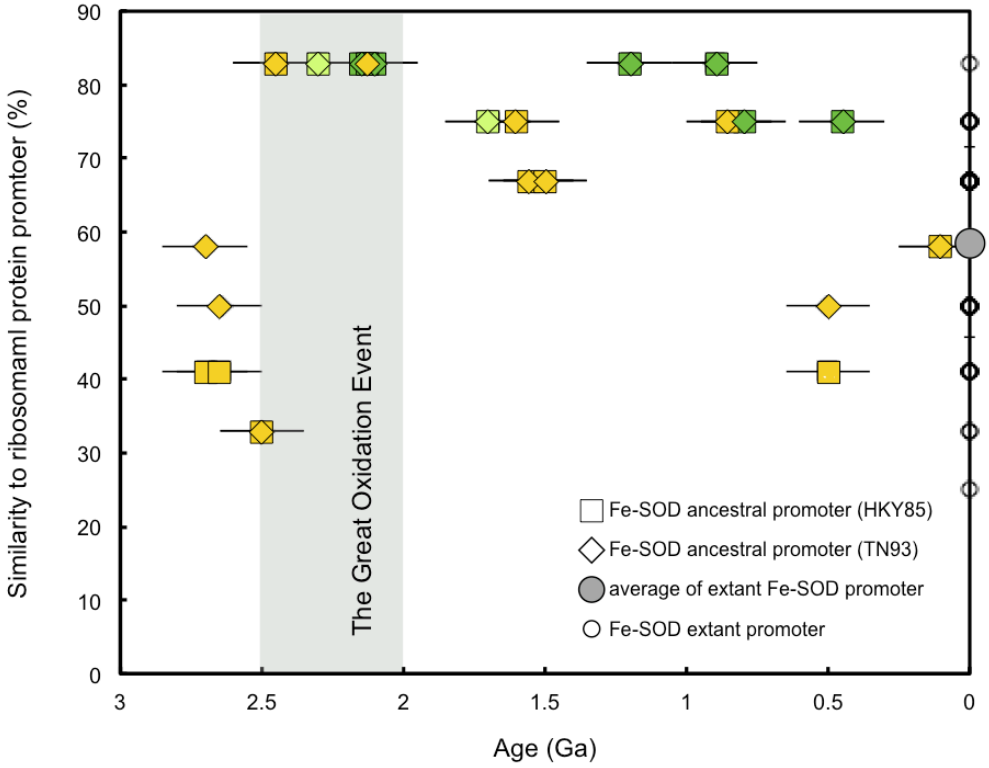

Fig 2.15 Time variation of similarity between ancestral promoters of ribosomal protein and Fe-SOD-effect of difference in morphologies. Multicellular (filamentous) cyanobacteria (green) and unicellular cyanobacteria (yellow). Ancestral morphologies were obtained from the literature (Blank and Sanchez-Baracaldo, 2010) (same as Fig. 2.14).

-

2.7.3. Future work: improvement of the methodology of the ancestral promoter analysis

In order to establish the ancestral promoter analysis as a methodology to estimate the adaptive evolution of life, efforts should be made for more accurate analysis. Although each step of the analysis (i.e., tree building, determination of extant promoter sequences, and estimation of ancestral sequences) should have some degree of uncertainty, the largest uncertainty may be in the determination of extant promoter sequences. In this study I determined the promoter sequences from alignment, which sometimes causes error in detecting promoter sequences that are not conserved. In addition, manual editing of the alignment might cause arbitrary choice of promoter sequences. To solve such problems, ideally, every promoter sequences should be determined experimentally. However, this would be impractical if the analysis were to made over one hundred species. Automatic determination of promoter sequences using computer programs would provide reproducible results without any subjective factors. Based on the known promoter sequences of bacteriophages and *E.coli*, program packages for promoter prediction have been developed (e.g, BPROM by Solovyev and Salamov (2011) and PromoterHunter Klucar et al. (2009)). There has also been an effort to develop promoter prediction programs based on the data of cyanobacteria (Vogel, 2003), nevertheless, the program are known to cause large number of false positives which probably due to the lack of data for the cyanobacterial promoters (Vogel, 2003). For accurate promoter detection by computer programs, more experimental data will be required.

Meanwhile, the results of this study show that the promoter determination by alignment works to some extent, especially in the case where promoters are well conserved. Thus, for better prediction of promoter sequences, it would be better to use a combined method including both the experiment and alignment. For the species whose promoters are highly conserved, the promoter sequences will be determined by the alignment, while, for species whose promoters are not well conserved, the species that would affect the critical ancestral nodes will be selected and the promoters will be determined more carefully by the experiment. Some degree of uncertainty may be in the tree building and estimation of ancestral sequences.

Sensitivity studies using different tree topology and statistical methods, and substitution models will be performed to check the robustness of results.

2.8. Summery of Part II

I evaluated adaptive evolution of cyanobacteria to the rise of O_2 by a novel methodology, in which ancestral promoter sequences were calculated to estimate the evolution in gene expression levels of O_2-related enzymes. I examined time variation of gene expression levels of RubisCO and Fe-SOD of cyanobacteria by comparing their ancestral promoter sequences to the promoter sequences of highly expressed protein and gene. I find that, st the onset of the GOE, gene expression of Fe-SOD increased from low to high levels in response to the rise of O_2. The changes in gene expression levels did not directly reflect the overshoot of O_2 and the Neoproterozoic rise of O_2. This is probably due to the delay in adaptation to the decreasing O_2 levels at the end of the overshoot, and the evolution of other defence mechanisms against oxidative stress, such as gene expression of other types of SOD and/or the function of enzymes in the Neoproterozoic. The gene expression levels of RubisCO did not change significantly over time, gradually decreasing from high levels in the origin of cyanobacteria. Contrary to Fe-SOD, the gene expression of RubisCO might not be simply controlled by the chemical composition of the environments but affected by habitats or morphologies of cyanobacteria.

The rise of O_2 in the Paleoproterozoic significantly changed redox state of Earth's surface environments, which results in a rise in gene expression of antioxidant enzymes for defence against toxic ROS in cyanobacteria. I showed that such adaptive evolution of life would be detected from the DNA sequences by phylogenetic analysis. The same methodology can be applied in evaluating the adaptive evolution of life to the other chemical evolution of environments, including the changes in biogeochemical cycles of sulphur, phosphorus, nitrogen, and other trace metals. The methodology will be improved to provide more accurate and objective results if combined with experimental studies in the future.

Conclusions

In order to reveal the linkage among the rise of atmospheric oxygen, snowball glaciation, and the evolution of life, I investigated environmental changes and evolution of life during the early Paleoproterozoic (2.5-2.0 Ga) by two different approaches. From the numerical calculation using biogeochemical cycle models (Part I), the trigger for the rise of oxygen was discussed. From this study, I proposed that the climate jump at the end of the snowball Earth event has triggered the rise of oxygen. Numerical results suggest that the super-greenhouse conditions after the deglaciation caused intense nutrient riverine input to the oceans via chemical weathering. This resulted in the massive bloom of cyanobacteria, causing a rapid transition from low ($< 10^{-5}$ PAL, PAL: Present Atmospheric Levels) to high ($> 10^{-2}$ PAL) O_2 steady states with an overshoot of oxygen to 0.1−1 PAL lasting for 10^6−10^8 years. Although sensitivity study suggest that the magnitude and time scales highly dependent on the initial CO_2 levels, calculation from one-dimensional ocean model suggests that only under the conditions assuming typical “hard snowball” Earth scenario, the extensive overshoot to ~1 PAL lasting for ~10^8 years occur. This causes the oxidation of deep oceans and the long-term accumulation of oceanic sulfate ions due to enhanced oxidative weathering of continental sulfides, which account for the geochemical records of O_2 overshoot. From the phylogenetic analysis of cyanobacterial promoter (Part II), I suggested that the gene expression levels of Fe-SOD in cyanobacteria increased at the nodes diverged at 2.5−2.2 Ga, possibly in response to the rise of atmospheric O_2. On the contrary, the gene expression levels of

RubsiCO have been continuously high through the history, independent on the changes in the oxygen levels. Such discrepancies might be owing to other biochemical factors that compensate the evolution of gene expressions, such as the improvement of the activity of the enzyme. Methodologies of ancestral promoter analysis developed in this study will become novel tools to provide the direct evidence of the biological evolution in response to the environmental changes in the Earth's history. Although I suggested the global climatic changes as a trigger for the rise of O_2 in Part I, the biological evolution of cyanobacteria could have caused the GOE. However, the results of Part II imply that there are no clear relationships between the rise of O_2 and the evolution of morphology and/or efficiency of carbon fixation. The evolution of the habitat of cyanobacteria, on the other hand, may have roughly coincided with the rise of O_2. Thus, from the results of Part I and Part II of this thesis, I suggest that the rise of O_2 in the Paleoproterozoic was triggered by the snowball Earth event, rather than by the evolution of cyanobacteria. The emergence of marine cyanobacteria might have occurred shortly before the snowball glaciation, allowing the massive bloom of cyanobacteria in response to the global climatic changes after the snowball deglaciation. The rise of O_2 has forced cyanobacteria to increase the gene expression levels of Fe-SOD, the trace of which can be detected by the ancestral promoter analysis. Although improvement of the methodology for the phylogenetic analysis and ancestral state estimation would be required, this study provides the first results to show the relationships between the rise of O_2, the snowball glaciation, and the evolution of life in the Plaeoproterozoic. In the future, comprehensive and interdisciplinary approaches employed in this work will contribute greatly to reveal the overall picture of co-evolution of life and environments in the Earth's history.

References

Akanuma, S., Nakajima, Y., Yokobori, S. -i., Kimura, M., Nemoto, N., Mase, T., Miyazono, K. -i., Tanokura, M., Yamagishi, A., 2013. Experimental evidence for the thermophilicity of ancestral life. Proc. Natl. Acad. Sci. 110, 11067–11072. doi:10.1073/pnas.1308215110

Amann, E., Brosius, J., Ptashne, M., 1983. Vectors bearing a hybrid trp-lac promoter useful for regulated expression of cloned genes in Escherichia coli. Gene 25, 167–178. doi:10.1016/0378-1119(83)90222-6

Anbar, A.D., Duan, Y., Lyons, T.W., Arnold, G.L., Kendall, B., Creaser, R. a, Kaufman, A.J., Gordon, G.W., Scott, C., Garvin, J., Buick, R., 2007. A whiff of oxygen before the great oxidation event? Science 317, 1903–1906. doi:10.1126/science.1140325

Andrews, T.J., Lorimer, G.H., 1978. Photorespiration-still unevoidable? FEBS Lett. 90, 1–9.

Badger, M.R., Price, G.D., 2003. CO2 concentrating mechanisms in cyanobacteria: Molecular components, their diversity and evolution. J. Exp. Bot. 54, 609–622. doi:10.1093/jxb/erg076

Bekker, A., Holland, H.D., 2012. Oxygen overshoot and recovery during the early Paleoproterozoic. Earth Planet. Sci. Lett. 317-318, 295–304. doi:10.1016/j.epsl.2011.12.012

Bekker, A., Holland, H.D., Wang, P.-L., Rumble, D., Stein, H.J., Hannah, J.L., Coetzee, L.L., Beukes, N.J., 2004. Dating the rise of atmospheric oxygen. Nature 427, 117–120. doi:10.1038/nature02260

Berner, R.A., 1994. Geocarb II: A revised model of atmospheric CO2 over phanerozoic time. Am. J. Sci. 294, 56–91.

Berner, R.A., 1991. A model for atmospheric CO2 over Phanerozoic time. Am. J. Sci. 291, 339–376.

Blank, C.E., Sánchez-Baracaldo, P., 2010. Timing of morphological and ecological innovations in the cyanobacteria--a key to understanding the rise in atmospheric oxygen. Geobiology 8, 1–23. doi:10.1111/j.1472-4669.2009.00220.x

Brosius, J., Erfle, M., Storella, J., 1985. Spacing of the -10 and -35 regions in the tac promoter. Effect on its in vivo activity. J. Biol. Chem. 260, 3539–3541.

Caldeira, K., Kasting, J.F., 1992. Susceptibility of the early Earth to irreversible glaciation caused by carbon dioxide clouds. Nature 359, 226–228.

Canfield, D.E., 2005. The early history of atmospheric oxygen: Homage to Robert M. Garrels. Annu. Rev. Earth Planet. Sci. 33, 1–36. doi:10.1146/annurev.earth.33.092203.122711

Canfield, D.E., Ngombi-Pemba, L., Hammarlund, E.U., Bengtson, S., Chaussidon, M., Gauthier-Lafaye, F., Meunier, A., Riboulleau, A., Rollion-Bard, C., Rouxel, O., Asael, D., Pierson-Wickmann, A.-C., El Albani, A., 2013. Oxygen dynamics in the aftermath of the Great Oxidation of Earth's atmosphere. Proc. Natl. Acad. Sci. U. S. A. 110, 16736–16741. doi:10.1073/pnas.1315570110

Capella-Gutierrez, S., Silla-Martinez, J.M., Gabaldon, T., 2009. trimAl: a tool for automated alignment trimming in large-scale phylogenetic analyses. Bioinformatics 25, 1972–1973. doi:10.1093/bioinformatics/btp348

Catling, D.C., Claire, M.W., 2005. How Earth's atmosphere evolved to an oxic state:

A status report. Earth Planet. Sci. Lett. 237, 1–20. doi:10.1016/j.epsl.2005.06.013

Chungjatupornchai, W., Fa-aroonsawat, S., 2014. The rrnA promoter as a tool for the improved expression of heterologous genes in cyanobacteria. Microbiol. Res. 169, 361–368. doi:10.1016/j.micres.2013.09.010

Claire, M.W., Catling, D.C., Zahnle, K.J., 2006. Biogeochemical modelling of the rise in atmospheric oxygen. Geobiology 4, 239–269. doi:10.1111/j.1472-4669.2006.00084.x

Dickson, A., Millero, F., 1987. A comparison of the equilibrium constants for the dissolution of carbonate acid in seawater media. Deep Sea Res. 34, 1733–1743.

El Albani, A., Bengtson, S., Canfield, D.E., Bekker, A., Macchiarelli, R., Mazurier, A., Hammarlund, E.U., Boulvais, P., Dupuy, J.-J., Fontaine, C., Fürsich, F.T., Gauthier-Lafaye, F., Janvier, P., Javaux, E., Ossa, F.O., Pierson-Wickmann, A.-C., Riboulleau, A., Sardini, P., Vachard, D., Whitehouse, M., Meunier, A., 2010. Large colonial organisms with coordinated growth in oxygenated environments 2.1 Gyr ago. Nature 466, 100–104. doi:10.1038/nature09166

Eppley, R., Peterson, B., 1979. Particulate organic matter flux and planktonic new production in the deep ocean. Nature 282, 677–680.

Evans, D.A., Beukes, N.J., Kirschvink, J.L., 1997. Low-latitude glaciation in the Palaeoproterozoic era. Nature 386, 262–266. doi:10.1038/386262a0

Farquhar, J., 2000. Atmospheric Influence of Earth's Earliest Sulfur Cycle. Science (80-.). 289, 756–758. doi:10.1126/science.289.5480.756

Farquhar, J., Peters, M., Johnston, D.T., Strauss, H., Masterson, A., Wiechert, U., Kaufman, A.J., 2007. Isotopic evidence for Mesoarchaean anoxia and changing atmospheric sulphur chemistry. Nature 449, 706–709. doi:10.1038/nature06202

Gaillard, F., Scaillet, B., Arndt, N.T., 2011. Atmospheric oxygenation caused by a change in volcanic degassing pressure. Nature 478, 229–232. doi:10.1038/nature10460

Galmés, J., Conesa, M.À., Díaz-Espejo, a., Mir, a., Perdomo, J. a., Niinemets, Ü., Flexas, J., 2014. Rubisco catalytic properties optimized for present and future climatic conditions. Plant Sci. 226, 61–70. doi:10.1016/j.plantsci.2014.01.008

Gaucher, E. a, Govindarajan, S., Ganesh, O.K., 2008. Palaeotemperature trend for Precambrian life inferred from resurrected proteins. Nature 451, 704–707. doi:10.1038/nature06510

Goldblatt, C., Lenton, T.M., Watson, A.J., 2006. Bistability of atmospheric oxygen and the Great Oxidation. Nature 443, 683–686. doi:10.1038/nature05169

Golubic, S., Seong-Joo, L., 1999. Early cyanobacterial fossil record: preservation, palaeoenvironments and identification. Eur. J. Phycol. 34, 339–348. doi:10.1080/09670269910001736402

Golubic, S., Sergeev, V.N., Knoll, A.H., 1995. Heterocystous Cyanobacteria.

Goto, K.T., Sekine, Y., Suzuki, K., Tajika, E., Senda, R., Nozaki, T., Tada, R., Goto, K., Yamamoto, S., Maruoka, T., Ohkouchi, N., Ogawa, N.O., 2013. Redox conditions in the atmosphere and shallow-marine environments during the first Huronian deglaciation: Insights from Os isotopes and redox-sensitive elements. Earth Planet. Sci. Lett. 376, 145–154. doi:10.1016/j.epsl.2013.06.018

Gough, D.O., 1981. Solar interior structure and luminosity variations. Sol. Phys. 74, 21–34.

Gunnars, A., Blomqvist, S., Martinsson, C., 2004. Inorganic formation of apatite in

brackish seawater from the Baltic Sea: an experimental approach. Mar. Chem. 91, 15–26. doi:10.1016/j.marchem.2004.01.008

Hawkesworth, C.J., Dhuime, B., Pietranik, a. B., Cawood, P. a., Kemp, a. I.S., Storey, C.D., 2010. The generation and evolution of the continental crust. J. Geol. Soc. London. 167, 229–248. doi:10.1144/0016-76492009-072

Hawkesworth, C.J., Kemp, a I.S., 2006. Evolution of the continental crust. Nature 443, 811–817. doi:10.1038/nature05191

Hoffman, P.F., Schrag, D.P., 2002. The snowball Earth hypothesis: testing the limits of global change. Terra Nov. 14, 129–155.

Hofmann, H.J., 1976. Precambrian Microflora, Belcher Islands, Canada: Significance and Systematics. J. Paleontol. 50, 1040–1073.

Hotinski, R.M., Kump, L.R., Najjar, R.G., Po, I., 2000. Opening Pandora ' s Box: The impact of open system modeling on interpretations of anoxia 15, 267–279.

Jenkyns, H.C., 2010. Geochemistry of oceanic anoxic events. Geochemistry, Geophys. Geosystems 11, n/a–n/a. doi:10.1029/2009GC002788

Karhu, J., Holland, H., 1996. Carbon isotopes and the rise of atmospheric oxygen. Geology 867–870.

Kasting, J., Liu, S., Donahue, T., 1979. Oxygen levels in the prebiological atmosphere. J. Geophys. Res. 84, 3079–3107. doi:10.1029/JC084iC06p03097

Kasting, J.F., Ackerman, T.P., 1986. Climatic consequences of very high carbon dioxide levels in the earth's early atmosphere. Science 234, 1383–1385.

Katoh, K., Misawa, K., Kuma, K., Miyata, T., 2002. MAFFT: a novel method for rapid multiple sequence alignment based on fast Fourier transform. Nucleic Acids Res. 30, 3059–3066. doi:10.1093/nar/gkf436

Kendall, B., Reinhard, C., Lyons, T., Kaufman, A.J., Poulton, S.W., Anbar, A.D., 2010. Pervasive oxygenation along late Archaean ocean margins. Nat. Geosci. 3, 647–652. doi:10.1038/ngeo942

Kirschvink, J.L., Gaidos, E.J., Bertani, L.E., Beukes, N.J., Gutzmer, J., Maepa, L.N., Steinberger, R.E., 2000. Paleoproterozoic snowball earth: extreme climatic and geochemical global change and its biological consequences. Proc. Natl. Acad. Sci. U. S. A. 97, 1400–1405.

Klemm, D., 2000. The formation of Palaeoproterozoic banded iron formations and their associated Fe and Mn deposits, with reference to the Griqualand West deposits, South Africa. J. African Earth Sci. 30, 1–24.

Klucar, L., Stano, M., Hajduk, M., 2009. PhiSITE: Database of gene regulation in bacteriophages. Nucleic Acids Res. 38, 366–370. doi:10.1093/nar/gkp911

Knoll, a H., Strother, P.K., Rossi, S., 1988. Distribution and diagenesis of microfossils from the lower Proterozoic Duck Creek Dolomite, Western Australia. Precambrian Res. 38, 257–79. doi:http://dx.doi.org/10.1016/0301-9268(88)90005-8

Knoll, A.H., Golubic, S., 1979. Anatomy and taphonomy of a precambrian algal stromatolite. Precambrian Res. 10, 115–151. doi:10.1016/0301-9268(79)90022-6

Kopp, R.E., Kirschvink, J.L., Hilburn, I.A., Nash, C.Z., 2005. The Paleoproterozoic snowball Earth: a climate disaster triggered by the evolution of oxygenic photosynthesis. Proc. Natl. Acad. Sci. U. S. A. 102, 11131–11136. doi:10.1073/pnas.0504878102

Kump, L.R., Barley, M.E., 2007. Increased subaerial volcanism and the rise of

atmospheric oxygen 2.5 billion years ago. Nature 448, 1033–1036. doi:10.1038/nature06058
Latifi, A., Ruiz, M., Zhang, C.C., 2009. Oxidative stress in cyanobacteria. FEMS Microbiol. Rev. 33, 258–278. doi:10.1111/j.1574-6976.2008.00134.x
Le Hir, G., Donnadieu, Y., Goddéris, Y., Pierrehumbert, R.T., Halverson, G.P., Macouin, M., Nédélec, A., Ramstein, G., 2009. The snowball Earth aftermath: Exploring the limits of continental weathering processes. Earth Planet. Sci. Lett. 277, 453–463. doi:10.1016/j.epsl.2008.11.010
Le Hir, G., Goddéris, Y., Donnadieu, Y., Ramstein, G., 2008. A geochemical modelling study of the evolution of the chemical composition of seawater linked to a " snowball " glaciation. Biogeosciences 5, 253–267.
Liu, Y., Zhou, R., Zhao, J., 2000. Molecular cloning and sequencing of the sodB gene from a heterocystous 1491, 248–252.
Lürling, M., Eshetu, F., Faassen, E.J., Kosten, S., Huszar, V.L.M., 2013. Comparison of cyanobacterial and green algal growth rates at different temperatures. Freshw. Biol. 58, 552–559. doi:10.1111/j.1365-2427.2012.02866.x
Lyons, T.W., Reinhard, C.T., Planavsky, N.J., 2014. The rise of oxygen in Earth's early ocean and atmosphere. Nature 506, 307–315. doi:10.1038/nature13068
Maddison, W.P., Maddison, D.R., 2008. Mesquite: A modular system for evolutionary analysis. Evolution (N. Y). 62, 1103–1118. doi:http://mesquiteproject.org
Mcclure, W.R., 1985. Mechanism and control of transcription initiation in prokaryotes. Annu. Rev. Biochem. 54, 171–204.
Millero, F.J., 2007. The marine inorganic carbon cycle. Chem. Rev. 107, 308–41. doi:10.1021/cr0503557
Mills, B., Watson, A.J., Goldblatt, C., Boyle, R., Lenton, T.M., 2011. Timing of Neoproterozoic glaciations linked to transport-limited global weathering. Nat. Geosci. 4, 861–864. doi:10.1038/ngeo1305
Moulton, K., West, J., Berner, R., 2000. Solute flux and mineral mass balance approches to the quantification of plant effects on silicate weathering. Am. J. Sci. 300, 539–570.
Murakami, T., Sreenivas, B., Sharma, S. Das, Sugimori, H., 2011. Quantification of atmospheric oxygen levels during the Paleoproterozoic using paleosol compositions and iron oxidation kinetics. Geochim. Cosmochim. Acta 75, 3982–4004. doi:10.1016/j.gca.2011.04.023
Nierzwicki-bauer, S.A., Curtis, S.E., 1985. Cotranscription of genes encoding the small and large subunits of ribulose-1 , 5-bisphosphate carboxylase in the cyanobacterium Anabaena 7120 82.
Ozaki, K., Tajika, E., 2013. Biogeochemical effects of atmospheric oxygen concentration, phosphorus weathering, and sea-level stand on oceanic redox chemistry: Implications for greenhouse climates. Earth Planet. Sci. Lett. 373, 129–139. doi:10.1016/j.epsl.2013.04.029
Papineau, D., Mojzsis, S.J., Schmitt, A.K., 2007. Multiple sulfur isotopes from Paleoproterozoic Huronian interglacial sediments and the rise of atmospheric oxygen. Earth Planet. Sci. Lett. 255, 188–212. doi:10.1016/j.epsl.2006.12.015
Parfrey, L.W., Lahr, D.J.G., Knoll, A.H., Katz, L.A., 2011. Estimating the timing of early eukaryotic diversification with multigene molecular clocks. Proc. Natl. Acad. Sci. 108, 13624–13629. doi:10.1073/pnas.1110633108

Partin, C. a., Bekker, a., Planavsky, N.J., Scott, C.T., Gill, B.C., Li, C., Podkovyrov, V., Maslov, a., Konhauser, K.O., Lalonde, S.V., Love, G.D., Poulton, S.W., Lyons, T.W., 2013. Large-scale fluctuations in Precambrian atmospheric and oceanic oxygen levels from the record of U in shales. Earth Planet. Sci. Lett. 369-370, 284–293. doi:10.1016/j.epsl.2013.03.031

Pavlov, A., Kasting, J., 2002. Mass-independent fractionation of sulfur isotopes in Archean Sediments: Strong Evidence for an Anoxic Archean Atomphere. Astrobiology 2, 27–41.

Payne, J.L., Boyer, A.G., Brown, J.H., Finnegan, S., Kowalewski, M., Krause, R. a, Lyons, S.K., McClain, C.R., McShea, D.W., Novack-Gottshall, P.M., Smith, F. a, Stempien, J. a, Wang, S.C., 2009. Two-phase increase in the maximum size of life over 3.5 billion years reflects biological innovation and environmental opportunity. Proc. Natl. Acad. Sci. U. S. A. 106, 24–27. doi:10.1073/pnas.0806314106

Paytan, A., McLaughlin, K., 2007. The oceanic phosphorus cycle. Chem. Rev. 107, 563–576. doi:10.1021/cr0503613

Planavsky, N.J., Bekker, A., Hofmann, A., Owens, J.D., Lyons, T.W., 2012. Sulfur record of rising and falling marine oxygen and sulfate levels during the Lomagundi event. Proc. Natl. Acad. Sci. U. S. A. doi:10.1073/pnas.1120387109/-/DCSupplemental.www.pnas.org/cgi/doi/10.1073/pnas.1120387109

Planavsky, N.J., Reinhard, C.T., Wang, X., Thomson, D., Mcgoldrick, P., Rainbird, R.H., Johnson, T., Fischer, W.W., Lyons, T.W., 2014. Low Mid-Proterozoic atmospheric oxygen levels and the delayed rise of animals. Science (80-.). 346, 635–638.

Planavsky, N.J., Rouxel, O.J., Bekker, A., Lalonde, S. V, Konhauser, K.O., Reinhard, C.T., Lyons, T.W., 2010. The evolution of the marine phosphate reservoir. Nature 467, 1088–1090. doi:10.1038/nature09485

Priya, B., Sivaprasanth, R.K., Jensi, V.D., Uma, L., Subramanian, G., Prabaharan, D., 2010. Characterization of manganese superoxide dismutase from a marine cyanobacterium Leptolyngbya valderiana BDU20041. Saline Systems 6, 6. doi:10.1186/1746-1448-6-6

Rasmussen, B., Bekker, A., Fletcher, I.R., 2013. Correlation of Paleoproterozoic glaciations based on U – Pb zircon ages for tuff beds in the Transvaal and Huronian Supergroups. Earth Planet. Sci. Lett. 382, 173–180. doi:10.1016/j.epsl.2013.08.037

Rich, P.R., 2003. The molecular machinery of Keilin's respiratory chain. Biochem. Soc. Trans. 31, 1095–1105. doi:10.1042/BST0311095

Rippka, R., Deruelles, J., Waterbury, J.B., Herdman, M., Stanier, R.Y., 1979. Generic Assignments, Strain Histories and Properties of Pure Cultures of Cyanobacteria. J. Gen. Microbiol. 111, 1–61. doi:10.1099/00221287-111-1-1

Rosenberg, M., Court, D., 1979. Regulatory Sequences Involved in the Promotion and Termination of RNA Transcription. Annu. Rev. Genet. 13, 319–353. doi:10.1146/annurev.ge.13.120179.001535

Rossi, J.J., Soberon, X., Marumoto, Y., McMahon, J., Itakura, K., 1983. Biological expression of an Escherichia coli consensus sequence promoter and some mutant derivatives. Proc. Natl. Acad. Sci. U. S. A. 80, 3203–3207. doi:10.1073/pnas.80.11.3203

Rye, R., Holland, H.D., 1998. Paleosols and the evolution of atmospheric oxygen: a critical review. Am. J. Sci. 298, 621–672.

Sahoo, S.K., Planavsky, N.J., Kendall, B., Wang, X., Shi, X., Scott, C., Anbar, A.D., Lyons, T.W., Jiang, G., 2012. Ocean oxygenation in the wake of the Marinoan glaciation. Nature 489, 546–549. doi:10.1038/nature11445

Sánchez-Baracaldo, P., Hayes, P.K., Blank, C.E., 2005. Morphological and habitat evolution in the Cyanobacteria using a compartmentalization approach. Geobiology 3, 145–165. doi:10.1111/j.1472-4669.2005.00050.x

Sánchez-Baracaldo, P., Ridgwell, A., Raven, J.A., 2014. A Neoproterozoic Transition in the Marine Nitrogen Cycle. Curr. Biol. 24, 652–657. doi:10.1016/j.cub.2014.01.041

Savir, Y., Noor, E., Milo, R., Tlusty, T., 2010. Cross-species analysis traces adaptation of Rubisco toward optimality in a low-dimensional landscape. Proc. Natl. Acad. Sci. U. S. A. 107, 3475–3480. doi:10.1073/pnas.0911663107

Schirrmeister, B.E., de Vos, J.M., Antonelli, A., Bagheri, H.C., 2013. Evolution of multicellularity coincided with increased diversification of cyanobacteria and the Great Oxidation Event. Proc. Natl. Acad. Sci. U. S. A. 110, 1791–6. doi:10.1073/pnas.1209927110

Schirrmeister, B.E., Gugger, M., Donoghue, P.C.J., 2015. Cyanobacteria and the Great Oxidation Event: evidence from genes and fossils. Palaeontology n/a–n/a. doi:10.1111/pala.12178

Schröder, S., Bekker, a., Beukes, N.J., Strauss, H., van Niekerk, H.S., 2008. Rise in seawater sulphate concentration associated with the Paleoproterozoic positive carbon isotope excursion: evidence from sulphate evaporites in the ~2.2–2.1 Gyr shallow-marine Lucknow Formation, South Africa. Terra Nov. 20, 108–117. doi:10.1111/j.1365-3121.2008.00795.x

Scott, C., Lyons, T.W., Bekker, a, Shen, Y., Poulton, S.W., Chu, X., Anbar, a D., 2008. Tracing the stepwise oxygenation of the Proterozoic ocean. Nature 452, 456–9. doi:10.1038/nature06811

Sekine, Y., Suzuki, K., Senda, R., Goto, K.T., Tajika, E., Tada, R., Goto, K., Yamamoto, S., Ohkouchi, N., Ogawa, N.O., Maruoka, T., 2011a. Osmium evidence for synchronicity between a rise in atmospheric oxygen and Palaeoproterozoic deglaciation. Nat. Commun. 2, 502. doi:10.1038/ncomms1507

Sekine, Y., Tajika, E., Tada, R., Hirai, T., Goto, K.T., Kuwatani, T., Goto, K., Yamamoto, S., Tachibana, S., Isozaki, Y., Kirschvink, J.L., 2011b. Manganese enrichment in the Gowganda Formation of the Huronian Supergroup: A highly oxidizing shallow-marine environment after the last Huronian glaciation. Earth Planet. Sci. Lett. 307, 201–210. doi:10.1016/j.epsl.2011.05.001

Sheng, Y., Abreu, I. a., Cabelli, D.E., Maroney, M.J., Miller, A.F., Teixeira, M., Valentine, J.S., 2014. Superoxide dismutases and superoxide reductases. Chem. Rev. 114, 3854–3918. doi:10.1021/cr4005296

Shi, T., Falkowski, P.G., 2008. Genome evolution in cyanobacteria: the stable core and the variable shell. Proc. Natl. Acad. Sci. U. S. A. 105, 2510–2515. doi:10.1073/pnas.0711165105

Shih, P.M., Wu, D., Latifi, A., Axen, S.D., Fewer, D.P., Talla, E., Calteau, A., Cai, F., Tandeau de Marsac, N., Rippka, R., Herdman, M., Sivonen, K., Coursin, T., Laurent, T., Goodwin, L., Nolan, M., Davenport, K.W., Han, C.S., Rubin, E.M.,

Eisen, J.A., Woyke, T., Gugger, M., Kerfeld, C.A., 2013. Improving the coverage of the cyanobacterial phylum using diversity-driven genome sequencing. Proc. Natl. Acad. Sci. 110, 1053–1058. doi:10.1073/pnas.1217107110

Silvestro, D., Michalak, I., 2012. RaxmlGUI: A graphical front-end for RAxML. Org. Divers. Evol. 12, 335–337. doi:10.1007/s13127-011-0056-0

Solovyev, V., Salamov, a, 2011. Automatic annotation of microbial genomes and metagenomic sequences. Metagenomics its Appl. Agric. Biomed. Environ. Stud. (Ed. RW Li), Nov. Sci. Publ. 61–78.

Tajika, E., 2003. Faint young Sun and the carbon cycle: implication for the Proterozoic global glaciations. Earth Planet. Sci. Lett. 214, 443–453. doi:10.1016/S0012-821X(03)00396-0

Tavare, S., 1986. Some probabilistic and statistical problems in the analysis of DNA sequences. Am. Math. Soc. Lect. Math. Life Sci.

Tcherkez, G.G.B., Farquhar, G.D., Andrews, T.J., 2006. Despite slow catalysis and confused substrate specificity, all ribulose bisphosphate carboxylases may be nearly perfectly optimized. Proc. Natl. Acad. Sci. U. S. A. 103, 7246–7251. doi:10.1073/pnas.0600605103

Tomitani, A., Knoll, A.H., Cavanaugh, C.M., Ohno, T., 2006. The evolutionary diversification of cyanobacteria: molecular-phylogenetic and paleontological perspectives. Proc. Natl. Acad. Sci. U. S. A. 103, 5442–7. doi:10.1073/pnas.0600999103

Tsu-Ming Han, B.R., 1992. Megascopic Eukaryotic Algae from the 2.1 - Billion-Year-Old Negaunee Iron Formation. Science 82008, 232–234.

Turner, E.C., Bekker, A., 2015. Thick sulfate evaporite accumulations marking a mid-Neoproterozoic oxygenation event (Ten Stone Formation, Northwest Territories, Canada). Geol. Soc. Am. Bull. B31268.1. doi:10.1130/B31268.1

Vogel, J., 2003. Experimental and computational analysis of transcriptional start sites in the cyanobacterium Prochlorococcus MED4. Nucleic Acids Res. 31, 2890–2899. doi:10.1093/nar/gkg398

Walker, J.C.G., Hays, P.B., Kasting, J.F., 1981. A negative feedback mechanism for the long-term stabilization of Earth's surface temperature. J. Geophys. Res. 86, 9776–9782. doi:10.1029/JC086iC10p09776

Weiss, R., 1974. Carbon dioxide in water and seawater: the solubility of a non-ideal gas. Mar. Chem. 2, 203–215.

Williamson, M.A., Rimstidt, J.D., 1994. The kinetics and electrochemical 58, 5443–5454.

Yamanaka, Y., Tajika, E., 1996. The role of the vertical fluxes of particulate organic matter and calcite in the oceanic carbon cycle: Studies using an ocean biogeochemical general circulation model. Global Biogeochem. Cycles 10, 361–382.

Yang, Z., Kumar, S., Nei, M., 1995. A new method of inference of ancestral nucleotide and amino acid sequences. Genetics 141, 1641–1650. doi:8601501

Young, G.M., 2002. Stratigraphic and tectonic settings of Proterozoic glaciogenic rocks and banded iron-formations: relevance to the snowball Earth debate. J. African Earth Sci. 35, 451–466. doi:10.1016/S0899-5362(02)00158-6

Young, J.N., Rickaby, R.E.M., Kapralov, M. V., Filatov, D. a., 2012. Adaptive signals in algal Rubisco reveal a history of ancient atmospheric carbon dioxide.

Philos. Trans. R. Soc. B Biol. Sci. 367, 483–492. doi:10.1098/rstb.2011.0145
Zahnle, K., Claire, M.W., Catling, D.C., 2006. The loss of mass-independent fractionation in sulfur due to a Palaeoproterozoic collapse of atmospheric methane. Geobiology 4, 271–283. doi:10.1111/j.1472-4669.2006.00085.x